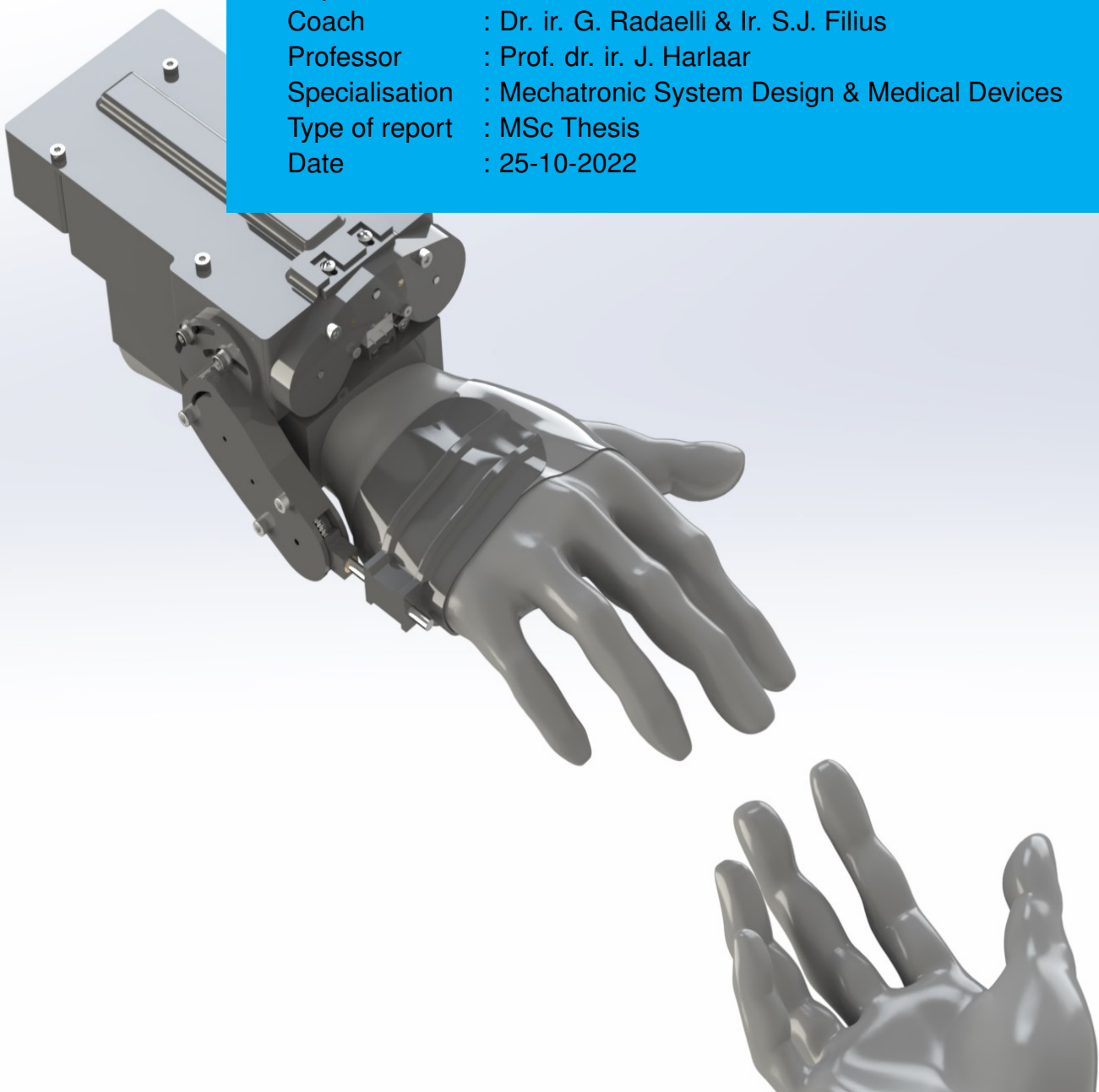


Department of Precision and Microsystems Engineering

Constant torque gravity compensation

B.J. van der Burgh

Report no : 2022.064
Coach : Dr. ir. G. Radaelli & Ir. S.J. Filius
Professor : Prof. dr. ir. J. Harlaar
Specialisation : Mechatronic System Design & Medical Devices
Type of report : MSc Thesis
Date : 25-10-2022



Constant torque gravity compensation

Designing a wrist support for Duchenne
Muscular Dystrophy patients

by

B.J. van der Burgh

to obtain the degree of Master of Science
at the Delft University of Technology,
to be defended publicly on Tuesday October 25, 2022 at 9:30 AM.

Student number:	4570308	
Thesis committee:	Prof. dr. ir. J. Harlaar,	TU Delft, Chair
	Dr. ir. G. Radaelli,	TU Delft, Supervisor
	Ir. S. J. Filius,	TU Delft, Supervisor
	Dr. ir. G. Smit,	TU Delft
	Dr. ir. D. Farhadi,	TU Delft

This thesis is confidential and cannot be made public until January 1, 2024.

An electronic version of this thesis is available at <http://repository.tudelft.nl/>.

Preface

It's an experience like no other experience I can describe, the best thing that can happen to a scientist, realizing that something that's happened in his or her mind exactly corresponds to something that happens in nature. It's startling every time it occurs. One is surprised that a construct of one's own mind can actually be realized in the honest-to-goodness world out there. A great shock, and a great, great joy
Leo Kadanoff

Every journey sooner or later comes to an end. As such with this thesis my journey of becoming an engineer has come to a closure. It is often said that the journey is more important than the destination, which I can now say is also applicable to this thesis. It was a challenging but rewarding journey as it has taught me valuable lessons in very diverse subjects, ranging from managing my own project to conducting experiments with human participants but also in mechanical design. Furthermore, I was confronted with some unexpected challenges in the course of this project. For instance, I had to learn how to operate a sowing machine to make the human interface for one of my umpteenth prototypes.

Nonetheless, as I have reached the end of this journey, of almost a lifetime of education, it is merely the start of a new one, the start of my professional career as an engineer. However, no matter what road lies ahead, I will never stop learning and investigating what interests me.

This thesis would not have been possible without the assistance of many people. First of all, I would like to thank my supervisors Giuseppe and Suzanne for their valuable feedback and for keeping me focussed on the project when I went too much into detail. Secondly, I would like to thank professor Harlaar for the insights he gave me while setting up and performing my experiments with human participants. Thirdly, my gratitude goes to Ali and Mariska for the interesting discussions on the implementation and implications of my ideas. Furthermore, to my fellow students for their help with my experiments and the interesting informal discussions. And of course, to the support staff of PME and BME for their assistance with performing and setting up my experiments. Lastly, I would like to thank my parents and family for their support throughout this journey, it would not have been possible without them.

*B.J. van der Burgh
Delft, October 2022*

Contents

Introduction	1
1 Duchenne Muscular Dystrophy	3
1.1 Disease progression	3
1.2 Microbiological Manifestation	3
1.3 Classification	4
1.4 Arm function in Duchenne Muscular Dystrophy.	4
1.5 Treatment.	5
2 Simplified balancing	7
2.1 Biomechanics of the arm.	7
2.2 Modelling of the arm	8
2.3 Balancing a mass.	10
2.3.1 1 DOF balancer.	10
2.3.2 Orientation independent balancer	11
3 The effectiveness of different torque profiles for gravity compensation of the hand	13
4 Design of an adjustable constant force mechanism for gravity compensation	25
5 Design of a wrist support	37
5.1 Design case.	37
5.1.1 Adjustable constant force	37
5.1.2 Negative stiffness.	39
5.1.3 Positive stiffness	40
5.1.4 Transmission	40
5.1.5 Complete mechanism design	40
5.1.6 Interface.	40
5.2 Design.	41
6 Discussion	43
7 Conclusion	45
7.1 Recommendations	45
A Description of the experimental setup	47
A.1 Fixating and positioning the forearm.	47
A.2 Applying a force to the hand	47
A.3 Generating the different force/torque profiles	48
A.4 Indicating the position of the hand.	49
B Three springs	51
B.1 Model	51
B.2 Sensitivity analysis	52
B.3 Experimental validation	53
C 3D cam	55
C.1 Model	55
C.2 Prototype	57

D	Curved and prestressed flexures	59
D.1	Curved flexures	59
D.2	Prestressed flexures	60
D.3	Experimental evaluation	61
D.3.1	method	61
D.3.2	results and discussion: Experiment 1	61
D.3.3	Conclusion: Experiment 1	63
D.3.4	Results and discussion: Experiment 2	64
D.3.5	Conclusion: Experiment 2	65
D.4	Conclusion	65
E	Experimental results of inclined flexures	67
E.1	Results and discussion	68
E.2	Evaluation of final configuration	69
E.2.1	results and discussion	69
E.3	Constant force mechanism.	70
F	Interface	71
F.1	Transmission	71
F.2	Attachment	72
F.2.1	Prototypes	72
G	Interface models	75
G.1	Cable and Bowden cable.	75
G.2	Slider hinge	76
H	Wrist support evaluation	79
H.1	Method	79
H.2	Results	79
H.3	Discussion	79
H.4	Conclusion	80
I	Interaction effects	81
I.1	Extensor muscle	81
I.1.1	Interaction effects.	82
I.2	Flexor muscle.	82
I.2.1	Interaction effects.	82
I.3	Discussion	83
J	Manufacturing	85
J.1	Prototype	85
J.2	Monolithic design	86
K	Concept generation	89
	References	91

Introduction

Duchenne Muscular Dystrophy (DMD) is a genetic disorder, occurring in approximately 1 in 5000 male births, causing a progressive loss of skeletal muscle function and increased joint impedance [1–3]. Thus, as the disease progresses the patients lose the strength to move their legs and arms making them more reliant on others and assistive devices, such as wheelchairs and arm supports, to assist them in their daily activities.

In recent years a considerable amount of effort has been put in the development of arm supports within the Flexion A-Gear project as a collaboration between the Delft University of Technology, VU Medical Centre, Technical University of Twente and Radboud University Medical Centre [4–8]. Currently, this research is being continued within the Wearable Robotics Consortium, to develop an arm exoskeleton and wrist support [9]. However, for both the arm exoskeleton and wrist support there are multiple challenges which have to be solved, such as the user interaction and weight compensation. Consequently, in this thesis an attempt is made to address the issue of weight compensation of the hand.

Compensating the weight of the hand is challenging, because of the complexity of the wrist joint and its manoeuvrability through space, making the level of compensation dependent on the orientation of the arm. So far only a few wrist supports have been developed capable of providing assistance in activities of daily living [10]. However, most of these devices are limited to specific orientations or are large and complex. Therefore, in this thesis a novel method is being investigated to reduce device complexity for compensating the weight of the hand. This method relies on balancing the hand only approximately using a constant torque of which the magnitude depends on the orientation of the forearm. Using such a constant torque allows for the use of a semi-passive type of wrist support, decreasing the complexity of control and the energy consumption of the support. However, as the use of a constant torque has not been used so far in weight compensation of the human body, its effectiveness in reducing the muscle effort must be evaluated. Subsequently, this thesis describes the experimental evaluation of using a constant torque to compensate the weight of the hand.

To be of use in a wrist support a mechanism is required which is capable of generating a constant force/torque output. Here a constant force output, implies that the output force remains approximately constant throughout a specific range of motion. Besides requiring a constant force, this force must also be adjustable as the level of compensation is dependent on the orientation of the arm. While a considerable effort has been put in the development of (adjustable) constant force mechanism in different fields of study [11], only in recent years the application of standard constant force mechanism in exoskeleton gained some interest [12, 13]. However so far, no attempts have been made to use adjustable constant force mechanisms for gravity compensation of a limb.

This thesis describes the development of an adjustable constant force mechanism as a proof of principle for a novel wrist support to compensate the weight of the hand. To discuss the different aspects related to the development of this wrist support this thesis is structured as follows. In the first chapter the disease DMD will be introduced and how it affects the functioning of the arm. Successively the second chapter describes how the mass of the hand can be compensated. The third chapter presents an article discussing the experimental evaluation of the effectiveness of the proposed compensation method in healthy subjects. The consecutive chapter presents an article discussing the design and evaluation of the adjustable constant force mechanism. The fifth chapter addresses the implementation of the results from the previous two chapter in a prototype of a wrist support. Finally, the outcomes of this thesis will be discussed, conclusions drawn and recommendations for future research given.

Duchenne Muscular Dystrophy

Muscle weakness or limited muscle control can have a serious impact on people's lives. This limited muscle functioning can have various causes such as a stroke, injury or diseases such as muscular dystrophies. There are multiple types of muscular dystrophies each being caused by a mutation in one of the genes responsible for the muscle functioning [1–3]. Of these muscular dystrophies Duchenne Muscular Dystrophy (DMD) is the most common, occurring in approximately 1 in 5000 male births [1–3, 14]. DMD is an inheritable disease caused by a mutation in the gene coding for the protein dystrophin, which lays on the X-chromosome. Being a recessive mutation, it follows X-linked recessive inheritance. Because of this, the disease almost exclusively occurs in boys. However, around 10% of the female carriers of the mutation do show some form of muscle weakness [3, 15]. Although the disease is known to be inheritable, in up to one-third of the patients it is caused by a new mutation [15, 16].

1.1. Disease progression

DMD is a progressive disease, affecting the large muscle groups at first more than the smaller groups. An overview of the disease progression is depicted in Fig. 1.1. The first symptoms, such as walking difficulties, become generally visible around the age of 2-3 years [17]. Furthermore, around the age of 10-14 most boys are wheelchair bound [18]. In the following years loss of function becomes also more apparent in the upper limbs. Additionally, since the breathing muscles are affected, breathing support is generally required around the age of 20 [19]. Not only the skeletal muscles are affected but also respiratory, cardiac and skeletal problems can occur directly or indirectly as a result of DMD [20]. However, due to improvements in treatment the median age of death has increased over the years [21]. In literature, median life expectancies of 28 up to 40 are being reported [22–24], where the cause of death is commonly due to heart or lung failure [23, 24].

1.2. Microbiological Manifestation

The deficiency or malformation of dystrophin has various consequences for the muscle cells, contributing to their progressive weakening. First of all, the muscle cells are less capable of supporting mechanical stresses, making them more susceptible to damage when contracting. Furthermore, in healthy people exercise will increase the blood perfusion of the muscles. However, this increase in blood flow is limited in DMD patients, potentially damaging the muscles due to a lack of oxygen. Besides that the muscles become damaged more easily, their regenerative potential is also limited [15]. As not all damaged muscle fibres are repaired, they can become necrotic and induce an inflammatory response, which increases the formation of fatty and fibrotic tissue, replacing the damaged muscle tissue [25]. An additional consequence of this build-up of fatty and fibrotic tissue is that the muscles can generate less force. Additionally, due to the increased joint impedance, more force must be exerted by these muscles to enable motion [26–28]. Dystrophin not only is important for the skeletal muscle functioning, but it also plays a role in the function of other tissues. Consequently, the manifestation of the disease is not solely in the skeletal muscles. For instance, it has been found that the prevalence of mental disorders is higher within DMD patients compared with the general population [29], while cardiomyopathy (disease of the heart muscle) occurs in almost all patients by the age of 18 [1].

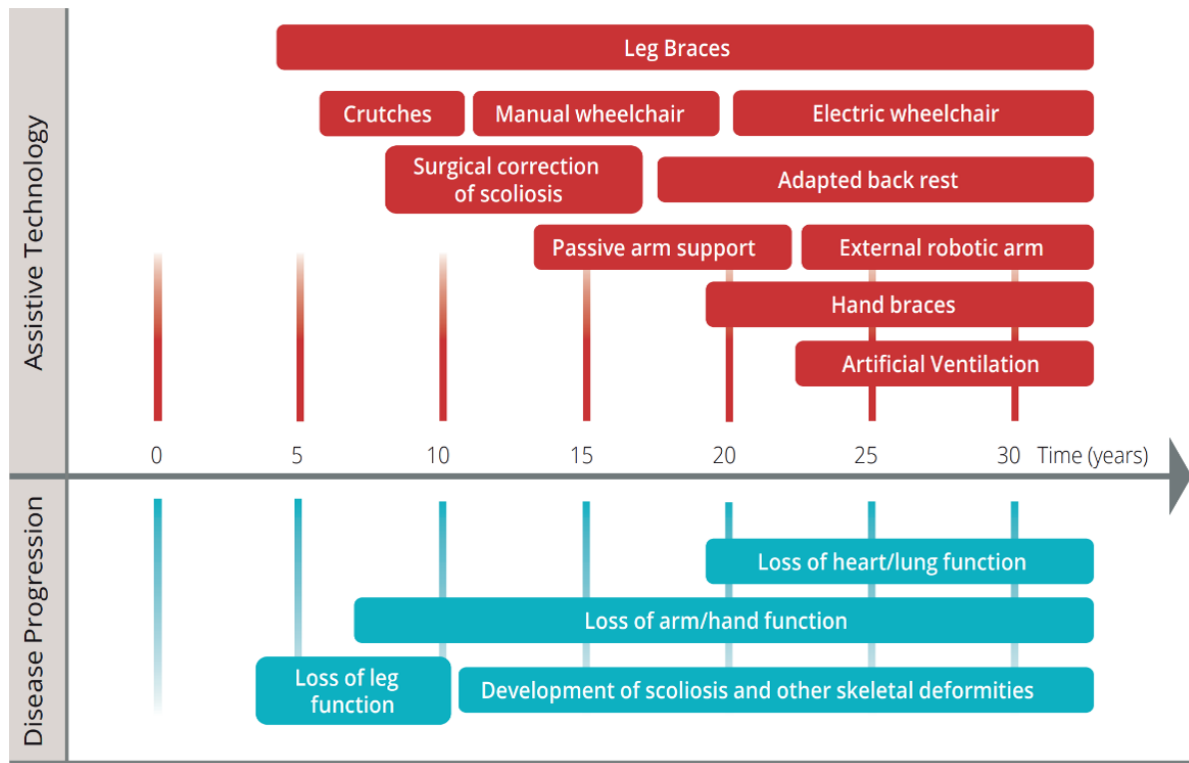


Figure 1.1: Disease progression and dependence on assistive devices for Duchenne Muscular Dystrophy patients. Retrieved from [4, 5]

1.3. Classification

The progression of DMD can be divided in different stages based on the remaining functional abilities of the patients. An example of such a division, which focusses on the upper extremity function, is the Brooke scale. This scale ranges from 1 to 6, where 1 is the least and 6 is the most severe (Table 1.1). Other scales such as the Vignos scale focus more on lower extremity function [30]. When focussing specifically on the wrist a decline in wrist function starts to become apparent around a Brooke scale of 3 [27] as the available joint torques become insufficient as considered required for all activities of daily living [31].

1.4. Arm function in Duchenne Muscular Dystrophy

As previously discussed, the upper extremity function decreases over time in DMD patients. The median age of the onset of Brooke scale 2 is found to be around the age of 11 years [32]. Thus, the arm

Table 1.1: Description of the various stages of the Brooke scale [30]

Brooke scale	Description
1	Starting with arms at the sides, the patient can abduct the arms in a full circle until they touch above the head
2	Can raise arms above head only by flexing the elbow or using accessory muscles
3	Cannot raise hands above head, but can raise a 200 ml glass of water to the mouth
4	Can raise hands to the mouth, but cannot raise a 200 ml glass of water to the mouth
5	Cannot raise hands to the mouth, but can use hands to hold a pen or pick up pennies from the table
6	Cannot raise hands to the mouth and has no useful function of hands

function is often already affected before the patients start using a wheelchair. However the disease progression can strongly differ between patients. Patients having a Brooke scale of 2, generally only feel a limited increase in joint impedance in the arms, however as of a Brooke scale of 3 severe joint impedance is observed [32]. This increase in stiffness as the disease progresses, is also found by Cornu et al. who measured the stiffness around the elbow joint [26]. This increased joint impedance is partially caused by the increased stiffness of the muscles themselves. For instance, Lacourpaille et al. found a significantly higher shear modulus in the biceps brachii and triceps brachii in DMD patients [33, 34]. Furthermore, muscle activation in DMD patients is closer to their maximal contraction level, indicating that the remaining functional muscles are put to more stress [35, 36]. This increase in joint impedance and decrease in strength decreases the range of movement. Additionally, the formation of contractures results in a further decrease. After the age of 13, contractures in the elbow and wrist are very common [37]. This increase in contracture incidence in these joints is related to the longer periods of inactivity of the limbs [37]. This was also observed by Janssen et al. where the maximum active and passive joint angles declined almost simultaneously with the disease progression. They attribute this to the decrease of active joint movement which cause the joint to be statically positioned for a longer duration of time, thus increasing the formation of contractures [27]. Additionally, a low level of physical activity in general results in a faster decline in functionality (e.g., the difference in performs between the dominant and non-dominant hand increases with increasing age in DMD patients) [38, 39].

When focussing on the wrist it has been found that the active range of motion is considerably lower in DMD patients with Brooke 3 or higher. Janssen et al. found for instance a decrease by almost a half in maximal active joint angle of wrist extension. However, due to the small sample size it could not be regarded as a significant difference [27]. Furthermore, they observed that patients with Brooke 3> were not able to generate enough torque to perform all activities of daily living (ADL) when performing wrist flexion or extension. Additionally, Wagner et al. observed that most subjects older than 14 years (Brooke 3 and higher) had difficulty extending their wrist through a full range of motion against gravity [40].

1.5. Treatment

Currently there is no cure for the disease. So, the available treatments focus on minimising the disease progression and maintaining a certain quality of life. A commonly used treatment is the use of corticosteroids [18], which by suppressing the inflammatory responses delays the disease progression [25]. Next to corticosteroids, several therapeutics are being investigated in DMD patients which for instance attempt to delay disease progression [41]. Other examples of treatments are providing ventilation support [42] or physical therapy [43, 44]. A more extensive overview of the management of DMD is provided by Birnkrant et al. [44–46]. However, once a function is lost, it cannot in general be retrieved. This is especially clear when looking at patients with Brooke scale of 3 or 4. Although they can still move their arms and hands, their range of movement is limited [27]. Furthermore, because of the limited movement as well as the replacement of muscle tissue by fibrotic and fatty tissue the risk of the formation of contractures is increased (decrease of passive range of motion), further decreasing their mobility. This development of contractures occurs especially after the patient has become wheelchair bound [37, 47].

As the disease progresses DMD patients become more dependent on assistive devices for their daily activities (Fig. 1.1). For instance, to improve or maintain the functionality of the arms and hands and to prevent the onset of contractures, external supports or exoskeletons can be used. Examples of such systems available on the market are the SeaboMas [48] and the devices developed by Armon [49], which aim to compensate the weight of the arm, decreasing the required effort to move the arm. Additionally, a considerable amount of effort was and is being put in the development of new devices. For instance, within the Wearable Robotics project [9] an exoskeleton is being developed specifically for DMD patients. However, these (commercial) devices primarily focus on supporting the arm, whereas these patients will also likely benefit from some support of the hand. As such, in recent years the development of such a support for the hand has gained interest [5, 7, 50]. However, several challenges still remain, such as compensating the weight of the hand, which will be further discussed in the next chapter.

2

Simplified balancing

To be able to compensate the weight of the hand, knowledge is required about its potential energy or the joint torques generated by gravity. To this end, a model has been developed of the arm. However, to be able to properly model the arm, information is needed about the biomechanics of the arm. Accordingly, a brief discussion will be given on the arm biomechanics followed by the description of the model and its simplifications. Based on this model various methods to compensate the weight of the hand will be discussed.

2.1. Biomechanics of the arm

Each arm consists of three distinct joints, namely the shoulder, elbow and wrist with a total of seven degrees of freedom (DOFs): three at the shoulder joint (Glenohumeral joint, spherical joint: flexion-extension, abduction-adduction, endo- and exorotation of upper arm), one at the elbow (Revolute joint: flexion-extension lower arm), two at the wrist (Universal joint: palmar-dorsal flexion, radial-ulnar deviation of the hand) and one distributed between the elbow and the wrist (Revolute joint: pronation-supination of the lower arm) [51–54]. Next to the joints in the arms themselves, the joints in the pectoral girdle also play a role in arm movement. These are the acromioclavicular joint (between the collarbone and shoulder blade) and the sternoclavicular joint (between the breastbone and the collarbone). These joints enable circumduction and elevation-depression of the shoulders [51], adding an additional two degrees of freedom [55].

Although the wrist joint is often considered as a universal joint, it is a complex joint involving the interaction of multiple bones. The palmar-dorsal flexion and ulnar-radial deviation of the wrist are enabled by a combination of two joints, the radiocarpal joint and the midcarpal joint (Fig. 2.1) [54, 56]. The radiocarpal joint, commonly referred to as the wrist joint, is the joint formed by the radius and three of the proximal carpals (scaphoid, lunate and triquetrum). The midcarpal joint is formed by the proximal carpals (scaphoid, lunate and triquetrum) and the distal carpals (trapezium, trapezoid, capitate and hamate). Next to this, some sliding movement between the different carpals is possible. However, this has a limited contribution to the movement of the wrist [54, 56, 57]. Because of this structure, the wrist has a large range of motion. The wrist can normally palmar flex up to 70-80 degrees, dorsal flex up to 60-75 degrees, radial deviate up to 30-35 degrees and ulnar deviate up to 15-20 degrees [31, 54]. However, in the case of diseases affecting the muscle strength and/or joint impedance these ranges of motion can be greatly decreased [27].

In modelling of the wrist, the two movements are generally simplified as a rotation around a single point. However, the axes of rotation for palmar-dorsal flexion and ulnar-radial deviation do not intersect [58, 59]. This offset between the two axes is important to consider when designing exoskeletons to prevent joint misalignment during motion, to avoid excessive forces on the wrist. However, as in this work only the assistance of palmar-dorsal flexion is considered, the offset between the axes of rotation is not yet an issue.

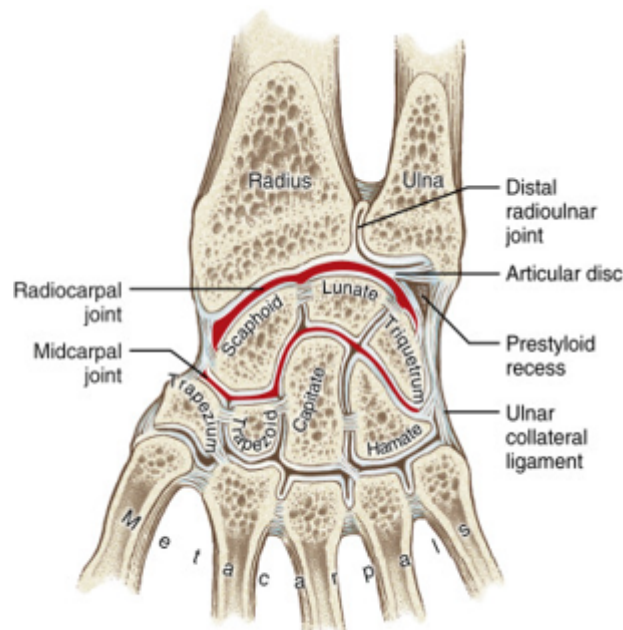


Figure 2.1: Bones and joints of the hand forming the wrist. Retrieved from [56]

2.2. Modelling of the arm

Based on the previous discussion the hand can be considered as being located at the end of a 7 DOF kinematic chain (ignoring the DOFs from the pectoral girdle). Subsequently, the hand can be moved almost freely through space, making the balancing of its weight around the wrist joint challenging, as the required balancing forces are dependent on the orientation of the arm. So, to determine the required balancing forces a model is constructed to describe the motion of the hand through space.

The model is made of the right arm with respect to the anatomical position, with the z-axis pointing upward, x-axis forward and y-axis to the left. The shoulder is modelled as having three degrees of freedom (endo-exorotation, abduction-adduction and flexion-extension). To describe the rotations around the shoulder a set of Euler angles can be used. For this, different orders of rotations are possible. However, here the order *zyx* is used in accordance to the rotation axes of an arm exoskeleton developed at the TU Delft. The elbow is modelled as a hinge joint around the local y-axis to describe flexion-extension of the elbow. The pronation-supination of the hand is caused by a combined movement at the elbow and wrist. However, as we are only interested in the orientation of the hand the pronation-supination motion is simplified to occur at the wrist. Consequently, the wrist is modelled as a spherical joint, following the same order of rotations as the shoulder (e.g., pronation-supination, palmar-dorsal flexion and radial-ulnar deviation). Two example positions of the arm are depicted in Fig. 2.2.

As the design of the wrist support is focussed on assisting with palmar-dorsal flexion the model can be simplified by constraining the radial-ulnar deviation of the hand. To be able to balance a mass, either the potential energy or the generated joint torque has to be known. So, based on the model an expression is sought for the gravitational potential energy.

According to Euler, a rotation in space can be described by three consecutive rotations around the coordinate systems axes. Thus, it should be possible to describe the orientation of the wrist by three rotations plus one additional rotation to describe the rotation of the hand around the wrist (e.g., the arm has some redundant DOFs). For this, different orders of Euler angles can be used, which result in equations for the potential energy of varying complexity. Thus, using Euler angles the position of the hand in space depends on 4 DOFs and therefore its potential energy can be expressed using

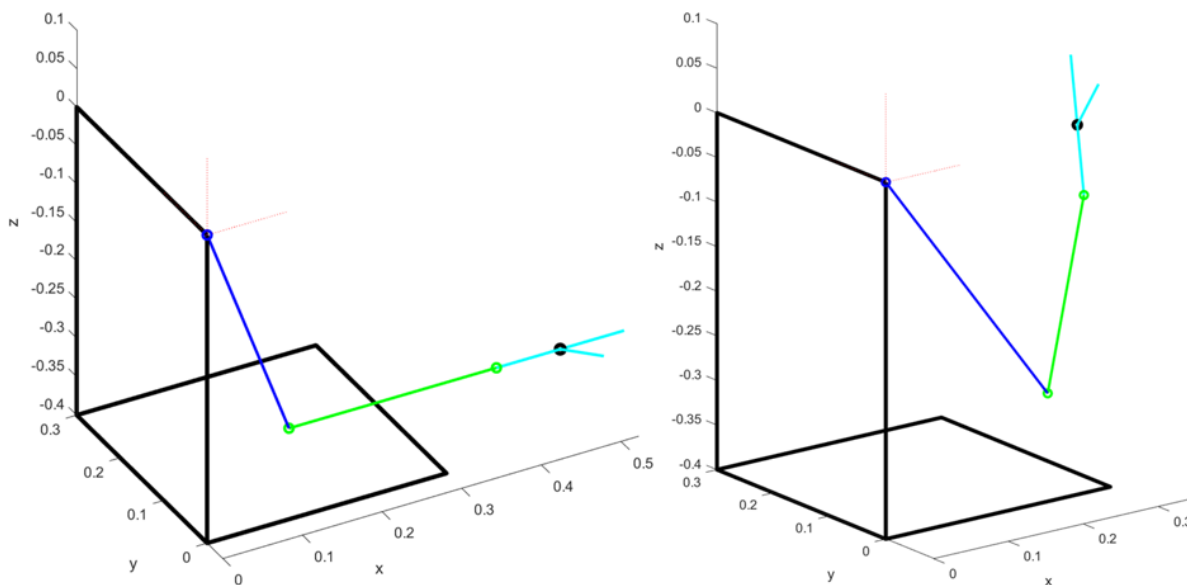


Figure 2.2: Arm model in two different orientations. Upper arm (blue line), forearm (green line), hand and thumb (cyan) and hand centre of mass (black dot). Left image 20° shoulder flexion and 70° elbow flexion. Right image 30° endorotation, 20° shoulder flexion, 30° abduction, 110° elbow flexion and 20° palmar flexion (movement occurred in this order)

four angles. The first three define the orientation of the wrist and the fourth the level of dorsal-palmar flexion of the hand. Based on this assumption a relatively simple expression can be found using a zxy order of rotations, which physically correspond to endo- exorotation (δ), abduction-adduction (ψ) of the shoulder, elbow flexion-extension (θ) and palmar-dorsal flexion (ϕ). Note that in the case of shoulder flexion-extension and pronation-supination of the forearm the physical meaning of these angles no longer holds. However, the model still applies.

$$V = -mgL \cos(\theta + \phi) \cos \psi \quad (2.1)$$

In this expression the angles are defined with respect to the anatomical position. Note that the potential energy is independent of the angle δ as a change of this angle does not result in a change in height of the hand. However, as the intended use of the wrist support is for wheelchair bound people a change of reference is more convenient (e.g., with respect to the hand lying on a desk). Therefore, the reference position is now taken at 90° elbow flexion with the hand in a pronated position. Due to this change of reference and coordinate system the potential energy is now given by

$$V = mgL \sin(\theta + \phi) \cos \psi \quad (2.2)$$

Where the angles are defined according to Fig. 2.3. Furthermore, the joint torques generated by gravity can be expressed as

$$T = mgL \cos(\theta + \phi) \cos \psi \quad (2.3)$$

Based on the use case of the Wearable Robotics integration project wrist support, some constraints can be placed on these angles. The minimum range of motion (ROM) for palmar flexion and dorsal flexion are respectively 50 and 25°. Thus, the angle ϕ ranges from -50 to 25°. For pronation-supination the minimum ROM is 80 and 50°, which approximately relates to ψ between 10 and 140° when θ is zero. However, as ψ also includes some abduction-adduction of the shoulder this range will be somewhat larger. Based on studies investigating the required ROM for common movements [60, 61], such as drinking from a glass, a rough estimate is made of the required θ , which is taken as -10 till 100° (considering the fact that the support is focused on DMD patients). Although, this involves a relatively large workspace, not all combinations of angles are performed in daily living. Additionally, the arm will predominantly be held in only a few specific orientations for longer periods of time (e.g. arms positioned as in working behind a desk). Consequently, not all orientations are of equal importance to consider for the wrist support.

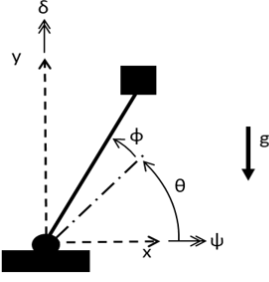


Figure 2.3: Model of the wrist/balancer, defining the used coordinate system

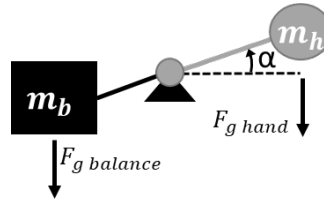


Figure 2.4: Example of a gravity balancer using a balance mass, which generates a sinusoidal torque profile around the joint as a function of α . Thus, compensating the gravity torques from the other mass.

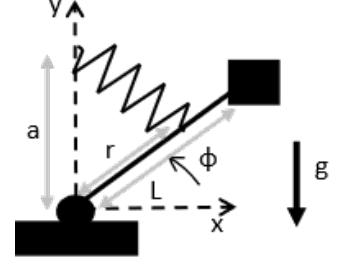


Figure 2.5: Example of a 1 DOF gravity balancer using a zero-free length spring

2.3. Balancing a mass

A mass can be balanced actively using actuators or passively using for instance a counterweight. Some of the drawbacks of using active balancing is its energy expenditure and the required control, which can become complex, especially when interaction with humans occurs (as with exoskeletons). On the contrary, passive balancing requires essentially no external energy and no control and possesses less safety risks. However, passive balancing is less flexible, as it has to be designed for each specific case. Nonetheless, because of its advantages passive balancing, more specifically passive gravity compensation, will be investigated for implementation in a wrist support.

Passive gravity compensation is a topic of interest in different fields, such as exoskeletons and robotics, as it decreases among others the requirements on actuators [62, 63]. Passive gravity compensation can be considered as a form of static balancing, which relies on keeping the potential energy constant throughout (a part) of the movement range [64]. This is generally achieved using springs or counterweights. Using a counterweight is perhaps the easiest method of balancing a mass (Fig. 2.4), examples of this can be found in bridge design, elevators, and robotics [62]. However, the use of counterweights is not always favourable due to its mass and required space. Springs on the contrary are in general lighter and take up less space. However, they have their drawbacks too, as it can be challenging to obtain the required spring characteristics.

2.3.1. 1 DOF balancer

An example of balancing a 1 DOF pendulum using a spring is depicted in Fig. 2.5. For this system the total potential energy is given by

$$V = mgL \sin \phi + \frac{1}{2}ku^2 \quad (2.4)$$

Here k is the spring stiffness, m the mass of the pendulum, L the arm length of the pendulum and g the gravitational acceleration. Furthermore, the elongation of the spring u is given by $u^2 = a^2 + r^2 - 2ar \sin \phi$, where r is the arm length of the spring and a the vertical offset of the spring. Accordingly, the total potential energy can be expressed as

$$V = mgL \sin \phi - kar \sin \phi + \frac{k}{2}(r^2 + a^2) \quad (2.5)$$

For the potential energy to be constant throughout its range motion, to compensate the weight, its derivative with respect to ϕ must equal zero throughout its range of motion.

$$\frac{\partial V}{\partial \phi} = mgL \cos \phi - kar \cos \phi = 0 \quad (2.6)$$

As this equality should hold for any value of ϕ the spring stiffness must be equal to $k = \frac{mgL}{ar}$. This methodology can be extended to balancing of mechanisms with more DOFs [64–67].

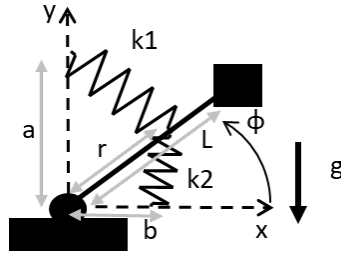


Figure 2.6: Balancer using two springs

2.3.2. Orientation independent balancer

When the orientation of the reference frame is changed, as is the case in the wrist model, balancing becomes considerably more difficult as it involves a phase shift and change of magnitude of the required balancing torque and potential energy (Equation 2.2 and 2.3). Changing the magnitude of the output force or torque is something investigated readily in literature and can be achieved by for instance changing the properties of the spring or its lever arm [68–71]. However, adjusting the phase is more challenging. A possible solution is to balance the entire kinematic chain the wrist belongs to (e.g., shoulder and elbow). When only considering motion in one plane, balancing can be achieved as proposed by for instance Agrawal and Agrawal [66]. Furthermore, when looking at 3D-motion, only examples can be found of balancers balancing across the shoulder and elbow joint [72, 73]. However, the size and the pronation-supination degree of freedom limits the extension of these mechanisms to the wrist. Two possible methods to solve this issue which will be considered next, are using a form of approximate balancing and using two parallel springs with adjustable stiffness.

Parallel springs Using trigonometric identities, the equation of the potential energy (equation 2.2) can be rewritten as

$$V = mgL \cos \theta \cos \psi \sin \phi + mgL \sin \theta \cos \psi \cos \phi \quad (2.7)$$

Considering the angles θ and ψ to be constant, the first term behaves similar as in the example of the 1 DOF balancer and can thus be balanced in the same way. Considering the second term, this as well can be balanced using a spring, resulting in the configuration as depicted in Fig. 2.6. To compensate the weight the required spring stiffness can now be expressed as

$$k_1 = \frac{mgL \cos \theta \cos \psi}{ar} \quad (2.8)$$

$$k_2 = \frac{mgL \sin \theta \cos \psi}{br} \quad (2.9)$$

Here to some extent similar methods can be used as described by van Dorsser et al. [68–71] to ensure equilibrium. Thus, either the coordinates of the spring must be changed (a and b or r) or its stiffness. However, these methods will only work for a certain range of θ and ψ as otherwise a change in sign has to occur of either the stiffness (negative stiffness) or spring coordinates, introducing additional difficulties. Although it is something of interest for further investigation it will not be considered any further here.

Approximate balancing Instead of perfect balancing, requiring a complex torque profile (Equation 2.3), it is of interest to look at more simplified balancing methods. Although the required effort by the user or system to move the mass around is no longer zero (theoretically), a reduction in movement effort can still be achieved throughout at least a part of the range of motion. Once again, the torques required for perfect balancing are given by the following equation of which some examples of the required balancing torques are illustrated in Fig. 2.7.

$$T = mgL \cos(\theta + \phi) \cos \psi \quad (2.10)$$

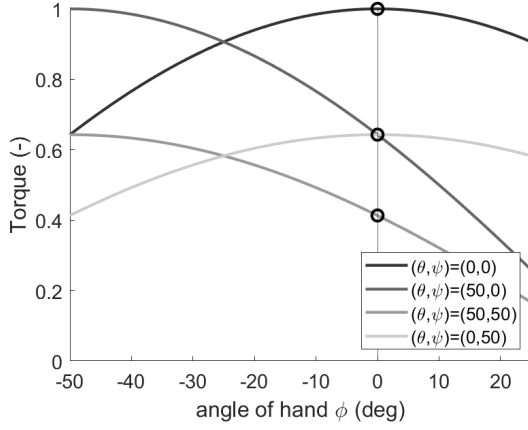


Figure 2.7: Torque profiles for different levels of θ and ψ . The circles indicate the required level of constant torque according to Equation 2.12. Note that for $(\theta, \psi) = (0, 50)$ and $(\theta, \psi) = (50, 0)$ require the same level of constant torque

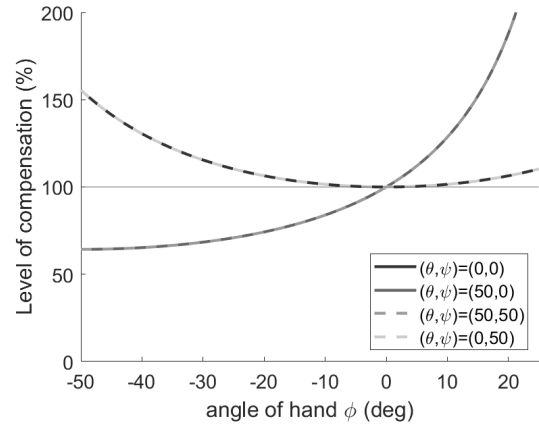


Figure 2.8: Level of compensation using a constant torque throughout the range of motion of the wrist for different levels of θ and ψ . Here 100% is considered as complete compensation, values larger than 100% overcompensation and lower than 100% undercompensation. Note that the level of compensation for different levels of ψ overlap.

By performing a Taylor expansion around the neutral wrist position $\phi=0$ the required balancing torque can be expressed as

$$T \approx mgL \cos \theta \cos \psi - mgL \sin \theta \cos \psi + \mathcal{O}(\phi^2) \quad (2.11)$$

This linear torque profile is equivalent to a prestressed spring ($T = k(\phi - \phi_0)$, with $k = -mgL \sin \theta \cos \psi$ and $\phi_0 = \frac{-1}{\tan \theta}$). Thus, an adjustment of the (effective) stiffness and its offset (ϕ_0) is required to ensure the balancing. Although there are several solutions available for the adjustment of stiffness [74–76], only a few are capable of adjusting their stiffness between positive and negative values [77, 78]. These mechanisms consist of a positive and negative stiffness element arranged in parallel of which the stiffness of one of these elements is adjusted. Although being of interest for further investigation, because of their complexity, an even simpler solution is sought. Consequently, considering only the first term of the Taylor expansion of the balancing torques, results in a constant force of which the magnitude depends only on the orientation of the mechanism/forearm. Accordingly, the balancing torque is given by

$$T \approx mgL \cos \theta \cos \psi \quad (2.12)$$

As constant force mechanisms find their application in numerous areas a considerable amount of effort has been put in literature in the development of such mechanisms [11]. Therefore, using a constant force seems like a good starting point for the development of a wrist support (Chapter 4). However, as the balancing potential of a constant torque is lower than of a sinusoidal torque (Fig. 2.8) the effectiveness of using a constant torque (as well as a linear torque) must be assessed (Chapter 3).

Conclusion

Based on an arm model a model was developed for the required torques to compensate the weight of the hand. Because of the complex control involved with an active support it was decided to use a (semi-) passive support. However, due to the complexity of the torque profile (e.g., dependence on several DOFs) an expression for an approximate balancing profile was derived, resulting in a constant torque profile of which the magnitude depends on the forearm orientation only.

3

The effectiveness of different torque profiles for gravity compensation of the hand

The effectiveness of different torque profiles for gravity compensation of the hand

B.J. van der Burgh^{1,2}, S.J. Filius¹, G. Radaelli² and J. Harlaar^{1,3*}

¹Department of Biomechanical Engineering, Delft University of Technology, Delft, The Netherlands. ²Department of Precision and Micro Engineering, Delft University of Technology, Delft, The Netherlands. ³Department of Orthopedics & Sports Medicine, Erasmus Medical Center, Rotterdam, The Netherlands.

*Corresponding author. E-mail: J.Harlaar@tudelft.nl

Keywords: Gravity compensation; wrist support; sEMG; constant torque

Abstract

People with muscular weakness might profit from a wrist support to compensate the weight of the hand. For the development of a novel type of passive mechanical wrist support the effectiveness of different compensation strategies was evaluated. Three different compensation strategies (applying a constant, linear or sinusoidal torque profile as a function of the wrist flexion angle) were compared to no support by assessment of the magnitude of the muscle activity through sEMG of the wrist flexors and extensors in different forearm and wrist positions. Based on the experiment with 8 healthy subjects it can be concluded that overall, there is a significant reduction of 47% up to 53% ($p < .001$) in the activity of the anti-gravity muscles (extensor muscle) in all used compensation strategies compared to no compensation, while there is no significant difference between the different compensation strategies. However, in all used compensation methods a significant increase of 44% up to 61% ($p = .005$) in flexor muscle activity is observed for large levels of palmar flexion. Indicating a possible limitation of the current compensation methods. Nonetheless, compared to the theoretically ideal sinusoidal profile, for a gravity compensating wrist support the simpler constant or linear torque profiles can be considered as effective alternatives.

1. Introduction

Muscular disorders can have a severe impact on people's lives. An example of such a disorder is Duchenne Muscular Dystrophy, a genetic disorder resulting in a progressive loss of muscle strength [1]. Due to the decreased muscle strength, the active range of motion (ROM) of the arms is reduced [2]. However, by compensating the weight of the upper extremities some ROM can be regained, for instance with a wrist support. Theoretically this requires a sinusoidal torque profile of which the magnitude and phase depend on the hand and forearm orientation (Supplementary material A). However, as the forearm can be moved in 3D space, compensating the weight of the hand over the wrist is challenging. This is because the wrist torques depend both on the position of the hand relative to the forearm and on the orientation in space of the forearm itself. As such, it is of interest to look at simplified torque profiles.

In literature, only a few examples can be found on studies showing the effect of wrist supports to compensate the weight of the hand. For instance, Hasegawa et al. designed a wrist support using a counterweight, which can generate a sinusoidal torque profile. With this they observed a considerable decrease in muscle activity [3]. Das et al. made use of pneumatic artificial muscles to construct a glove to assist with wrist movement. Using this glove they observed a decrease in the required muscle effort to move the hand [4]. Other examples are given by Gopura and Kiguchi [5, 6]. In these four studies, the evaluation was only performed with very few subjects ($n=1$, $n=2$, $n=3$ and $n=1$ respectively) consequently without statistical analysis. Additionally, no articles considered the use of simplified torque

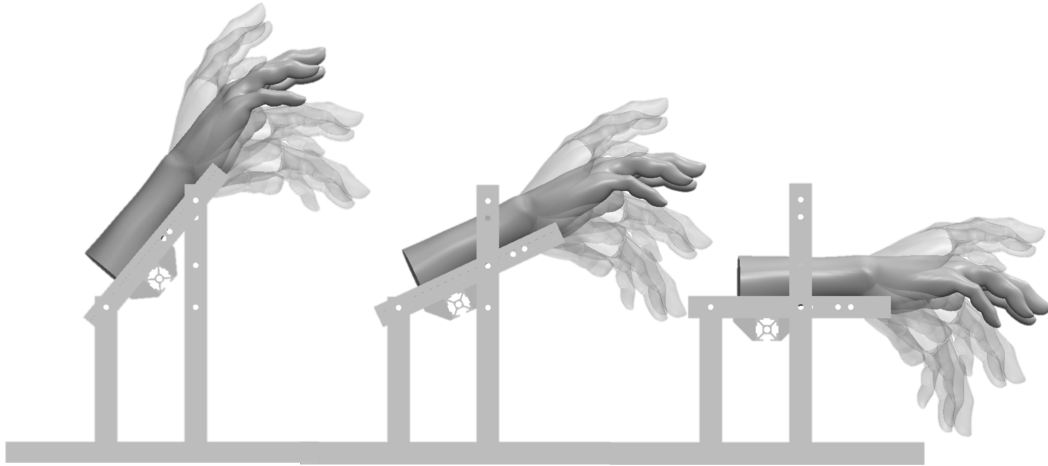


Figure 1. Schematic of the different positions of the forearm and hand. From left to right the forearm is positioned at 50, 25 and 0° with respect to the horizontal. Additionally, the hand can be positioned at 25° dorsal flexion (-25°), neutral (0°), 25° palmar flexion (25°) and 50° palmar flexion (50°) indicated by the transparent hands. Hand model adapted from [7].

profiles or the different orientations of the forearm. Therefore, a more rigorous evaluation of the use of a wrist support to compensate the weight of the hand is required. As such, the goal of this research is to assess the effectiveness of gravity compensation using simplified torque profiles to compensate the weight of the hand. More specifically, does a constant torque with respect to the palmar-dorsal flexion of the wrist (the simplest approximation of the sinusoidal torque profile) result in a similar decrease of the anti-gravity muscle effort as the theoretically ideal profile?

2. Method

2.1. Participants

For this study, healthy subjects were recruited from a university student population, with no history of injuries to the right wrist. Ethical approval was obtained from the Human Research Ethics Committee (HREC) from the Delft University of Technology. All participants gave written informed consent.

2.2. Experiment design

With the experiment the influence of three different factors on the muscle activity of the wrist flexor and extensor muscles based on the magnitude of the surface electromyograms (sEMG) are considered.

- The orientation of the forearm can be adjusted between 0, 25 and 50° with respect to the horizontal to simulate the effect of different levels of gravity loads (Fig. 1).
- The static position of the wrist at 25° dorsal flexion, 0°, 25° and 50° palmar flexion, with the hand in a pronated position. During each measurement all four orientations are assessed, by holding the hand in the specified position for 10 seconds, after which the hand is moved to the next position.
- The type of compensation method, involving no support, a constant, a linear, or a sinusoidal torque profile. The characteristics of these profiles depend on the biometric properties of the subject's hand in combination with the forearm orientation (Fig. 2). For the forearm orientation of 0° the linear torque profile is not considered as it behaves as a constant torque.

Both the order of the wrist positions as well as the compensation method are randomised as movement direction can affect muscle activity [8] (Supplementary material C). Additionally, the orientation of the fingers is kept constant by letting the subjects slightly hold a foam tube in their hand.

Additionally, Maximum Voluntary Contraction (MVC), Relative Voluntary Contraction (RVC) and rest measurements were performed to allow between and within subject comparison.

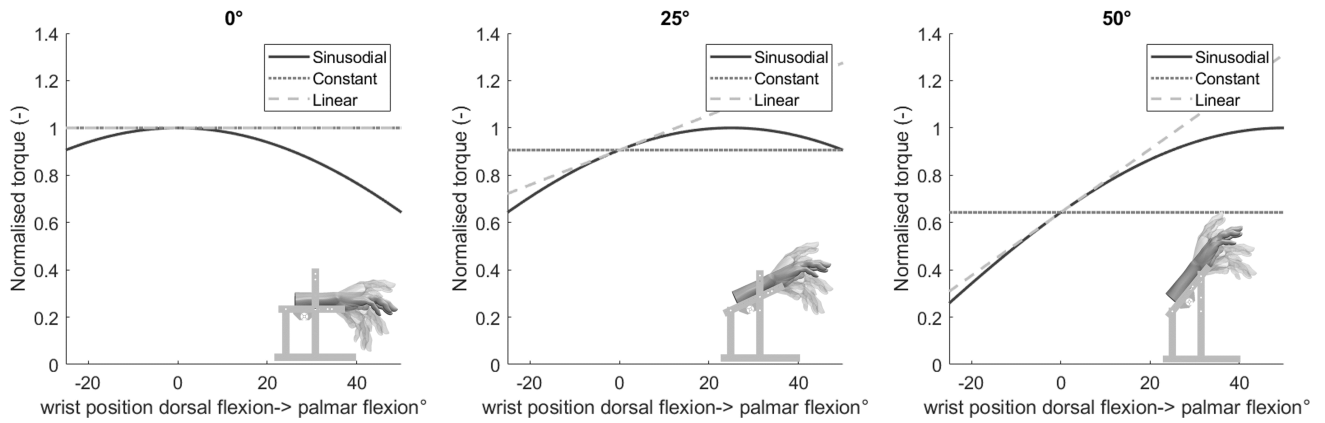


Figure 2. Torque profiles as a ratio of the maximum sinusoidal torque for the three different forearm orientations. Note that the constant torque is only constant with respect to the wrist flexion angle, while it is different for every forearm orientation.

2.3. Biometric data collection

To determine the required level of compensation, the weight and centre of mass of the participant's hand must be determined. The weight of the hand is evaluated by the mean outcome of two methods. 1.) Determining the volume of the hand by submerging the hand in a bucket of water and multiplying the displaced volume with an average density from literature [9]. 2.) Using the predictive equation proposed by Clauser et al. based on the dimensions of the hand [10]. The centre of mass is also determined using the predictive equations from Clauser et al. [10] as well as based on an adaptation of the equations from Chandler et al. [9] to adjust for the flexed position of the fingers.

2.4. Equipment

For the experiment a setup was developed which can fixate the forearm in different orientations and can provide different torque profiles to the wrist (Fig. 3). The constant torque profile is generated through a mass hanging from a pulley over a constant lever arm (Fig. 4). By combining from a set of six masses the desired torque can be approximated within an error of less than 3%. The linear profile is generated by combining the constant torque with a spring. By using different types of springs, the slope of the torque can be adjusted. For this, a choice is made between four different springs to approximate the desired stiffness (0.15, 0.19, 0.25 and 0.47 N/mm). The sinusoidal profile is generated by attaching a weight to a rigid rod. By varying the distance of the weight with respect to the hinge of the rod the magnitude of the profile can be adjusted (Fig. 4). This value can be adjusted continuously.

The EMG recordings were made using a Bagnoli™ EMG system with DE-2.1 Single Differential Surface EMG sensors from Delsys®, consisting of an 8-channel amplifier with an output voltage range of +/- 5 V (System noise (R.T.I) < $1.2\mu V_{rms}$). The amplifier gain was set separately for each participant to 1k or 10k depending on the signal strength, amount of powerline interference and the occurrence of amplifier saturation. The analog signal was sampled with a frequency of 2000 Hz with a 16-bit (+/- 10 V) ADC 4ch NI® 9215 with BNC (Input noise $3.7mV_{rms}$) and NI LabVIEW™ 2018. The discretized signal was stored on a computer for offline processing with MATLAB® R2021a and IBM SPSS® Statistic 28.

2.5. Sensor placement

EMG electrode placement is performed based on the recommendations from [8, 11] on the palpated muscle bellies of the extensor carpi radialis (ECR) and the flexor carpi radialis (FCR). The reference electrode is placed on the lateral epicondyle of the humerus. For skin preparation recommendations from Delsys® were followed (shaving and rubbing the skin with alcohol).

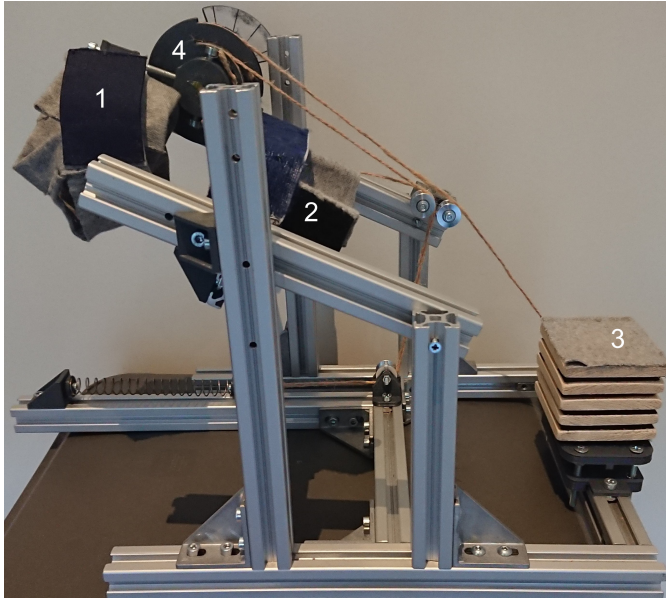


Figure 3. Overview of the setup. 1) Hand interface 2) Forearm interface 3) Elbow support 4) Transmission pulley for application of the different torque profiles.

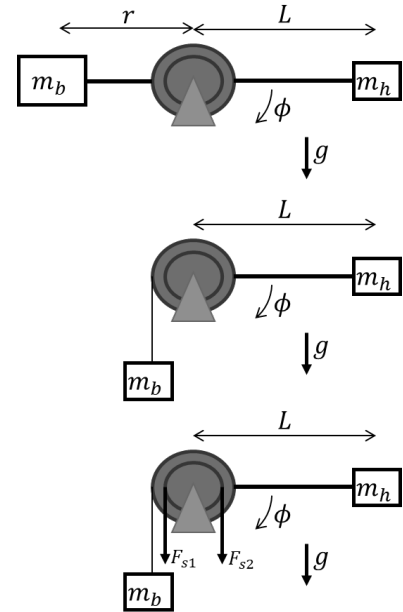


Figure 4. Schematic of the application of the sinusoidal (top), constant (middle) and linear (bottom) torque profiles to the hand. Here m_b and m_h are the balance mass and the mass of the hand respectively and F_s the force exerted by the spring.

2.6. Data acquisition and processing

For comparison of the compensation methods the mean magnitude of the sEMG envelope of the ECR and FCR muscles is used as a measure of the muscle activity required to hold the hand in place.

During each experiment all three experimental factors are assessed (forearm position, balancing method and wrist position) resulting in 44 measurements of 10 seconds. Additionally, all measurements are repeated three times. The MVC is defined as the maximum filtered EMG magnitude for each muscle from three MVC tasks of 3 seconds followed by 12 seconds rest. The two MVCs are performed by maximally flexing or extending the hand against a rigid surface with a straight wrist in a pronated position. During the MVC the participants are encouraged by the experimenter. For additional comparison a RVC measurement is performed following the protocol from Mathiassen et al. [8, 12] and a rest measurement by laying the forearm and hand relaxed on a table.

The digitized EMG-signal is filtered with a 2nd-order IIR Notch filter at 50 Hz to remove powerline interference, followed by a 6th order bandpass Butterworth filter with cut-off frequencies of 20 and 450 Hz [13]. The signal is then rectified by taking its absolute value. Finally, the signal envelope is determined through 3rd order lowpass Butterworth filtering of the signal with a cut-off frequency of 2 Hz. A low cut-off frequency is chosen to determine the envelope as the study involves quasistatic measurements [14]. As output measure the mean magnitude of the middle 5.5 s of the sEMG envelope of the three repetitions is used, expressed relative to the MVC [15, 16].

2.7. Statistics

For statistical analysis, a repeated measures analysis of variance (ANOVA) is performed on the outcome measures to assess the effects of the forearm orientation, wrist position and balancing method and their interactions on the EMG activity of the ECR and FCR muscles. Following the ANOVA, the results are analysed using a multiple comparison with Bonferroni adjustment [17]. P-values $< .05$ are interpreted as significant. Data is reported as mean \pm SD.

Table 1. Participant characteristics, reported as mean and standard deviation.

	Age (years)	Weight (kg)	Height (m)	Hand weight (g)	Centre of mass (mm)
N=8	24.4 ± 0.7	71.0 ± 1.7	1.78 ± 0.11	386 ± 61	44.9 ± 3.5

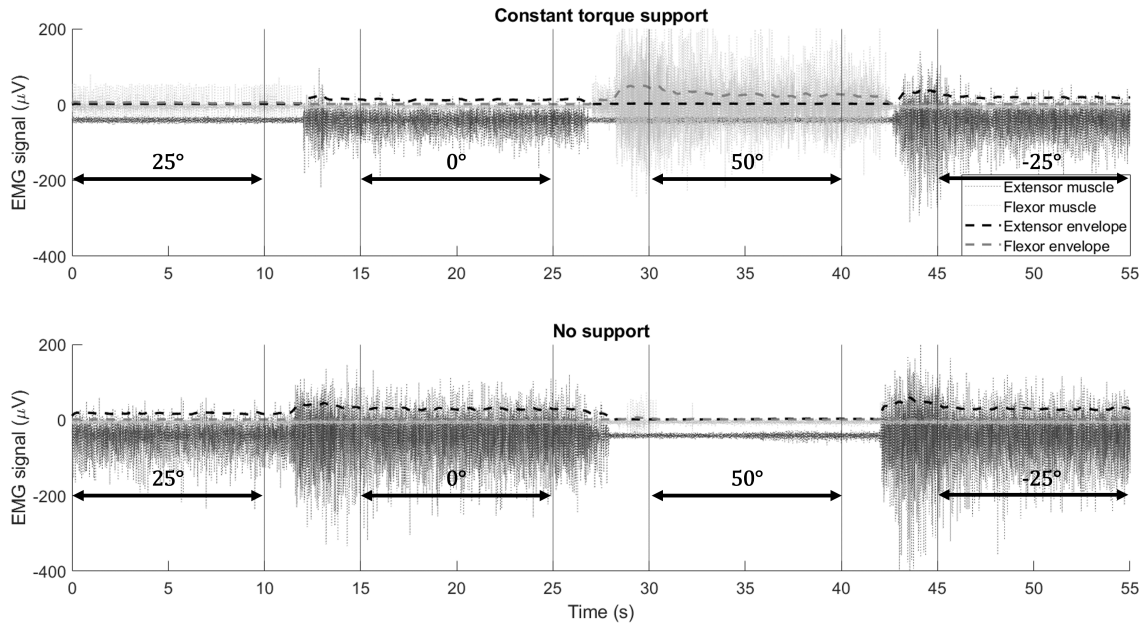


Figure 5. Raw EMG data and the signal envelope from one participant for a single measurement of constant torque support (top graph) and no support (bottom graph), for different levels of palmar flexion with the forearm at 0°. Note that the order of the wrist position is randomly assigned throughout the experiments. However, for clarity the results of two experiments of the same participant are depicted which follow the same order.

3. Results

3.1. Participants

A total of nine people participated in the experiment (five females and four males). All participants were right-handed. One female participant had to be excluded due to a technical error during the experiment. The characteristics of the participants are depicted in Table 1.

3.2. sEMG activity

An example of the raw EMG data is depicted in Fig. 5 for no support (bottom) and a constant torque (top). Overall, the extensor activity is lower for the constant torque support, while the flexor activity increases for larger levels of palmar flexion.

3.2.1. Extensor muscle

Using Mauchly's test it was observed that the assumption of sphericity had been violated for the main effects of wrist position, $\chi^2(5) = 21.04, p < .001$ and balance method $\chi^2(5) = 15.04, p = .011$. Consequently, the degrees of freedom were corrected using Greenhouse-Geisser estimates of sphericity. The effect of wrist position and balance method were observed to be significant ($p < .001$). A pairwise comparison showed that the activity using a form of support were 51%, 53% and 46% lower ($p < .001$) than without support (0.043 ± 0.012) for respectively constant (0.021 ± 0.0068), linear (0.020 ± 0.0058) and sinusoidal (0.023 ± 0.0061). No significant effects were observed between the different types of compensation. When looking at the interaction effects a significant interaction ($p = .002$) was observed between the wrist position and the balance method. This can also be seen from Fig. 6 showing an overall decrease in extensor muscle activity for larger levels of palmar flexion.

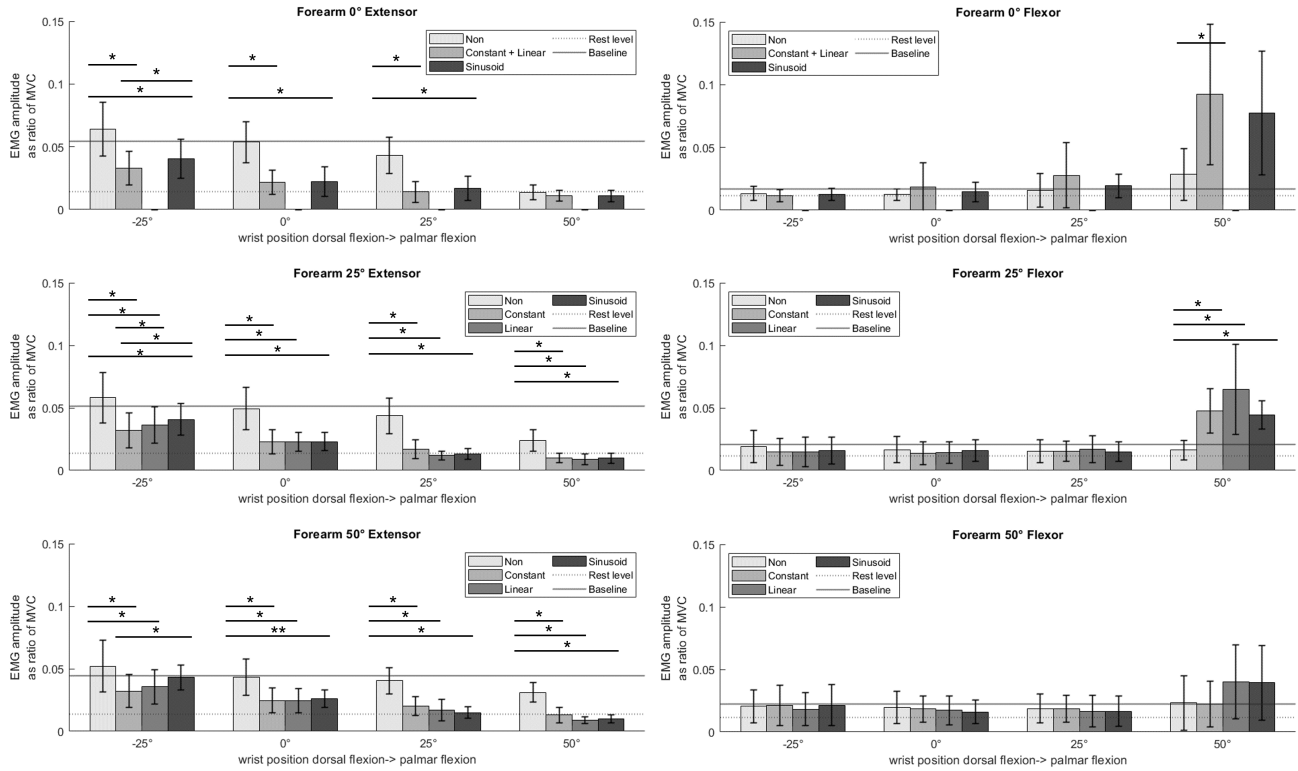


Figure 6. Mean sEMG magnitude relative to the MVC of the ECR (left) and FCR (right) for different forearm positions, wrist positions and balance methods. Reported as mean and standard deviation. * indicate a statistically significant difference. Note, for the 0° forearm position the linear force profile is combined with the constant force profile as they are the same for this orientation (therefore no separate measurements were performed).

3.2.2. Flexor muscle

Using Mauchly's test it was indicated that the assumption of sphericity had been violated for the main effects of wrist position, $\chi^2(5) = 29.78, p < .001$. Consequently, the degrees of freedom were corrected using Greenhouse-Geisser estimates of sphericity. The effect of wrist position ($p < .001$), balance method ($p < .001$) and forearm orientation ($p = .008$) were observed to be significant. A pairwise comparison showed that the activity using a form of support were 50% ($p = .012$), 61% ($p = .005$) and 44% ($p = .005$) higher than without support (0.018 ± 0.0096) for respectively constant (0.027 ± 0.013), linear (0.029 ± 0.014) and sinusoidal (0.026 ± 0.011). No significant effects were observed between the different types of compensation. When looking at the interaction effects a significant interaction was observed between the forearm and wrist position ($p = .047$), forearm position and balance method ($p < .001$) and wrist position and balance method ($p = .001$). This can also be observed from Fig. 6, showing a large increase in flexor activity at 50° palmar flexion when some form of support is used, especially at the horizontal forearm position.

4. Discussion

This study was performed to assess if simplified torque profiles show a similar muscle activity reduction as the standard gravity compensation strategies for compensation of the weight of the hand. From Fig. 6 it can be noticed that there is a noticeable difference between no support and with support, while the differences between the different compensation methods (constant, linear and sinusoidal) are only small. From the pairwise comparison it can be concluded that the difference between with and without support is indeed significant, both for the extensor and the flexor muscle, while the differences between the constant and sinusoidal profiles were in general non-significant. However, one important remark must be made here. Although the results from the extensor muscle are in favour of using a form of support. The results from the flexor muscle show a limitation of the use of the considered supports,

Table 2. Level of compensation of the simplified balancing methods compared to the sinusoidal profile for the specific wrist and forearm positions. Larger values than 100% indicate overcompensation whereas smaller values indicate undercompensation. For the balance method C=constant and L=linear, while the adjoining number indicates the forearm orientation. A more general overview of the level of compensation is depicted in Fig. 2

Balance method	Wrist position			
	-25	0	25	50
C 0	110%	100%	110%	156%
L 0	110%	100%	110%	156%
C 25	141%	100%	91%	100%
L 25	112%	100%	109%	141%
C 50	248%	100%	71%	64%
L 50	119%	100%	108%	131%

showing an increase of 134% (3.1 p.p. %MCV) in flexor muscle activity at 50° palmar flexion for the constant and sinusoidal torque and an increase of 187% (4.3 p.p. %MCV) for the linear profile with respect to no support. However, this is still less than 10% of MVC. When comparing Fig. 6 with the level of compensation as depicted in Table 2, overcompensation occurred when the flexor activity was high. However, an increase is also observed when there is no overcompensation (sinusoidal and C25). Consequently, it is hypothesised that this increase in activity for large flexion angles is (partially) a result of the inherent joint impedance. This assumes that when no support is provided the forces generated by gravity are large enough to overcome at least partially the joint impedance during flexion (the hand starts hanging). However, when the weight is compensated, additional forces are required to palmar flex the hand to overcome the joint impedance. The influence of this joint impedance is especially of importance when translating these findings to people with muscular weakness caused by for instance a chronic stroke or muscular dystrophy, as the joint impedance in these populations are in general considerably higher than in healthy people [18, 19].

From the data in Fig. 6 it can be observed that the differences for some of the conditions are large, both between and within subjects, showing a large standard deviation. This is especially the case for the flexor data, containing more outliers. This is likely caused by the fact that the activity was close to rest levels, making it more susceptible to noise (e.g., powerline interference). Additionally, some variation is potentially caused by estimation errors of the hand weight and centre of mass because a deviation in the level of compensation can influence the measured activity (See supplementary material B) [20, 21]. However, the estimated masses are comparable to literature [10, 22]. Moreover, the resolution of the constant and linear torques was finite. This was especially an issue for the linear profile. Other possible causes are differences in joint impedance and non-perfect alignment of the wrist joint with the mechanisms joint (e.g., wrist does not behave as a perfect hinge). Although for small angles of wrist flexion these effects are small, for larger angles these effects can be more dominant requiring more force to flex the wrist. Moreover, correctly palpating the muscle belly of the FCR was challenging in some participants, potentially resulting in a less ideal sensor placement, causing more crosstalk from other muscles. Lastly, the test setup could have biased the measured activity (e.g. providing already some support). However, as the activity at the 0° position of the wrist is similar to the baseline measurement (measurement without hand interface) this source of bias can be considered as minor.

Direct comparison of the results with literature is difficult as there are, to the authors knowledge, no articles which investigated different torque profiles to compensate the weight of the hand. Nonetheless, some studies investigated the effect of wrist supports on EMG activity and of gravity compensation of other parts of the body. Hasegawa et al. observed a decrease in the activity of the ECR during a reaching task, while using a sinusoidal torque profile [3]. In literature considering gravity compensation of the entire arm, a reduction in muscle activity was observed for the anti-gravity muscles, such

as the biceps brachii [2, 20, 23, 24]. Whereas no or only a limited effect was observed in the antagonistic muscles (biceps brachii against triceps brachii) [20, 23]. Furthermore, Prange et al. observed an increase (although nonsignificant) in activity of the triceps at the end of a reaching task (relatively large elbow extension) when compensation was used [25]. Although not further discussed in their article, the increase they observed could have been of similar nature as the increase observed in the FCR in this study. However, the comparability of all these studies is limited as they only involve, in some way, the use of a sinusoidal torque profile and are dynamic of nature.

5. Conclusion

This study has shown that using a constant or linear profile can be considered as an alternative for compensation of the weight of the hand. However, the increase in flexor muscle activity for all compensation methods could indicate a possible limitation of the current compensation strategies as they do not account for joint impedance. As such, more research is needed to assess this influence of joint impedance on compensation. Based on the findings from this study a wrist support will be developed capable of generating an adjustable constant torque which will be used for further validation with general movements in healthy people and people suffering from muscular weakness. Lastly, although this study only considered the wrist, the use of a constant torque could potentially be used for other joints in exoskeletons and orthoses, allowing for possibly simpler designs and/or controllers.

Supplementary material A: Torque models. When looking at current wrist supports [26, 27], which aim to support the hand against gravity, such as the Ambrose Dynamic Wrist Orthosis [28], they primarily focus on supporting palmar-dorsal flexion of the wrist. As such gravity compensation of the hand for palmar-dorsal flexion is considered here. Consequently, as only one degree of freedom of the wrist is considered it can be simplified as a revolute joint. Thus, the required torque to compensate the weight of the hand can be expressed as

$$T = mgL \cos(\theta - \phi) \cos \psi \quad (1)$$

Where m is the mass of the hand, L the distance from the wrist joint to the hand's centre of mass, g the gravitational acceleration, ϕ the angle of the wrist with respect to the forearm, θ the inclination of the forearm and ψ the pronation-supination angle at zero inclination (Fig. 7). The weight of the hand can be perfectly compensated by attaching a balance weight opposite to the centre of mass (Fig. 8), resulting in a sinusoidal torque profile. To simplify the required torque profile, it can be approximated using Taylor expansions. Here the 0th and 1st order expansion will be considered. The 0th order expansion around the neutral wrist position $\phi_0 = 0$ can be expressed as

$$T = mgL \cos \theta \cos \psi \quad (2)$$

From this it can be noticed that the required torque only depends on the orientation of the forearm and no longer on the position of the wrist. Thus, the torques are constant for each position of the wrist. The 1st order expansion is given by

$$T = mgL (\cos \theta + \phi \sin \theta) \cos \psi \quad (3)$$

Consequently, the torque depends linearly on the wrist position. This linear term can be considered as a torque generated by a linear spring with torsional stiffness $k_\phi = mgL \sin \theta$ or $k = mg \frac{L}{r^2} \sin \theta$ for an ordinary coil spring attached to a pulley of radius r .

The orientations considered during the experiment correspond to $\psi=0^\circ$, $\theta=0, 25, 50^\circ$ and $\phi=-25, 0, 25, 50^\circ$. The angle ψ is achieved physically through a combination of predominantly pronation of the forearm and a slight abduction of the shoulder. The different angles of θ are achieved through a combination of elbow and shoulder flexion. The different angles of ϕ are achieved through dorsal and palmar flexion of the wrist.

Supplementary material B: Effect of different levels of compensation. To assess the effect of different levels of compensation an additional experiment was performed for the constant torque by using different weights. This experiment was performed with one subject and each measurement was performed five times. In sets of three and two. This was done to reduce the experiment time as changing the weights costs time. The order of the level of compensation was randomised as well as the order of the wrist positions. The orientation of the forearm was held constant throughout the experiment.

The biometric data of the participant are depicted in table 3. The results of the experiment are shown in Fig. 9. From this it can be concluded that using more compensation results in a larger reduction in the activity of the anti-gravity muscle (extensor).

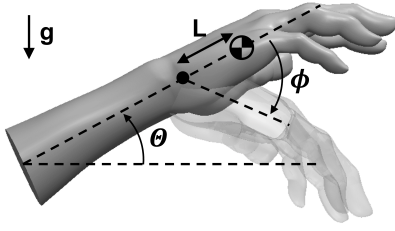


Figure 7. Model of the hand. Note that ϕ is chosen positive for palmar flexion.

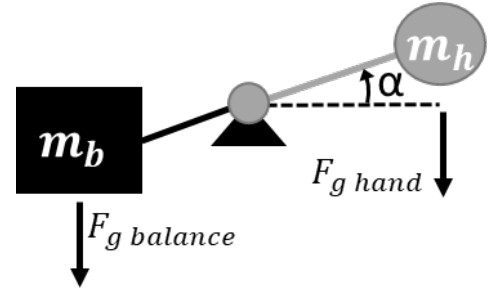


Figure 8. Example of a gravity balancer using a balance weight, which generates a sinusoidal torque profile as a function of α around the joint.

Table 3. Participant characteristics, reported as mean and standard deviation.

Gender	Age (years)	Weight (kg)	Height (m)	Hand weight (g)	Centre of mass (mm)
Male	24	61	1.88	353	43.6

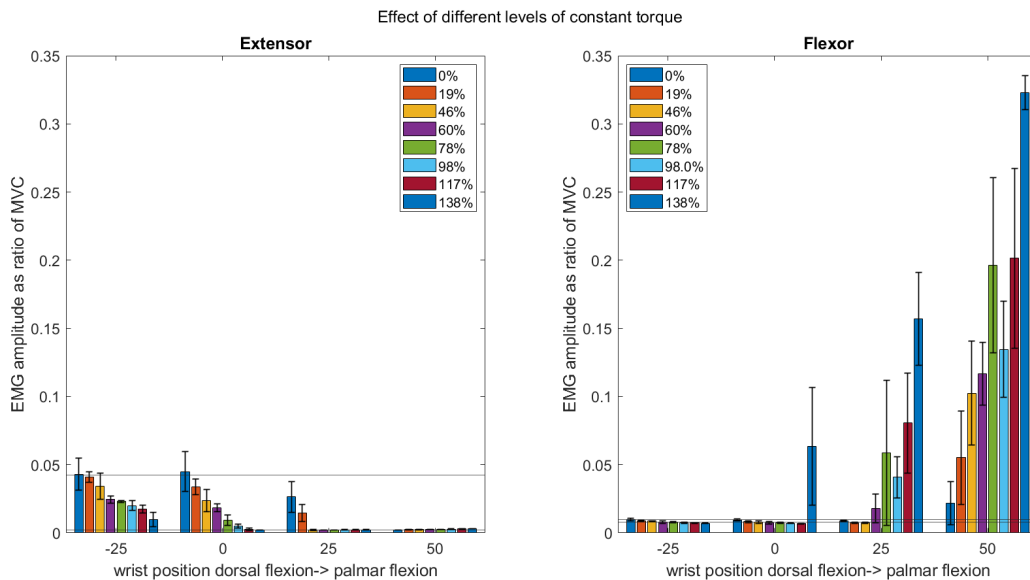


Figure 9. Mean normalised EMG amplitude for different levels of constant torque compensation of the extensor carpi radialis (left) and flexor carpi radialis (right). Error bars are one standard deviation.

However, a larger level of compensation results in an increase in the flexor muscle activity for palmar flexion. This can also be expected as for larger levels of compensation overcompensation occurs, requiring additional effort of the flexor muscles. When comparing these findings with literature, Coscia et al. observed a decrease in muscle activity of the anti-gravity muscles when increasing the level of support from no to full support [20]. Here they used perfect balancing which is comparable to the sinusoidal profile as discussed in this article. Note that in this experiment non-perfect balancing is used (a constant torque) and the levels are increased beyond the full compensation. A similar effect was observed by Runnals et al. [21]. Comparing the results of this additional experiment with the main experiment it can be observed that for the extensor the outcomes are similar when looking at 0% and 98% support. However, the flexor amplitude is considerably higher when support is used, compared to the mean results from the main experiment. However, this is likely caused by interindividual differences as also in the main experiment some participants showed similar results.

Supplementary material C: Effect of movement direction. To assess the effect of the movement order of the wrist on the muscle activity a separate experiment was performed. This experiment was performed with one subject and each measurement was performed 10 times. The participant was asked to move his hand from 25° dorsiflexion to 0° and then to 25° and 50° palmar flexion, after following the same order backwards. The orientation of the forearm was held constant throughout the experiment and no support was provided.

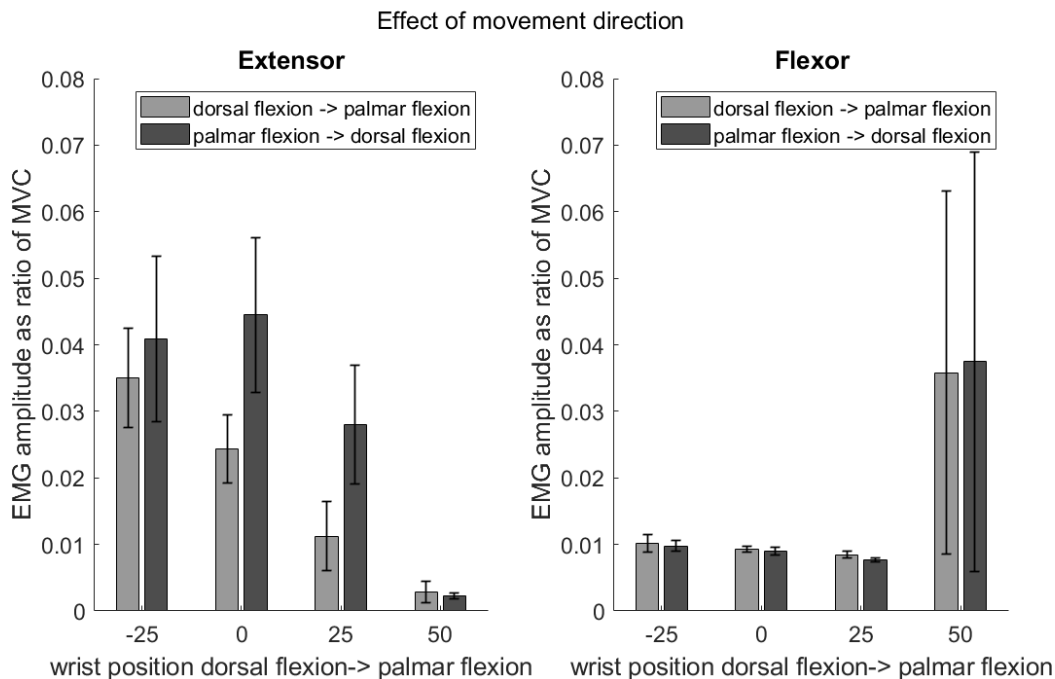


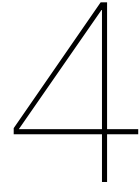
Figure 10. Mean normalised EMG-amplitude of the extensor carpi radialis (left) and flexor carpi radialis (right) for two movement directions. Error bars are one standard deviation.

The biometric data of the participant are depicted in Table 3. The results of the experiment are depicted in Fig. 10 showing in general a higher activity when moving from palmar to dorsal (against gravity) than from dorsal to palmar (with gravity). The first case (dorsal to palmar flexion) involves a concentric contraction (muscle shortens during contraction) while the second (palmar to dorsal flexion) involves an eccentric contraction (muscle lengthens during contraction). These results are also expected as in general the measured activity during a concentric contraction is larger than during eccentric contraction [8].

References

1. Mercuri, E., Bönnemann, C. G. & Muntoni, F. Muscular dystrophies. *The Lancet* **394**, 2025–2038. ISSN: 01406736. <https://linkinghub.elsevier.com/retrieve/pii/S0140673619329101> (Nov. 2019).
2. Jannink, M. *et al.* Reduction of muscle activity during repeated reach and retrieval with gravity compensation in stroke patients in 2007 IEEE 10th International Conference on Rehabilitation Robotics (IEEE, June 2007), 472–476. ISBN: 978-1-4244-1319-5. <http://ieeexplore.ieee.org/document/4428468/>.
3. Hasegawa, Y., Shimada, S. & Eguchi, K. Development of wrist support mechanism for muscle weakness person to work on desk work in 2014 International Symposium on Micro-NanoMechatronics and Human Science (MHS) (IEEE, Nov. 2014), 1–3. ISBN: 978-1-4799-6679-0. <http://ieeexplore.ieee.org/document/7006127/>.
4. Das, S., Lowell, C. & Kurita, Y. in, 239–245 (Springer Singapore, Singapore, 2018). http://link.springer.com/10.1007/978-981-10-4157-0_41.
5. Gopura, R. A. R. C. & Kiguchi, K. Development of an exoskeleton robot for human wrist and forearm motion assist in 2007 International Conference on Industrial and Information Systems (IEEE, 2007), 535–540. ISBN: 978-1-4244-1151-1. <http://ieeexplore.ieee.org/document/4579235/>.
6. Gopura, R. A. R. C. & Kiguchi, K. An Exoskeleton Robot for Human Forearm and Wrist Motion Assist -Hardware Design and EMG-Based Controller. *Journal of Advanced Mechanical Design, Systems, and Manufacturing* **2**, 1067–1083. ISSN: 1881-3054. http://www.jstage.jst.go.jp/article/jamdsm/2/6/2_6_1067/_article (2008).
7. Story, A. *Right Hand Reference* 2020. <https://grabcad.com/library/right-hand-reference-1>.
8. Criswell, E. C. J. R. *Cram's introduction to surface electromyography* English. ISBN: 9780763732745 (Jones and Bartlett, Sudbury, MA, 2011).
9. Chandler, R. F., Clauser, C. E., McConville, J. T., Reynolds, H. M. & Young, J. W. *Investigation of inertial properties of the human body* tech. rep. (1975).
10. Clauser, C. E., McConville, J. T. & Young, J. W. *Weight, volume, and center of mass of segments of the human body* tech. rep. (1969).
11. Barbero, M., Merletti, R. & Rainoldi, A. in *Atlas of Muscle Innervation Zones* 103–120 (Springer Milan, Milano, 2012). http://link.springer.com/10.1007/978-88-470-2463-2_9.

12. Mathiassen, S., Winkel, J. & Hägg, G. Normalization of surface EMG amplitude from the upper trapezius muscle in ergonomic studies — A review. *Journal of Electromyography and Kinesiology* **5**, 197–226. ISSN: 10506411. <https://linkinghub.elsevier.com/retrieve/pii/105064119400014X> (Dec. 1995).
13. Merletti, R. & Cerone, G. Tutorial. Surface EMG detection, conditioning and pre-processing: Best practices. *Journal of Electromyography and Kinesiology* **54**, 102440. ISSN: 10506411. <https://linkinghub.elsevier.com/retrieve/pii/S1050641120300821> (Oct. 2020).
14. Clancy, E. A., Negro, F. & Farina, D. in *Surface Electromyography : Physiology, Engineering, and Applications* 91–125 (John Wiley & Sons, Inc., Hoboken, New Jersey, Apr. 2016). <https://onlinelibrary.wiley.com/doi/10.1002/9781119082934.ch04>.
15. Burden, A. How should we normalize electromyograms obtained from healthy participants? What we have learned from over 25years of research. *Journal of Electromyography and Kinesiology* **20**, 1023–1035. ISSN: 10506411. <https://linkinghub.elsevier.com/retrieve/pii/S1050641110001008> (Dec. 2010).
16. Besomi, M. *et al.* Consensus for experimental design in electromyography (CEDE) project: Amplitude normalization matrix. *Journal of Electromyography and Kinesiology* **53**, 102438. ISSN: 10506411. <https://linkinghub.elsevier.com/retrieve/pii/S1050641120300808> (Aug. 2020).
17. Field, A. *Discovering statistics using IBM SPSS statistics* ISBN: 1446274586 (sage, 2013).
18. Cornu, C., Goubel, F. & Fardeau, M. Muscle and joint elastic properties during elbow flexion in Duchenne muscular dystrophy. *The Journal of Physiology* **533**, 605–616. ISSN: 0022-3751. <https://onlinelibrary.wiley.com/doi/10.1111/j.1469-7793.2001.0605a.x> (June 2001).
19. De Gooijer-van de Groep, K. L. *et al.* Estimation of tissue stiffness, reflex activity, optimal muscle length and slack length in stroke patients using an electromyography driven antagonistic wrist model. *Clinical Biomechanics* **35**, 93–101. ISSN: 02680033. <https://linkinghub.elsevier.com/retrieve/pii/S0268003316300274> (June 2016).
20. Coscia, M. *et al.* The effect of arm weight support on upper limb muscle synergies during reaching movements. *Journal of NeuroEngineering and Rehabilitation* **11**, 22. ISSN: 1743-0003. <http://jneuroengrehab.biomedcentral.com/articles/10.1186/1743-0003-11-22> (2014).
21. Runnalls, K. D., Anson, G., Wolf, S. L. & Byblow, W. D. Partial weight support differentially affects corticomotor excitability across muscles of the upper limb. *Physiological Reports* **2**, e12183. ISSN: 2051817X. <http://doi.wiley.com/10.14814/phy2.12183> (Dec. 2014).
22. Durkin, J. L. & Dowling, J. J. Analysis of Body Segment Parameter Differences Between Four Human Populations and the Estimation Errors of Four Popular Mathematical Models. *Journal of Biomechanical Engineering* **125**, 515–522. ISSN: 0148-0731. <https://asmedigitalcollection.asme.org/biomechanical/article/125/4/515/447637/Analysis-of-Body-Segment-Parameter-Differences> (Aug. 2003).
23. Iwamuro, B. T., Cruz, E. G., Connelly, L. L., Fischer, H. C. & Kamper, D. G. Effect of a Gravity-Compensating Orthosis on Reaching After Stroke: Evaluation of the Therapy Assistant WREX. *Archives of Physical Medicine and Rehabilitation* **89**, 2121–2128. ISSN: 00039993. <https://linkinghub.elsevier.com/retrieve/pii/S0003999308007946> (Nov. 2008).
24. Puchinger, M. *et al.* *The Retrainer Light-Weight Arm Exoskeleton: Effect of Adjustable Gravity Compensation on Muscle Activations and Forces in 2018 7th IEEE International Conference on Biomedical Robotics and Biomechatronics (Biorob)* (IEEE, Aug. 2018), 396–401. ISBN: 978-1-5386-8183-1. <https://ieeexplore.ieee.org/document/8487218/>.
25. Prange, G. *et al.* Influence of gravity compensation on muscle activity during reach and retrieval in healthy elderly. *Journal of Electromyography and Kinesiology* **19**, e40–e49. ISSN: 10506411. <https://linkinghub.elsevier.com/retrieve/pii/S1050641107001393> (Apr. 2009).
26. Heo, P., Gu, G. M., Lee, S.-j., Rhee, K. & Kim, J. Current hand exoskeleton technologies for rehabilitation and assistive engineering. *International Journal of Precision Engineering and Manufacturing* **13**, 807–824. ISSN: 2234-7593. <http://link.springer.com/10.1007/s12541-012-0107-2> (May 2012).
27. Bos, R. A. *et al.* A structured overview of trends and technologies used in dynamic hand orthoses. *Journal of NeuroEngineering and Rehabilitation* **13**, 62. ISSN: 1743-0003. <http://jneuroengrehab.biomedcentral.com/articles/10.1186/s12984-016-0168-z> (Dec. 2016).
28. *Ambroise Dynamische Polsorthese • Ambroise* <https://www.ambroise.nl/armorthesen/polsorthesen/ambroise-dynamische-polsorthese/>.



Design of an adjustable constant force mechanism for gravity compensation

Design of an adjustable constant force mechanism for gravity compensation

B.J. van der Burgh^{a,b}, S.J. Filius^b and G. Radaelli^{a,*}

^a*Department of Precision and Micro Engineering, Delft University of Technology, Delft, The Netherlands*

^b*Department of Biomechanical Engineering, Delft University of Technology, Delft, The Netherlands*

ARTICLE INFO

Keywords:

Static balancing

Adjustable constant force

Zero stiffness

Negative stiffness

ABSTRACT


Adjustable constant force mechanisms find their use in numerous applications, such as in the field of gravity compensation. However so far, only a few mechanisms have been developed which can continuously adjust their constant force output across a negative to positive range, which is beneficial for implementation in for instance a wrist support. Consequently, this article investigates the development of a novel adjustable constant force mechanism. This adjustable constant force is achieved by combining fixed guided beams, having a negative stiffness, with a set of coil springs, having a positive stiffness, resulting in a zero-stiffness mechanism. Through prestressing of the coil spring, the level of constant force can be adjusted. Additionally, a novel configuration of the fixed guided beams is proposed to enable a compact design while still achieving a large stroke, by stacking the beams in different parallel planes. The performance of the mechanism is evaluated through simulations and experiments, showing a substantial difference in stiffness between the simulations and experiment. Nonetheless, from the experiment it could be concluded that the mechanism is capable of providing a constant force, which is adjustable towards both positive and negative levels of force.

1. Introduction

Passive gravity compensation has gained a lot of interest in the fields of robotics and exoskeletons to decrease the required actuator power or the user's effort [1, 8]. Providing some form of gravity compensation can be among others helpful for people with severe forms of muscle weakness to regain some freedom of movement. However, passive gravity compensation can be challenging as the required balancing forces depend on the orientation of the body part. This is especially an issue for the hand. As it can be moved in 3D space, the required balancing forces are both dependent on the wrist and forearm orientation, making it difficult to compensate. However, the required effort to move the hand against gravity can also be decreased by more approximate balancing methods, such as applying a constant torque, of which the magnitude only depends on the forearm orientation. Such a constant torque/force mechanism is a mechanism of which the output force remains constant across a range of input displacements [33]. For such a mechanism to be applicable in a wrist support the mechanism must be compact and capable of adjusting its constant output force between negative and positive force levels. This article investigates the development of such an adjustable constant force mechanism.

Adjustable constant force mechanisms can be found in various areas such as vibration isolation [4, 21], robotics [7, 18] and medical instruments [20]. However, the reasons for using a constant force within these areas differ, such as to prevent excessive forces during grasping or to suppress external vibrations. These devices can be divided in two groups. The first group consists of mechanisms having a fixed constant force in combination with a transmission to obtain different outputs [2, 3, 4, 16, 20]. For instance, Lan et al. changed the lever arm of a constant torque mechanism to adjust the constant force output of a surgical forceps [20]. A similar method has been used by Keung and Chen where the constant force is achieved with a spring-cam mechanism [16]. Using a roller along a variable elliptic curve Asai et al. made a force amplification mechanism to variably amplify the force of a constant force spring [4]. The second group consists of mechanisms where the properties of the constant force mechanism themselves are adjusted through preloading of a spring. Examples are mechanisms consisting of a combination of negative and positive stiffness

*Corresponding author

 G.Radaelli@tudelft.nl (G. Radaelli)

elements [7, 10, 11, 24], of which the positive element is preloaded, or a specifically oriented combinations of springs [6, 17, 18, 19, 21, 25, 34] of which one is preloaded. To obtain the required negative stiffness Liu et al. used a cam in combination with a coil spring [24]. Using a set of three springs Lan et al. designed an adjustable constant force mechanism, by mounting two of the springs oblique to the movement direction. By prestressing the straight spring the level of constant force can be adjusted, whereas by prestressing the oblique springs the flatness of the load-displacement curve can be tuned [21]. Although it is a simple mechanism capable of obtaining both a negative and a positive output, a large device is required to obtain the desired properties as the constant force region is otherwise very small. On the contrary, Chen and Lan made use of a monolithic design consisting of a shape-optimized bi-stable beam and a planar spring [7]. Similarly, Gan et al. used a fixed guided beam and a circular beam to obtain the negative and positive stiffness respectively [10]. Hao et al. also made use of fixed guided beams, but used a planar spring for the positive stiffness [11]. These three different mechanisms have in common that they cannot adjust their constant force output in both positive and negative ranges. Additionally, just as in the design proposed by Lan et al. the mechanisms become very wide if a large negative stiffness region is required. Consequently, although their working mechanisms do show potential, the proposed mechanisms are not directly applicable to a wrist support.

The objective of this paper is to propose a new design for an adjustable constant force mechanism. This mechanism differs from similar mechanism found in literature, as it is capable of adjusting its constant force output in a range of positive till negative forces, whereas in most examples from literature only one direction is considered. Additionally, a novel configuration is proposed, making use of a parallel stack of flexures, which enables a more compact design, while still achieving a large stroke. This paper is structured as follows. In the method section an overview will be presented on how to obtain a constant force. Followed by a discussion on modelling of the mechanism and the presentation of a case study. Subsequently, the result section consists of two parts. First of all, the experimental results of the adjustable constant force mechanism will be presented. Secondly, the negative stiffness mechanism will be discussed in more detail as it is a key component of the constant force mechanism. In the discussion section a comparison will be made between the results of the simulations and experiments, for both the adjustable constant force mechanism and the negative stiffness mechanism. Consequently, some of their limitations will be discussed and suggestions will be made for improvements of both the simulations and the design.

2. Method

2.1. Obtaining a constant force

There are various methods to generate a constant force [33]. These mechanisms rely either on a variable transmission ratio, obtained with for instance cams [26] or linkages [19], or on the combination of a negative stiffness with a positive stiffness, such that they cancel each other out. For this, the stiffness magnitude of the positive and negative elements must be the same, but with a different sign across the desired motion range. By connecting these two elements in parallel, the negative and positive stiffness add up resulting in a zero-stiffness mechanism (Fig. 1). This combination of negative with positive stiffness can be inherent, through for instance the optimisation of a beam shape such that the geometrical and material stiffness cancel each other out [15, 30, 31]. Another solution is by combining a separate negative and positive stiffness spring or mechanism. Using this last method has some advantages. First of all, similar to the optimised beams, friction is minimal as no moving contact potentially occurs. Additionally, the mechanism can be made adjustable relatively straightforward, requiring only an additional preloading of the positive stiffness element (e.g., ordinary coil spring). As such, this article will focus on this type of mechanism.

The constant positive stiffness can be obtained relatively straightforward with the help of for instance an ordinary coil spring. Obtaining the constant negative stiffness is more challenging and is in general only achieved approximately. Some examples of techniques used to obtain a negative stiffness are through cams, magnets, oblique springs or buckling of beams [22]. The current design will be based on buckling of beams. Using buckled beams, an approximately constant negative stiffness can be achieved in three manners; prestressing straight flexures [32], pre-curved beams, e.g., by mimicking the buckled shape of the previous method [29] or inclined straight flexures (fixed guided beam) [14, 23, 35, 36]. Of these the inclined straight flexures are the easiest to use, as they do not require prestress to obtain the negative stiffness. On the other hand, pre-curved beams are more difficult to fabricate, while the flexures for the fixed guided beam can be cut out of a flat sheet. Consequently, the fixed guided beam is chosen as the method to obtain the desired stiffness.

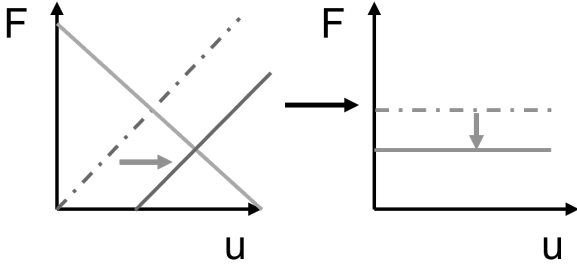


Figure 1: Obtaining an adjustable constant force mechanism, by combining a negative stiffness spring with a positive stiffness spring

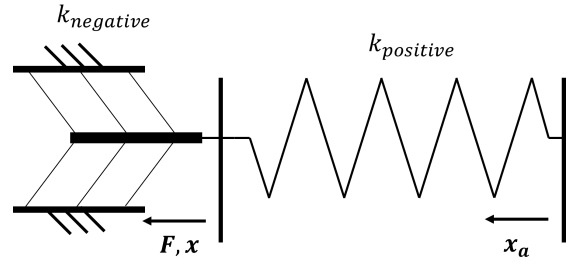


Figure 2: Negative and positive spring configuration. Here F and x denote the input/output force and displacement respectively and x_a denotes the displacement for adjustment

2.2. Modelling of the mechanism

As the fixed guided beams involve large displacements no simple analytical models are available to simulate its performance. Common methods used are Finite Element Analysis (FEA) [9], elliptic integrals [12, 14] and the beam constrained model [27]. With FEA, extra attention must be paid to the modelling as it could otherwise give physically unrealistic buckling modes (only the 1st and 2nd mode generally occur). Thus the model must be forced in these lower buckling modes, either by applying a small initial curvature [9] or an offset load or displacement. Here both FEA and elliptic integrals will be used. The FEA is used to simulate the influence of boundary conditions and imperfections, while due to its low computational expenses the elliptic integral method is used for a sensitivity analysis. The used FEA code makes use of a co-rotational Euler-Bernoulli beam formulation based on the work of Battini [5]. For the elliptic integral method, code based on the book “Handbook of Compliant Mechanisms” has been used [14]. Both methods neglect the effect of shear, however as long as the flexures are thin compared to their length this effect is negligible.

2.3. Constant force model

During buckling the fixed guided beams show an approximately constant negative slope (e.g. Fig. 8). As such, to simplify the consecutive model, the fixed guided beams will be modelled as a linear spring with a negative slope, being loaded as depicted in Fig. 2. Accordingly, the forces within this spring can be expressed as

$$F_n = k_n x + F_0 \quad (1)$$

Where k_n is the approximated linear stiffness of the fixed guided beams, x the displacement and F_0 the offset force. Here an offset force F_0 is required as the approximate linear part of the load-displacement curve of the fixed guided beams do not intersect the origin (e.g., Fig. 8). The forces exerted by the positive stiffness spring with the adjustment are given by

$$F_p = k_p (x - x_a) \quad (2)$$

Here k_p is the spring stiffness and x_a the adjustment displacement. Combining these two forces and assuming the stiffness of the positive and negative spring to cancel each other out perfectly ($k_n = -k_p$) the output force can be expressed as a function of the adjustment.

$$F = F_0 - k_p x_a \quad (3)$$

Rewriting this equation gives an expression for the level of adjustment x_a required to obtain the desired force output

$$x_a = \frac{F_0 - F}{k_p} \quad (4)$$

Although adjustment in both directions is possible only positive values for x_a will be considered as this is required to go from a positive to a negative output force.

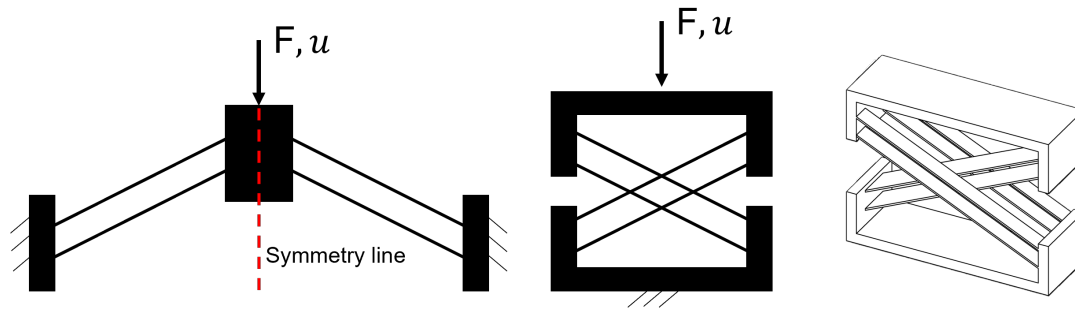


Figure 3: Two different configuration for the fixed guided beams. Left, standard configuration. Middle, proposed configuration. Right, 3D-view of proposed configuration

2.4. Design

In literature the fixed guided beams are constructed in one plane. Although this allows for a monolithic design it results in a wide mechanism. If, however the width of the mechanism is constrained, as in a wrist support, the use of such a configuration is limited. However, these flexure can also be stacked resulting in an adaptation of the Cross-Axis Flexural Pivot as depicted in Fig. 3 [13]. To prevent in-plane deflections during loading the mechanism must be symmetric. For this, three sets of flexures can be used by mounting them in alternating order (e.g., right, left, right). Here the outer two sets must be twice as small as the central set to ensure the symmetry (or the central set can be constructed of two sets similar to the external once). With this new configuration the width of the mechanism can be decreased by half. Additionally, changing the number of flexures has the same effect on the stiffness as changing the flexures width. As such, by increasing the number of flexures the overall thickness of the mechanism can be minimised. By connecting this element in parallel with a positive stiffness spring having the same stiffness, such as a coil spring, a constant force mechanism can be constructed.

To evaluate the performance of this adjustable constant force mechanism a prototype was made. Based on a use case for a wrist support the following requirements were determined. Constant force range of at least 12 mm, with a total range of at least 18 mm and a constant force adjustability of ± 25 N. Additionally, the free length of the flexures was set at 50 mm (dimensional constraint), with a desired stiffness of 2.5 N/mm (corresponding to the stiffness of a set of coil springs). Consequently, 16 flexures being 5.1 mm wide each were used, which were grouped in sets of four (Fig. 4). To obtain the required stroke under the given dimensional constraint the flexures are placed under an angle of 18° . The flexures are cut to size from 0.2 mm stainless spring steel sheets (ANSI 301) having a tensile strength of 1500-1700 MPa. The prestress was controlled electronically using an actuator (Pololu 100:1 Micro Metal Gearmotor HP 6V) and an Arduino nano. The level of adjustment was determined using a quadrature encoder attached to the motor shaft. To transmit the rotational motion of the motor to a linear motion for prestressing the spring, a transmission with a power screw was used. As the power screw is non-backdriveable no power is consumed by the motor once the desired level of adjustment has been achieved.

2.5. Experimental setup

To determine the characteristics of the mechanism tensile and compressive test were performed, with a 45 N load cell (futek) and a motion stage (PI M-505.4DG) (Fig. 5). The force and displacement were recorded using NI LabVIEW™ 2018. Further data processing is performed using MATLAB® R2021a. For the measurement of the constant force four adjustment levels are considered (6.25, 12.5, 18.75 and 25 mm). Besides the total mechanism, also the characteristics of the separate components were evaluated. The adjustment is performed at the initially unloaded position. To estimate the stiffness from the experimental data, a linear curve fit is performed through the region of interest.

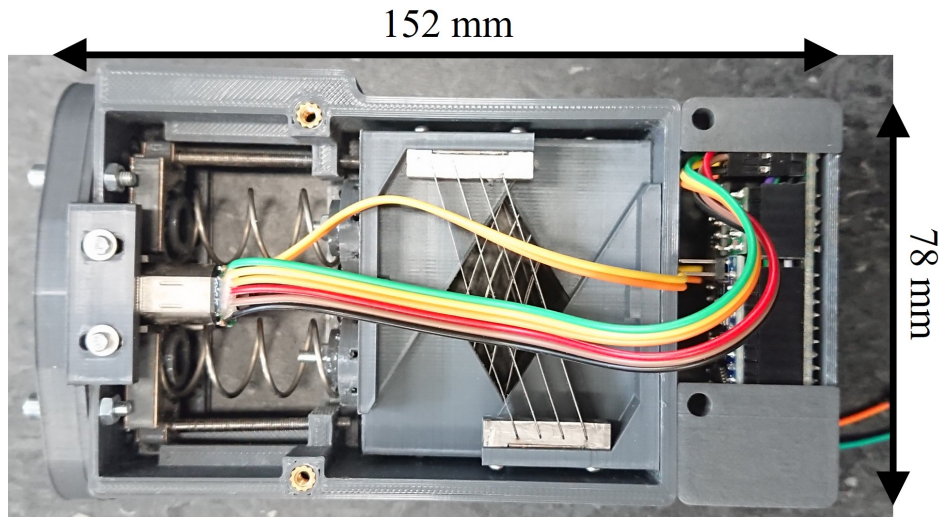


Figure 4: Overview of the mechanism. A DC motor, power transmission and electronics have been added to control the adjustment.

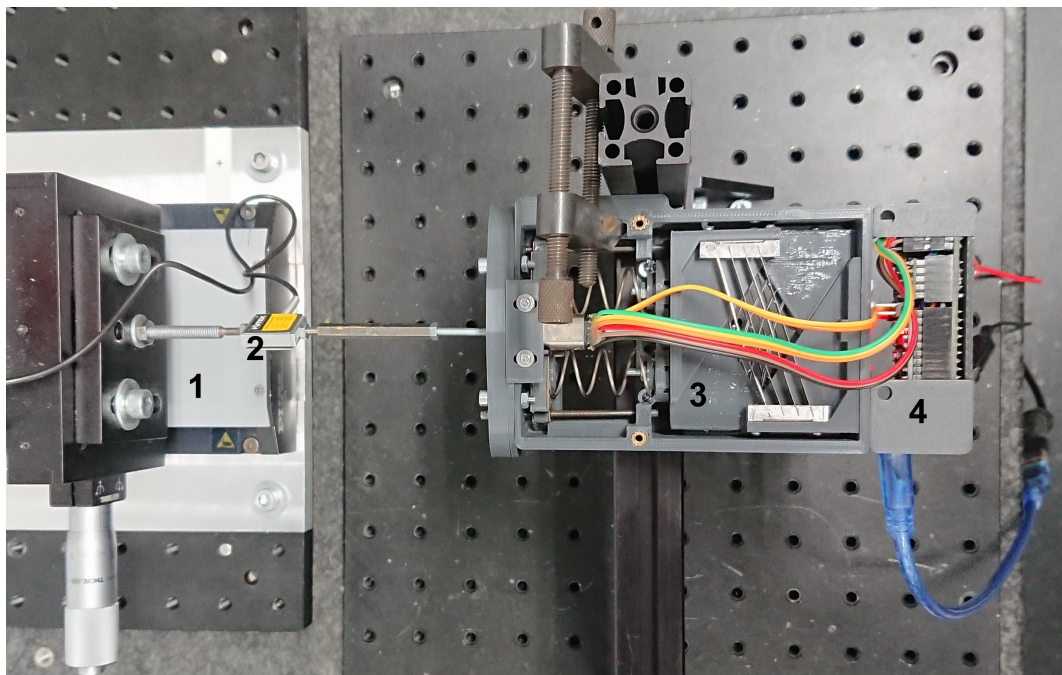


Figure 5: Constant force mechanism and test setup. 1. Motion stage, 2. Force sensor, 3. Constant force mechanism, 4. Electronics for adjustment mechanism

3. Results

3.1. Adjustable constant force mechanism

The results of the experiment to verify the adjustability and the load-displacement characteristics are shown in Fig. 6. From this figure it can be observed that the force output of the mechanism can be varied from positive till negative levels of force, while achieving an approximately constant force across a range of 12 mm. During the experiment it was observed that contact occurred between two flexures, which can be seen as the small force peak between 12 and 14 mm in Fig. 6. Additionally, some contact occurred between the negative stiffness element and the sidewalls due to a minor rotation of the element.

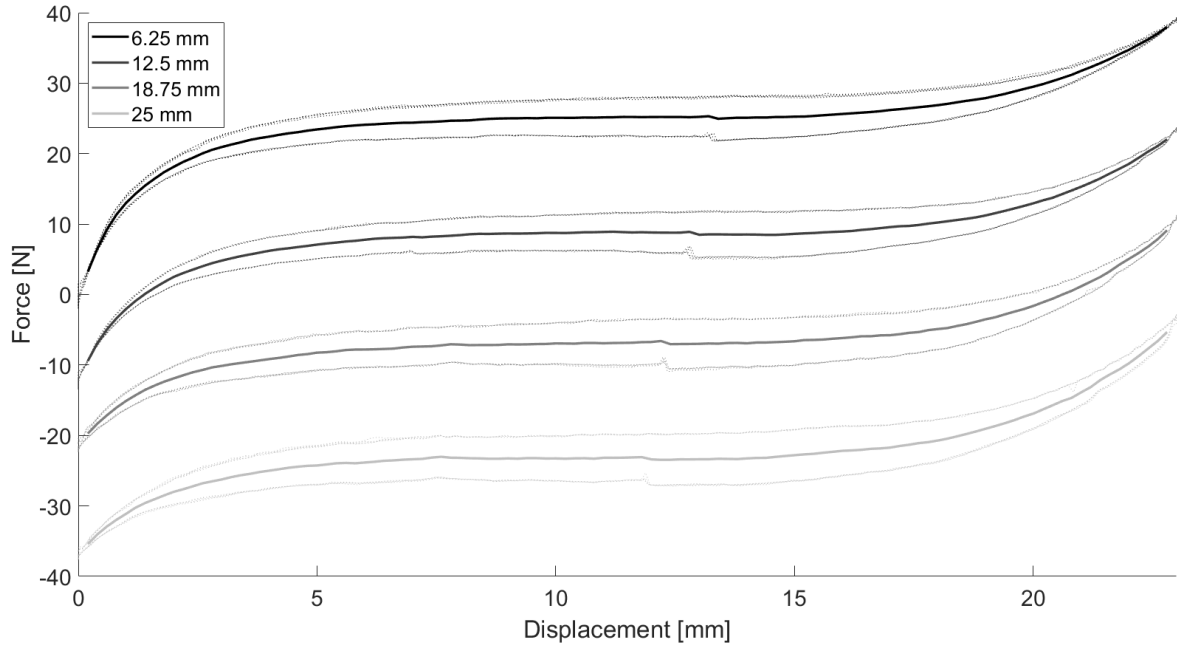


Figure 6: Load-displacement relation for four levels of adjustment. The dotted lines indicate the results of different experiments whereas the solid represents the mean of this data.

A comparison of the adjustment model to the data is depicted in Fig. 7. For the magnitude of the constant force the mean force is taken between a displacement of 5 and 17 mm of the mechanism. The parameters of the model are obtained from the experimental results of the separate components (e.g., coil spring and negative stiffness mechanism). From this figure it can be observed that although the simulation results match the experimental results there is a considerable difference in stiffness deviation.

3.2. Negative stiffness mechanism

As the negative stiffness element is the critical component in the overall behaviour of the mechanism some additional simulations and experiments were performed to assess the influence of different parameters on its behaviour.

3.2.1. Sensitivity analysis

A sensitivity analysis was performed using the elliptic integral method to assess the influence of the different parameters on the stiffness (K), negative stiffness range (s) and maximum stresses (σ_{max}). From this study it was observed that the different parameters are approximately proportional to

$$K \propto f(\gamma) \left(\frac{t}{L}\right)^3 Ew \quad (5)$$

$$s \propto L \sin \gamma \quad (6)$$

$$\sigma_{max} \propto \frac{t}{L} E\gamma \quad (7)$$

The dependency of the stiffness on the angle can be expressed by the following expression. The value of 0.425 is an estimate based on the sensitivity analysis.

$$f(\gamma) \approx (1 - 0.425 \cos \gamma) \quad (8)$$

However, for small angles the stiffness remains nearly constant as from 3° to 30° the stiffness increases by only 9%. This is also observed experimentally as depicted in Fig. 8, showing a difference of approximately 2%. This is different from the observations made by Hao et al. who stated that the stiffness was independent of the angle [11]. Furthermore, increasing the angle also influences the linearity of the negative stiffness curve, as a larger angle results

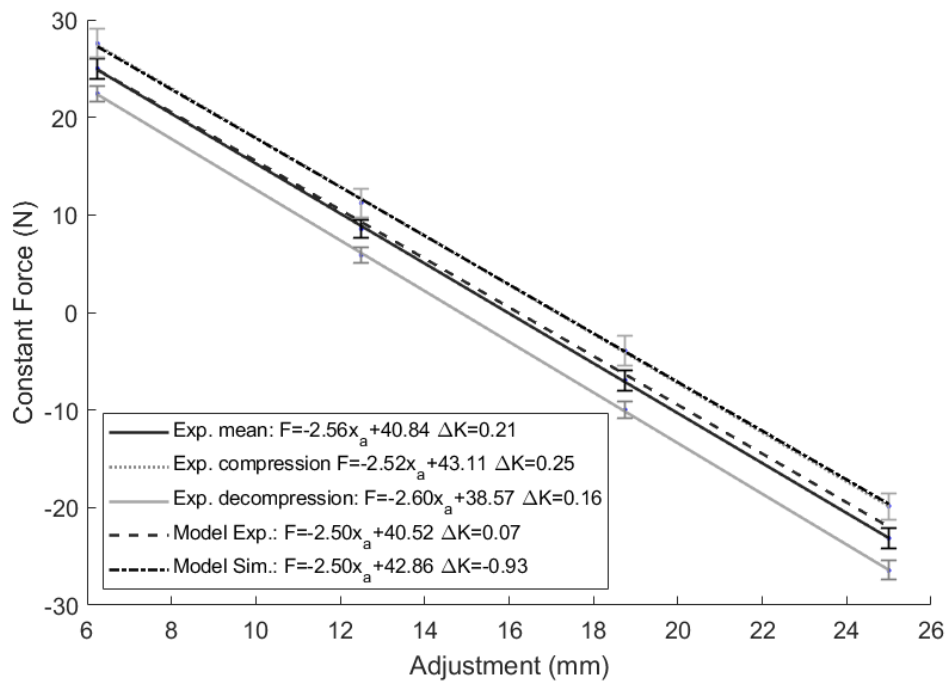


Figure 7: Influence of adjustment on the constant force. The error bars indicate 2SD. ΔK indicates the mean deviation of the stiffness with respect to zero (constant force) in N/mm. Here ΔK is the slope of the line drawn through the force at a displacement of 5 and 17 mm of the mechanism (not to be confused with the adjustment).

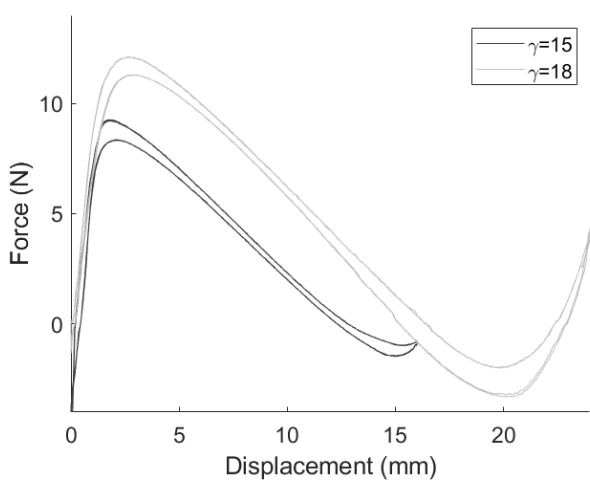


Figure 8: Experimental result for two different angles. At $\gamma = 15^\circ$ the mean stiffness between 5 and 10 mm is 0.94 N/mm and at $\gamma = 18^\circ$ the mean stiffness is 0.92 N/mm. For both experiments 8 flexures of 4.2 mm wide and a free length of 50 mm were used.

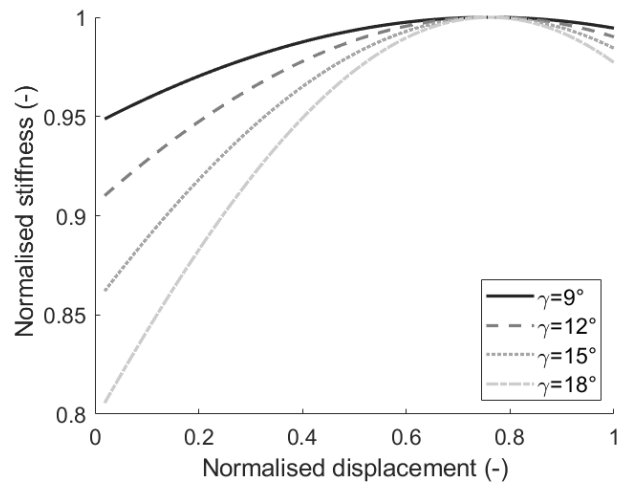


Figure 9: Influence of various levels of inclination on stiffness. The displacement is normalised with respect to the largest displacement in the negative stiffness region and the stiffness is normalised with respect to the largest negative stiffness.

in larger differences in stiffness (Fig. 9). Additionally increasing the angle even further, up to approximately 60° a nearly constant force can be achieved throughout a part of the motion range [28]. However the adjustment of the output force using the method discussed in this article is no longer possible.

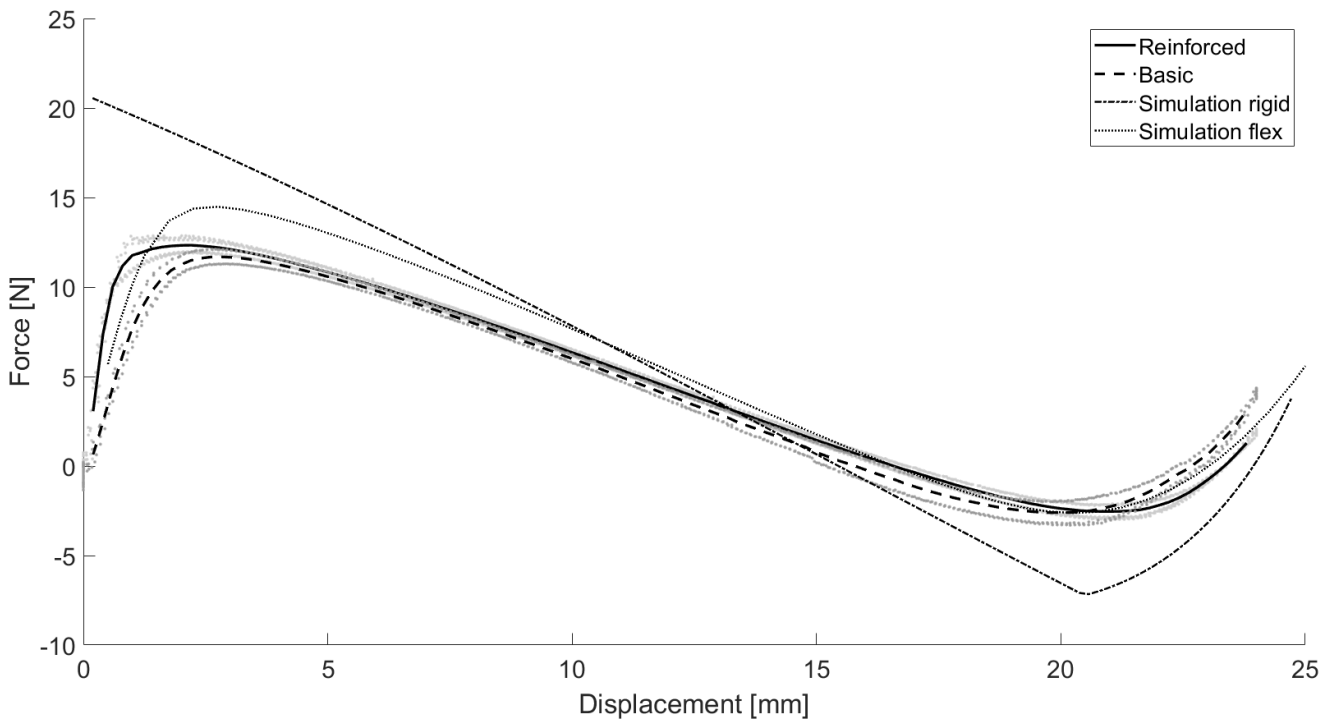


Figure 10: Influence of mounting reinforcement and comparison with simulations. The light grey dots indicate the actual measurement data

3.2.2. Influence of support stiffness

With the elliptic integral method it is assumed that the support of the flexures is rigid. However, in reality this is rarely the case (e.g., in the current prototype the support frame is 3D-printed from PLA). Consequently, the influence of this support structure is assessed experimentally using two different clamps for the flexures. 1.) The flexures are mounted in a 3D-printed block of PLA. 2.) The same blocks, but now reinforced with steel plating. The results of these two clamping methods are depicted in Fig. 10, showing an increase in the negative stiffness region by increasing the support stiffness. When comparing the experimental results with simulations using the same parameters a clear difference can be observed. First of all, the simulation immediately starts with a negative stiffness. Secondly, the stiffness from the simulation is considerably higher compared with the experiments (1.4 N/mm compared to 0.9 N/mm). Thirdly, a difference can be observed between the locations of the unstable and stable equilibria. Using FEA, the effect of some support stiffness was considered as well ($k \approx 2E5N/m$), showing a more similar result with experiment than with the simulations with a rigid support.

4. Discussion

4.1. Adjustable constant force mechanism

Based on the results of the experiment as depicted in Fig. 6 it can be concluded that the proposed mechanism is capable of providing a constant force for both positive and negative forces. However, there is still room for improvement of the mechanism. For instance, the hysteresis within the mechanism is quite high. This can be attributed to several factors. First of all, during compression the negative stiffness element started to rotate slightly, coming into contact with the sidewall. Secondly, due to the loading of the coil springs the two halves of the negative stiffness element came into contact. Thirdly, some contact occurred between two flexures, resulting in a noticeable force spike between 12-14 mm (Fig. 1).

Considering the model of the constant force mechanism it can be concluded from Fig. 7 that both the model parameters based on the experimental data of the separate components as well as the model parameters of the simulation match with the experimental results. However, for the simulation model there is a considerable offset in stiffness, caused

by the higher negative stiffness obtained from the simulations. Due to this large deviation, direct comparison with the simulation results is not of interest. Nonetheless, when considering the experimental results of the separate components a good agreement is obtained, showing the validity of the model. This is in line with the observations made by Chen and Lan [7] and Hao et al. [11].

Although adjustable constant force mechanisms find their application in numerous areas, this article focused on the application of a wrist support. Based on the experimental results, it can be concluded that the mechanism indeed shows promise for application in a wrist support as it meets the requirements on both adjustability and range of motion. However, the current prototype served as a proof of principle and thus is not fully optimised. Nonetheless, the total device already only weighs 260 g. Thus, there is still room for improvement on for instance its weight, size and output force. By using stiffer springs and increasing the number of flexures the output force can be increased. Additionally, by combining the mechanism with a transmission the required stroke of the mechanism can be decreased, which allows for further miniaturisation of the mechanism.

4.2. Negative stiffness mechanism

When comparing the results of the experiments with the simulations a considerable difference in stiffness and overall behaviour could be observed. These differences are a result of several factors related to the manufacturing and the loading conditions. With the elliptic integral method, it is assumed that the flexures are perfectly straight. However the presence of some curvature is very likely to occur. Simulating the flexures with some initial curvature using a nonlinear FEA solver does show a significant influence of the curvature on the overall behaviour, as also observed by Hao et al. [11]. Another factor which can have a considerable effect is the free length, as a 1% increase in free length already results in a decrease in stiffness of 3%. This increase in free length can be a result of manufacturing inaccuracies, but also due to the occurrence of microslip in the clamping of the flexures. After the experiment, it was observed that the flexure sets had become slightly bigger, as the flexures had moved inside the clamping. This did not only result in an increase of free length, but also in the build-up of compressive stresses. Since the flexure sets are placed opposite to one another, any change in length will result in a build-up of compressive stresses inside the mechanism. However, the presence of these compressive stresses does not necessarily have a negative influence on the mechanism's behaviour. Instead, based on some preliminary investigation with FEA it seems as if the approximate linear region of negative stiffness increases through the application of compressive stresses. Consequently, applying prestress to a fixed guided beam is something worth further investigation.

Other factors which influence the mechanism's behaviour, although their effect is minor, are slight differences in angle and width of the flexures. Due to these small errors the buckling directions differed between some of the flexures causing them to come into contact with each other.

When considering the loading conditions, in the simulations it is assumed that the support of the flexures is rigid. However, in reality the support has some elasticity of which the influence could already be observed by reinforcing the flexure mounts. Thus, when simulating similar mechanisms, which have a relatively low support stiffness, the stiffness must be included in the simulation as it has a considerable impact on simulation behaviour.

As previously mentioned, some rotation occurred inside the negative stiffness mechanism during compression. Which is caused by the relatively low torsional stiffness of the negative stiffness mechanism in combination with some off-centre loading. To increase the torsional stiffness, the flexures can be placed further apart within each flexure set. However, a trade-off has to be made here as placing the flexures further from the centre line, will increase the overall size of the mechanism. Additionally, by mounting the flexures away from the centre line, the distance between some of the flexures becomes smaller, increases the risks of flexures coming into contact if they exhibit opposite buckling modes. However, from the experiments it was observed that when opposite buckling occurred away from the centre line there is a larger torsional stiffness than if the flexures buckled towards the centre line or in the same direction. This increase in torsional stiffness is expected as buckling away from the centre line results in a larger second polar moment of area and thus a larger torsional stiffness. Thus, controlling the buckling mode through for instance the addition of imperfections is a possible method to influence the torsional stiffness.

5. Conclusion

This paper presented a new adjustable constant force mechanism based on a novel configuration of fixed guided beams, to enable a compact design with a large constant force stroke. This constant force can be adjusted continuously over a large range of forces. This was evaluated with a prototype showing a constant force region of approximately 12 mm and an output force which can be varied between +25 and -25 N. Upon future improvements, such as a reduction of hysteresis, the proposed mechanism will be further investigated for possible implementation in a novel wrist support to assist people with muscular weakness.

Besides the experimental analysis of the constant force mechanism, the performance of the negative stiffness mechanism has been evaluated both experimentally and numerically. This showed a significant difference between the numerical and experimental results. However, the observed errors are of predictable nature, such as manufacturing imperfections, curvature of flexures, influence of support stiffness and the occurrence of microslip. Consequently, extra care must be taken when simulating buckling behaviour in the presence of a low support stiffness. Additionally, optimisation of the negative stiffness mechanism, such as its torsional stiffness, are of interest for future research.

References

- [1] Arakelian, V., 2016. Gravity compensation in robotics. *Advanced Robotics* 30, 79–96. URL: <http://www.tandfonline.com/doi/full/10.1080/01691864.2015.1090334>, doi:10.1080/01691864.2015.1090334.
- [2] Araki, Y., Asai, T., Kimura, K., Maezawa, K., Masui, T., 2013. Nonlinear vibration isolator with adjustable restoring force. *Journal of Sound and Vibration* 332, 6063–6077. URL: <https://linkinghub.elsevier.com/retrieve/pii/S0022460X13005701>, doi:10.1016/j.jsv.2013.06.030.
- [3] Araki, Y., Asai, T., Masui, T., 2009. Vertical vibration isolator having piecewise-constant restoring force. *Earthquake Engineering & Structural Dynamics* 38, 1505–1523. URL: <https://onlinelibrary.wiley.com/doi/10.1002/eqe.915>, doi:10.1002/eqe.915.
- [4] Asai, T., Araki, Y., Kimura, K., Masui, T., 2017. Adjustable vertical vibration isolator with a variable ellipse curve mechanism. *Earthquake Engineering & Structural Dynamics* 46, 1345–1366. URL: <https://onlinelibrary.wiley.com/doi/10.1002/eqe.2859>, doi:10.1002/eqe.2859.
- [5] Battini, J.M., 2002. Co-rotational beam elements in instability problems. Ph.D. thesis.
- [6] Chen, C.C., Lan, C.C., 2018. An Accurate Force Regulation Mechanism for High-Speed Handling of Fragile Objects Using Pneumatic Grippers. *IEEE Transactions on Automation Science and Engineering* 15, 1600–1608. URL: <https://ieeexplore.ieee.org/document/8077767/>, doi:10.1109/TASE.2017.2757527.
- [7] Chen, Y.H., Lan, C.C., 2012. An Adjustable Constant-Force Mechanism for Adaptive End-Effector Operations. *Journal of Mechanical Design* 134. URL: <https://asmedigitalcollection.asme.org/mechanicaldesign/article/doi/10.1115/1.4005865/475509/An-Adjustable-ConstantForce-Mechanism-for-Adaptive>, doi:10.1115/1.4005865.
- [8] Dunning, A.G., Herder, J.L., 2013. A review of assistive devices for arm balancing, in: 2013 IEEE 13th International Conference on Rehabilitation Robotics (ICORR), IEEE. pp. 1–6. URL: <http://ieeexplore.ieee.org/document/6650485/>, doi:10.1109/ICORR.2013.6650485.
- [9] Dunning, A.G., Tolou, N., Plumiers, P.P., Kluit, L.F., Herder, J.L., 2012. Bistable Compliant Mechanisms: Corrected Finite Element Modeling for Stiffness Tuning and Preloading Incorporation. *Journal of Mechanical Design* 134. URL: <https://asmedigitalcollection.asme.org/mechanicaldesign/article/doi/10.1115/1.4006961/467019/Bistable-Compliant-Mechanisms-Corrected-Finite>, doi:10.1115/1.4006961.
- [10] Gan, J., Xu, H., Zhang, X., Ding, H., 2022. Design of a compliant adjustable constant-force gripper based on circular beams. *Mechanism and Machine Theory* 173, 104843. URL: <https://linkinghub.elsevier.com/retrieve/pii/S0094114X22001100>, doi:10.1016/j.mechmachtheory.2022.104843.
- [11] Hao, G., Mullins, J., Cronin, K., 2017. Simplified modelling and development of a bi-directionally adjustable constant-force compliant gripper. *Proceedings of the Institution of Mechanical Engineers, Part C: Journal of Mechanical Engineering Science* 231, 2110–2123. URL: <http://journals.sagepub.com/doi/10.1177/0954406216628557>, doi:10.1177/0954406216628557.
- [12] Holst, G.L., Teichert, G.H., Jensen, B.D., 2011. Modeling and Experiments of Buckling Modes and Deflection of Fixed-Guided Beams in Compliant Mechanisms. *Journal of Mechanical Design* 133. URL: <https://asmedigitalcollection.asme.org/mechanicaldesign/article/doi/10.1115/1.4003922/467359/Modeling-and-Experiments-of-Buckling-Modes-and>, doi:10.1115/1.4003922.
- [13] Howell, L.L., Magleby, S.P., Olsen, B.M., 2013. Elements of Mechanisms, in: *Handbook of Compliant Mechanisms*. John Wiley & Sons Ltd, Oxford, UK, pp. 155–191. URL: <https://onlinelibrary.wiley.com/doi/10.1002/9781118516485.ch11>, doi:10.1002/9781118516485.ch11.
- [14] Jensen, B., 2013. Modeling of Large Deflection Members, in: *Handbook of Compliant Mechanisms*. John Wiley & Sons Ltd, Oxford, UK, pp. 45–54. URL: <https://onlinelibrary.wiley.com/doi/10.1002/9781118516485.ch4>, doi:10.1002/9781118516485.ch4.
- [15] Jutte, C.V., Kota, S., 2008. Design of Nonlinear Springs for Prescribed Load-Displacement Functions. *Journal of Mechanical Design* 130. URL: <https://asmedigitalcollection.asme.org/mechanicaldesign/article/doi/10.1115/1.2936928/418190/Design-of-Nonlinear-Springs-for-Prescribed>, doi:10.1115/1.2936928.

- [16] Keung, G., Chen, C., 2019. Novel Design of An Adjustable Constant Force Mechanism based on Cam and Spring, in: Uhl, T. (Ed.), *Advances in Mechanism and Machine Science*. Springer International Publishing, Cham, pp. 1481–1490. URL: http://link.springer.com/10.1007/978-3-030-20131-9_146, doi:10.1007/978-3-030-20131-9_{_}146.
- [17] Kuo, Y.L., Huang, S.Y., Lan, C.C., 2019. Sensorless Force Control of Automated Grinding/Deburring Using an Adjustable force regulation mechanism, in: 2019 International Conference on Robotics and Automation (ICRA), IEEE. pp. 9489–9495. URL: <https://ieeexplore.ieee.org/document/8794058/>, doi:10.1109/ICRA.2019.8794058.
- [18] Kuo, Y.L., Lan, C.C., 2020. A Two-Dimensional Adjustable Constant-Force Mechanism. *Journal of Mechanical Design* 142. URL: <https://asmedigitalcollection.asme.org/mechanicaldesign/article/doi/10.1115/1.4044917/975678/A-TwoDimensional-Adjustable-ConstantForce>, doi:10.1115/1.4044917.
- [19] Lambert, P., Herder, J.L., 2017. An Adjustable Constant Force Mechanism Using Pin Joints and Springs, in: Wenger, P., Flores, P. (Eds.), *New Trends in Mechanism and Machine Science*. Springer International Publishing, Cham, pp. 453–461. URL: http://link.springer.com/10.1007/978-3-319-44156-6_46, doi:10.1007/978-3-319-44156-6_{_}46.
- [20] Lan, C.C., Wang, J.Y., 2011. Design of adjustable constant-force forceps for robot-assisted surgical manipulation, in: 2011 IEEE International Conference on Robotics and Automation, IEEE. pp. 386–391. URL: <http://ieeexplore.ieee.org/document/5979556/>, doi:10.1109/ICRA.2011.5979556.
- [21] Lan, C.C., Yang, S.A., Wu, Y.S., 2014. Design and experiment of a compact quasi-zero-stiffness isolator capable of a wide range of loads. *Journal of Sound and Vibration* 333, 4843–4858. URL: <https://linkinghub.elsevier.com/retrieve/pii/S0022460X1400399X>, doi:10.1016/j.jsv.2014.05.009.
- [22] Li, H., Li, Y., Li, J., 2020. Negative stiffness devices for vibration isolation applications: A review. *Advances in Structural Engineering* 23, 1739–1755. URL: <http://journals.sagepub.com/doi/10.1177/1369433219900311>, doi:10.1177/1369433219900311.
- [23] Liu, X., Huang, X., Hua, H., 2013. On the characteristics of a quasi-zero stiffness isolator using Euler buckled beam as negative stiffness corrector. *Journal of Sound and Vibration* 332, 3359–3376. URL: <https://linkinghub.elsevier.com/retrieve/pii/S0022460X13000813>, doi:10.1016/j.jsv.2012.10.037.
- [24] Liu, Y., Yu, D.p., Yao, J., 2016. Design of an adjustable cam based constant force mechanism. *Mechanism and Machine Theory* 103, 85–97. URL: <https://linkinghub.elsevier.com/retrieve/pii/S0094114X16300489>, doi:10.1016/j.mechmachtheory.2016.04.014.
- [25] Liu, Z., Niu, F., Gao, H., Yu, H., Ding, L., Li, N., Deng, Z., 2018. Design, analysis, and experimental validation of an active constant-force system based on a low-stiffness mechanism. *Mechanism and Machine Theory* 130, 1–26. URL: <https://linkinghub.elsevier.com/retrieve/pii/S0094114X18305950>, doi:10.1016/j.mechmachtheory.2018.07.019.
- [26] López-Martínez, J., García-Vallejo, D., Arrabal-Campos, F.M., Garcia-Manrique, J.M., 2018. Design of Three New Cam-Based Constant-Force Mechanisms. *Journal of Mechanical Design* 140. URL: <https://asmedigitalcollection.asme.org/mechanicaldesign/article/doi/10.1115/1.4040174/367597/Design-of-Three-New-CamBased-ConstantForce>, doi:10.1115/1.4040174.
- [27] Ma, F., Chen, G., 2017. Bi-BCM: A Closed-Form Solution for Fixed-Guided Beams in Compliant Mechanisms. *Journal of Mechanisms and Robotics* 9. URL: <https://asmedigitalcollection.asme.org/mechanismsrobotics/article/doi/10.1115/1.4035084/473131/BiBCM-A-ClosedForm-Solution-for-FixedGuided-Beams>, doi:10.1115/1.4035084.
- [28] Ma, F., Chen, G., Wang, H., 2020. Large-Stroke constant-Force mechanisms utilizing second buckling mode of flexible beams: Evaluation metrics and design approach. *Journal of Mechanical Design, Transactions of the ASME* 142. URL: <https://asmedigitalcollection-asme-org.tudelft.idm.oclc.org/mechanicaldesign/article/142/10/103303/1074272/Large-Stroke-Constant-Force-Mechanisms-Utilizing>, doi:10.1115/1.4046242/1074272.
- [29] Qiu, J., Lang, J., Slocum, A., 2004. A Curved-Beam Bistable Mechanism. *Journal of Microelectromechanical Systems* 13, 137–146. URL: <http://ieeexplore.ieee.org/document/1284352/>, doi:10.1109/JMEMS.2004.825308.
- [30] Radaelli, G., Herder, J., 2016. A monolithic compliant large-range gravity balancer. *Mechanism and Machine Theory* 102, 55–67. URL: <https://linkinghub.elsevier.com/retrieve/pii/S0094114X16300088>, doi:10.1016/j.mechmachtheory.2016.03.015.
- [31] Rahman, M.U., 2014. Design of constant force compliant mechanisms. Ph.D. thesis.
- [32] Vangbo, M., 1998. An analytical analysis of a compressed bistable buckled beam. *Sensors and Actuators A: Physical* 69, 212–216. doi:10.1016/S0924-4247(98)00097-1.
- [33] Wang, P., Xu, Q., 2018. Design and modeling of constant-force mechanisms: A survey. *Mechanism and Machine Theory* 119, 1–21. URL: <https://linkinghub.elsevier.com/retrieve/pii/S0094114X17302525>, doi:10.1016/j.mechmachtheory.2017.08.017.
- [34] Yang, Z.W., Lan, C.C., 2015. An adjustable gravity-balancing mechanism using planar extension and compression springs. *Mechanism and Machine Theory* 92, 314–329. URL: <https://linkinghub.elsevier.com/retrieve/pii/S0094114X1500110X>, doi:10.1016/j.mechmachtheory.2015.05.006.
- [35] Zhao, J., Jia, J., He, X., Wang, H., 2008. Post-buckling and Snap-Through Behavior of Inclined Slender Beams. *Journal of Applied Mechanics* 75. URL: <https://asmedigitalcollection.asme.org/appliedmechanics/article/doi/10.1115/1.2870953/475080/Postbuckling-and-SnapThrough-Behavior-of-Inclined>, doi:10.1115/1.2870953.
- [36] Zhou, Z., Gao, Y., Sun, L., Dong, W., Du, Z., 2020. A bistable mechanism with linear negative stiffness and large in-plane lateral stiffness: design, modeling and case studies. *Mechanical Sciences* 11, 75–89. URL: <https://ms.copernicus.org/articles/11/75/2020/>, doi:10.5194/ms-11-75-2020.

5

Design of a wrist support

In the previous chapters the mechanism to generate a constant force and the applicability of a constant force to a wrist support have been discussed. In this chapter a more elaborate discussion regarding the design decisions of the mechanism and interface is presented. Additionally, the incorporation of the different components in a prototype of a wrist support is briefly addressed.

5.1. Design case

Based on the use case from the Wearable Robotics integration project wrist support, the required range of motion is determined as 50° palmar flexion to 25° dorsal flexion. Furthermore, as the goal is to compensate the weight of the hand an estimate of the mass and centre of mass is required. Based on a combination of several studies investigating the anthropometric properties of the human body, the hand's mass is assumed to be 420 g and the centre of mass located 54 mm from the wrist joint [79–82]. For this estimate only anthropometric data of males was considered as DMD patients are almost exclusively males. Thus, based on the hand's mass and centre of gravity the maximum torque required for balancing is 0.22 Nm. Comparing this to the maximal torques available in healthy people and DMD patients in Table 5.1, it can be observed that the torques required for balancing the hand against gravity are for DMD patients already a large fraction of the maximum torques they can exert. Consequently, compensating the weight of the hand is likely to assist these patients.

For a wrist support to be wearable, the size and mass are also important factors to consider. However, as the current design is a proof of principle no clear constraints are set on these parameters. Nonetheless, during the design process some attempts are made to decrease the overall size. Furthermore, as the mechanism needs to adjust itself during an orientation change of the arm, the adjustment must be quick enough. However, for now no constraints are placed on the adjustment speed.

5.1.1. Adjustable constant force

Before coming to the final concept of an adjustable constant force mechanism other solutions were investigated focussing on compensation of the full torque profile by for instance using a change of stiffness or a transmission. For this, the problem was divided in three subproblems: energy storage, creating the required torque/force profile and adjusting the profile. Examples of solutions of these subproblems can be found in Appendix K. Furthermore, some of these solutions were combined in more

Table 5.1: Required torque to lift the hand against gravity compared to the maximum available wrist torques generated by the flexors and extensor muscles, for healthy subjects and DMD patients. Maximum wrist torques obtained from Janssen et al. [27]. Note the relatively small sample size of the DMD patients.

	Healthy (n=20)	Brooke 1 (n=5)	Brooke 2 (n=7)	Brooke 3 (n=3)	Brooke 4 (n=3)	Brooke 5 (n=2)
Wrist flexors	2.6%	7.6%	11%	15%	20%	27.5%
Wrist extensors	2.8%	6.9%	10%	12%	55%	27.5%

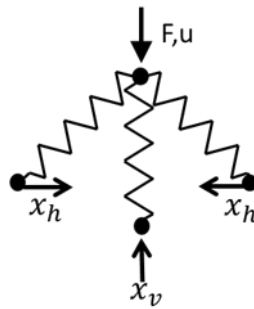


Figure 5.1: Schematic of the three springs mechanism. Here x_h and x_v correspond to horizontal and vertical adjustment of the mechanism.

complete concepts, which are depicted in the second part of Appendix K. However, most of these solutions were fundamental solutions and not necessarily design solutions (e.g., their function had yet to be proven). Consequently, the following process followed more an exploratory search instead of a design process. Following on this, it was decided to focus on the simplification of the problem by using a constant force (Chapter 2).

As already discussed in the previous chapter an adjustable constant force can be obtained in two ways. The first method involves a constant force spring in combination with a variable transmission, such as a lever arm. Thus, when a different output force is required the length of the lever arm is adjusted. The second method involves combining a positive with a negative stiffness spring, by prestressing the positive stiffness spring the output force can be adjusted. When comparing the two methods the design challenge of the first method is in the transmission (as off the shelf (constant force) springs can be used), requiring the output to be scaled between positive and negative forces. Whereas, in the second method obtaining the constant force can be considered as the most challenging, while the adjustment is performed by prestressing a spring of which solutions are readily available. However, examples of mechanisms capable of generating a constant force can be found in literature [11]. For both methods some ideas were investigated (Appendix K). This resulted in two concepts, called the 3D-cam mechanism and the three springs mechanism, which were evaluated through simulations and prototyping.

The 3D-cam mechanism relies on a cam to generate the constant force profile, while energy is stored in springs through movement of the follower as a result of a rotation of the cam. To enable different levels of constant force output the shape of the cam is varied in its thickness direction, such that by moving the position of the follower in the thickness direction of the profile a different output force is generated. A more detailed description of the mechanism can be found in Appendix C.

The three springs mechanism is based on the vibration isolator discussed by Lan et al. [83]. This mechanism relies on two oblique springs (generating a negative stiffness) and one vertical spring (positive stiffness) (Fig. 5.1). By adjusting the level of prestress in the vertical spring the magnitude of the output force can be adjusted. Additionally, by prestressing the oblique springs the flatness of the constant force region can be adjusted. However, a more detailed description of the mechanism can be found in Appendix D.

Based on the prototypes it was observed that for the 3D-cam adjustment was still a challenge due to the friction between the cam and follower. Additionally, the manufacturability of a 3D-cam with the required surface hardness is something of concern. Although these problems are likely not insurmountable, it was decided to continue with the working principle of the three springs as it already showed the desired behaviour. However, although the three springs mechanism did show the desired behaviour (e.g., adjustability and approximately constant force) the overall size of the mechanism was large. Consequently, although continuing with the same same working principle as the three springs mechanism, another solution for the negative stiffness was sought.

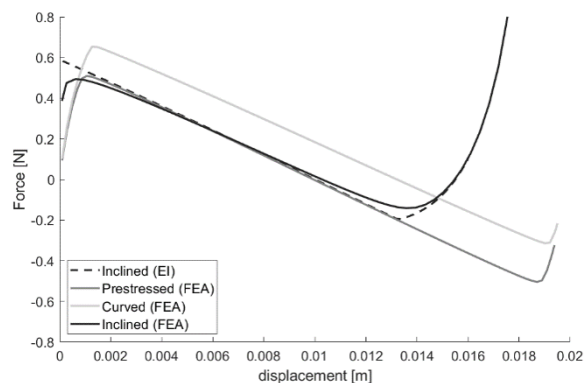


Figure 5.2: Load displacement curve of the different types of flexures using approximately the same properties (e.g. material, length, thickness and width). EI: Elliptic Integral method, FEA: Finite Element analysis. For the FEM solution of the inclined flexure a small curvature was added to the beam to force the physically correct buckling mode to occur [88]. Note that the prestressed curves are shifted to the right, while in fact it is symmetric around zero.

Table 5.2: Comparison of the maximum stresses for the different flexures, having approximately the same dimensions

	Inclined	Prestressed	Curved
Tension	1.1E7	1.3E7	2.6E7
Compression	-1.3E7	-1.4E7	-4.4E7

5.1.2. Negative stiffness

As discussed in chapter 4 there are several methods to obtain a negative stiffness, such as through buckling of beams, cams, and magnets. However of these methods the use of magnets is restricted in a wrist support due to possible interference with nearby electrical components.

Considering the buckling of beams there are three possible solutions, using pre-curved beams, prestressed beams, or straight beams under an inclination (fixed guided beams). Each of these methods was investigated further.

Using pre-curved beams allows for more flexibility to tune the stiffness characteristics of the curve. In literature several articles can be found on the optimization of a beam shape to obtain a specific force-deflection behaviour [84–86]. Here however, the beam shape is based on the work of Qiu et al. [87]. Although these beams are capable of generating a negative stiffness (See Appendix D), manufacturing the flexures with the required stiffness is more difficult than using the other two methods. Namely, for the other two methods the flexures can be cut out of a flat sheet. Consequently, the use of prestressed beams was investigated. However, applying the right amount of prestress posed to be challenging in the proposed flexure configuration, resulting in a more complex design. As such, the use of fixed guided beams was investigated as they did not require additional prestress. Consequently, making the design of the negative stiffness mechanism considerably simpler.

To compare the different methods, simulations were performed using a set of flexures of approximately similar dimensions and material properties (PLA, width=0.01 m, length=0.05 m, thickness= 0.4 mm). Comparing the force displacement behaviour of the different methods it can be observed that the magnitude of the negative stiffness is nearly the same (Fig. 5.2). The region of negative stiffness is for the curved and prestressed beams approximately equal, but for the fixed guided beam it is significantly smaller. Looking at the maximum stresses occurring in the flexures (Table 5.2) it can be noticed that the stresses inside the curved flexures are the largest, while the stresses in the inclined and prestressed beam are comparable. Despite the smaller negative stiffness region, it was decided to use the inclined flexures, because it resulted in the simplest design (Appendix E). Additionally, as the inclined flexures can be cut from a flat sheet it allows for thinner flexures than could be achieved for the curved flexures. Although thinner flexures decrease the stiffness it also decreases the stresses allowing for a smaller design. Nonetheless, the use of prestressed or curved flexures is worth further investigation.

5.1.3. Positive stiffness

To obtain the positive stiffness it was decided to use coil springs, due to their availability, costs, ease of use and linearity of the load-displacement curve. The use of beams subjected to bending was also investigated. However, it was observed that for the desired stroke the length of the beams became too large or for shorter beams the force-displacement started to deviate too much from a linear behaviour to be of use to compensate the negative stiffness.

5.1.4. Transmission

One of the requirements of the transmission mechanism for the adjustment was that it should be non-backdriveable. This is of importance to decrease power consumption of the mechanism, as the actuator can be turned off when the desired level of adjustment is achieved. Additionally, as the adjustment involves a displacement of the springs, the output of the transmission should be a linear motion. Possible solutions to ensure non-backdriveability is through a worm wheel, ball screw, lead screw, high transmission ratio or a ratchet and paw. To generate a linear motion possible solutions are ball screws, lead/power screw, rack and pinion, belt drive or linkage. Both ball screw and lead screw are both solutions for the backdriveability and the linear motion. As ball screws are considerably more expensive than lead screws it was decided to use a lead screw for the adjustment mechanism. To actuate the lead screw a geared DC motor was used, because of its small size. Furthermore, to control the level of adjustment a quadrature encoder was attached to the motor shaft resulting in a theoretical resolution of 0.7 μm , ignoring backlash and play.

5.1.5. Complete mechanism design

For the mechanism to be capable of generating a constant torque ranging from -0.22 Nm to 0.22 Nm the required stroke and output force should be determined. For this, it is useful to look at the required energy consumed during motion. Thus, when considering the required range of motion of 75° (50° palmar flexion and 25° dorsal flexion) the work done by the constant torque equals 0.29 J. Thus, for the stroke and maximum output force of the mechanism it should hold that

$$F_m s > 0.29J \quad (5.1)$$

So, a trade-off has to be made here between the output force and the stroke. Based on the sensitivity analysis in the previous chapter it can be noticed that the stroke is proportional to $L \sin \gamma$. Thus, if a large stroke is desired either the length of the flexures or the level inclination must be large. Increasing the level of inclination increases the stresses in the material while decreases the linearity of the negative stiffness region. Consequently, the allowable increase of γ is limited. Increasing the length to increase the stroke results in a larger mechanism. When aiming for a large force instead of a large stroke either the level of adjustment must be increased or the stiffness of the positive and negative elements. A large force results in larger forces being exerted on the support structure, thus requiring a stiffer structure. Additionally, a large force requires a larger adjustment stroke, potentially requiring longer springs. The increase in adjustment stroke can be prevented by using stiffer springs, but this increases the demands on the motor and the size of the negative stiffness mechanism. Based on this trade-off it was decided to design the mechanism with a negative stiffness stroke of 12 mm and a force of 25 N. However, further optimisation is still possible.

5.1.6. Interface

An issue which is often faced in exoskeleton design is aligning the mechanism with the body such that the assistive forces are applied correctly. If the mechanism is not properly aligned it can result in additional (unwanted) forces being exerted on the body, resulting in discomfort or even pain and injury [89]. Proper alignment is often difficult because the human joints do not act as standard mechanical joints (e.g., revolute joint) and the exact axis of rotation is often unknown. For example, the wrist consists of two joints working in tandem, as such the centre of rotation shifts during movement, resulting in a potential misalignment of the exoskeleton joint for large flexion angles. An example to solve this problem is presented by Ates et al. for a wrist support assisting wrist extension [90, 91]. Here they used a double parallelogram mechanism to transmit the wrist flexion-extension to an elastic tension cord attached to the forearm (Fig. 5.3). Using this mechanism, the rotation is decoupled from the translation, preventing misalignment between the device and the human joint. However, the mechanism has some

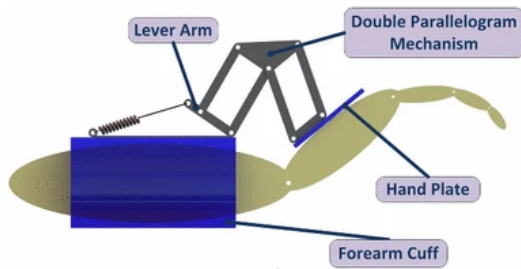


Figure 5.3: Mechanism of the SCRIPT passive orthosis using a double parallelogram mechanism to prevent misalignment. Retrieved from [91]

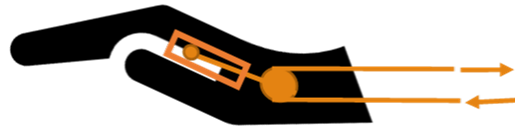


Figure 5.4: Schematic of the proposed interface. The support force is always directed perpendicular to the hand. As the point of application of the force can move slightly with respect to the hand, misalignment is prevented

drawbacks. It is relatively large and the relation between the input and output is nonlinear. Thus, if a constant force is provided as an input, the same force magnitude is no longer applied to the output. Consequently, other solutions are investigated (Appendix F). Instead of a rigid mechanism a flexible connection (such as strings) can be used to prevent misalignment. However, this also results in a nonlinear relation between input and output as the moment arm changes depending on the position of the wrist. Additionally, strings are only capable of providing a tensile force, thus an interface with both the palmar and dorsal side is required. As such, it was decided to use a hinge attached to the side of the wrist, which is attached through a lever to the hand. To prevent misalignment some sliding is allowed between the lever and the attachment point to the hand (Fig. 5.4). Although this introduces some deviation, it results in only a minor error in the torques. For instance, based on a mathematical model of the mechanism (Appendix G) a misalignment of 5 mm results in a maximum deviation from the constant torque of 10% at 50° palmer flexion.

5.2. Design

Taking all the previous design steps into account results in the final prototype as depicted in Fig. 5.5 and Fig. 5.6. To convert the rotary motion of the hand to the linear motion of the mechanism a tooth rack is used in combination with a gearbox to obtain the correct angle-displacement relation. Additionally, the gearbox is used to pass the gap between the mechanism and the joint axis of the wrist as the mechanism cannot be mounted directly on top of this axis as it would hinder wrist motion. These components are used because of their availability and costs. However, they are not necessarily the best solution and thus it is a topic for further investigation.

With the prototype of the wrist support some preliminary experiments were performed to test its functioning. However, as the experiments were primarily exploratory the results will not be considered here, but are discussed in Appendix H.

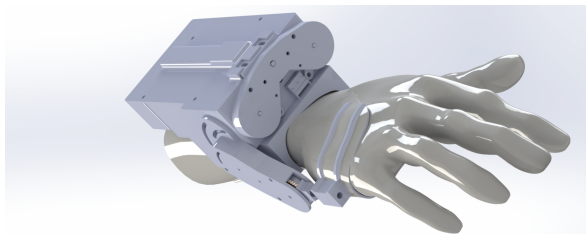


Figure 5.5: Render of the final version of the prototype

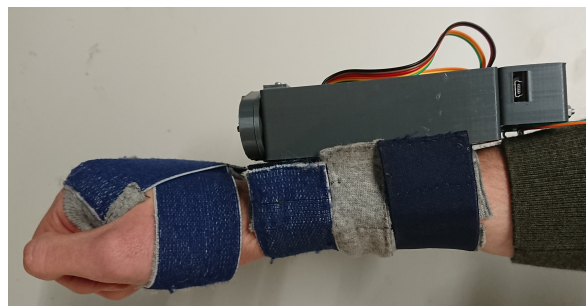


Figure 5.6: Photograph of the prototype

6

Discussion

This study focused on the use of a simplified torque profile (constant torque with respect to the wrist flexion angle) for gravity compensation of the hand, for (future) implementation in a wrist support for DMD patients. From the results of the Chapter 3, it can be noticed that using a constant torque results in a similar decrease in activity of the anti-gravity muscle (extensor muscles) as the sinusoidal profile, which is considered as the theoretically ideal method of balancing. When considering the antagonists (flexor muscle) an increase in activity was observed for all compensation methods at 50° palmar flexion. Indicating a possible influence of the joint impedance, which is not accounted for in the different compensation methods. Furthermore, using constant torque balancing results in some under- or overcompensation when the wrist is at a flexed position compared to the sinusoidal profile. Although non-significant, a general trend was observed in the presence of under- or overcompensation. For instance, overcompensation resulted in a slightly larger decrease in the extensor muscle activity and slightly larger increase in flexor muscle activity compared to the sinusoidal profile. The opposite was true for undercompensation. However, this under- or overcompensation is only with respect to the sinusoidal profile, which is also an approximation of the physically required torque profile. Consequently, based on this research it is difficult to draw conclusions on how much better or worse a constant torque is compared to the sinusoidal torque. Nonetheless, for the considered orientations there is on average no significant differences between the two methods. However, a somewhat more elaborate discussion of the results of the experiment, focussing on the different interaction effects can be found in Appendix I.

In this study the hand was modelled as a frictionless pendulum, which can be considered as an oversimplification, due to among others the presence of joint impedance [92–95]. Consequently, based on the experiments it is hypothesised that especially for larger flexion angles the joint impedance is of substantial influence on the level of required compensation. Subsequently, when translating the findings of this study to DMD patients, the presence of joint impedance becomes a concern, as it is elevated in most of these patients compared to healthy people. Nevertheless, it is expected that despite this increased joint impedance, the patients will benefit from the presented wrist support, as the increase in flexor activity is primarily observed for larger flexion angles. Additionally, by incorporating the joint impedance in the model for the required balancing torques, it is also potentially possible to compensate for, at least partially, this impedance using a constant torque.

Although this study focussed on compensation of the weight of the hand, the proposed balancing methods can be used to compensate for an additional weight, e.g., when picking something up. This can be achieved by adjusting the level of constant torque, as otherwise done when to orientation of the arm is changed. However, for this to be possible the weight of the picked-up mass must be known or estimated during the process, which is currently a topic of active research. Additionally, the required level of constant torque is currently determined based on the neutral position of the wrist $\phi = 0$, but it is not limited to this. For instance, if a more palmar flexed position is preferred, the amount of torque can be adjusted to this position, e.g. adjustment is also possible for a fixed forearm orientation.

The current prototype of the adjustable constant force mechanism has shown to be able to be adjustable and generate a constant force (showing an average increase of stiffness across its constant force motion range of at most 0.25 N/mm). This deviation from the constant force is partially caused by the deviation in stiffness between the negative stiffness element and coil springs. Additionally, although in the modelling it is assumed that the negative stiffness mechanism generates a constant negative stiffness throughout its range of motion, this is not the case. So, still improvements can be made to increase performance of the constant force mechanism. First of all, by including an additional transmission the required constant force stroke can be reduced, making it possible to place the flexures under a smaller inclination, resulting in a more constant behaviour (for smaller angles the negative stiffness region behaves more linearly). However, this requires a larger output force, but this can be achieved relatively straightforward by increasing the stiffness through adding additional flexures or making the flexures a bit wider. Secondly, reconsidering the use of pre-curved flexures. Although with these flexures manufacturing constraints and tolerances are more of importance, the advantage is that the shape of the flexures can be tuned to improve the negative stiffness behaviour.

Within the prototype a considerable amount of hysteresis was observed. This friction has primarily two origins: contact between the two halves of the negative stiffness elements and contact between the negative stiffness mechanism and the support structure. The first point is a result of misalignment during loading, resulting in a slight twist of the mechanism. By increasing the tolerances between the two parts, preventing contact, a considerable reduction in friction can be achieved (Appendix E). Another solution is including some form of constraints, through for instance bearings, constraining the mechanisms motion. This will also be a solution to the second issue, as this is caused by a minor rotation of the mechanism during motion. However, adding bearings is not the ideal solution as it also adds friction, while the mechanism itself is compliant. A better solution would be to increase the torsional stiffness of the mechanism, preventing the occurrence of contact in the first place. A straightforward solution is to place the flexures further away from the centre line (e.g., considering stacking of a couple of flexures). Another solution would be to reconsider pre-curved flexures as they can potentially be optimised for a higher torsional stiffness.



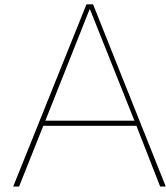
Conclusion

In this thesis it has been shown experimentally that using an adjustable constant torque shows a similar performance in reducing the muscle effort than the commonly used compensation methods for different positions of the wrist and arm. Consequently, using an adjustable constant torque seems to be an alternative for compensation of the weight of the hand. What furthermore becomes clear from the experiment is the possible influence of joint impedance on the weight compensation. This will be especially something to consider when translating these findings to DMD patients as their joint impedance is significantly higher than in healthy people.

To implement this torque profile in a wrist support an adjustable constant force mechanism was designed and validated experimentally. These experiments showed an approximately constant force across the required range of motion, while being able to adjust this force between positive and negative values. However, there is still room for improvement of the mechanism as a considerable amount of hysteresis was observed inside the mechanism.

7.1. Recommendations

Although this research provided some new answers it also resulted in new questions which are worth investigating. First of all, the influence of joint impedance. As this thesis focussed on balancing the weight of the hand, the joint impedance was ignored. However, from the experiments it could be observed that joint impedance potentially influences the level of required compensation. Consequently, it is of interest to investigate the interaction between joint impedance and gravity compensation, by for instance performing the experiment with people with an increased joint impedance, such as DMD patients. Secondly, in this research only a few positions of the arm were considered. Consequently, an area of future research is to investigate the influence of using adjustable constant torque compensation in the case of general motion. However, for this the proposed wrist support should be developed further. Thirdly, the adjustable constant force mechanism has not been optimised thoroughly and thus there is still room for improvement related to its weight and size. Possible areas worth investigation are: reconsidering curved flexures by using 3D printing or waterjet cutting, a monolithic design (e.g. see the second part of Appendix J for an example) or using a larger transmission such that the negative stiffness mechanism can be decreased in size. Fourthly, although being investigated in the experiment the generation of a linear profile has not been considered in the design of the wrist support yet. Although for the investigated range of motion the linear profile did not show any advantages over the constant profile, this might be the case for larger motion ranges or increased levels of joint impedance. Fifthly, currently the adjustment requires a considerable amount of force, which is delivered through a motor. However, applying a prestress is something which can be theoretically statically balanced, further reducing the power consumption of the mechanism and perhaps allowing for a fully passive device. Lastly, this study has only focussed on the wrist. However, the proposed method of using a constant torque for gravity compensation is potentially also of interest for gravity compensation across other joints, as it simplifies the control and in theory decreases energy consumption compared to fully active systems.



Description of the experimental setup

For the experiment to assess the effectiveness of different torque profiles for gravity compensation of the hand a test setup was developed. This setup needed to be able to fixate the arm in different positions, while additionally being able to apply different forces to the hand. As the setup was going to be used with an experiment involving human subjects HREC guidelines were followed in the design, requiring approval of the design by one of the TU Delft safety officers.

The design had to fulfil the following requirements

- Fixating/positioning the forearm in different positions
- Applying a force/torque to the hand
- Generating different torque profiles
- Indicate the flexion/extension angle of the wrist

To limit the safety risks involved with the setup it was decided to make the setup completely passive, thus relying on purely mechanical means to generate the required forces and indicating the position of the hand. Furthermore, to limit the complexity of both the experiment and test setup only static measurements were performed (e.g., measuring the muscle activity when the hand is held still in a specific position).

A.1. Fixating and positioning the forearm

The frame of the setup is constructed from aluminium frames in which holes are drilled to be able to adjust the angle of the forearm position. With these holes the forearm can orientated at 0, 25 and 50° with respect to the horizontal plan (Fig. A.2). To attach the forearm to the setup, the forearm is placed in a cup following the shape of the forearm where it is fixated to through elastic bands with Velcro®. As the length of the forearm varies between participants the forearm mount can be shifted sideways and forward and backwards by loosening a set of bolts. However, because of the flexibility of the skin with respect to the underlying structures some movement of the arm is still possible. So, to provide additional support to the arm a cloth covered pad is placed underneath the elbow (Fig. A.5). To accommodate different arm sizes and the different positions of the mechanism the position and height of the pad can be adjusted.

A.2. Applying a force to the hand

The forces are applied to the hand through a rod attached to the medial side of the hand and a pulley (Fig. A.1). Thus, rotation of the pulley results in a movement of the hand. The interface with the hand consists of a 3D printed part following the shape of the hand, with a mount for the rod (For a more detailed description see Appendix F). The printed part is covered with cloth for comfort and is fixated to the hand through elastic bands with Velcro®. The centre of the pulley can be aligned with the centre

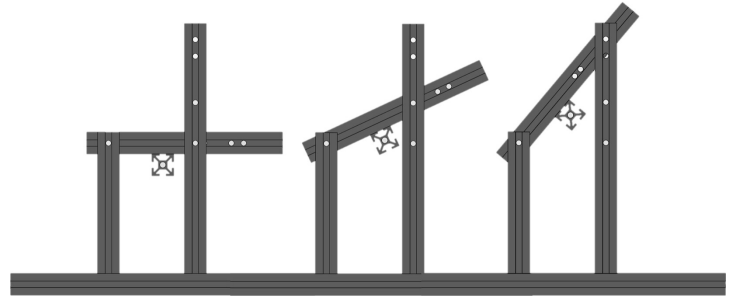
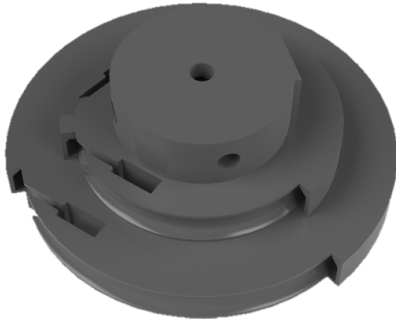


Figure A.1: Close up of the main pulley used to apply the different torque profiles to the hand

Figure A.2: Frame of the setup in the different orientations. From left to right 0°, 25° and 50°

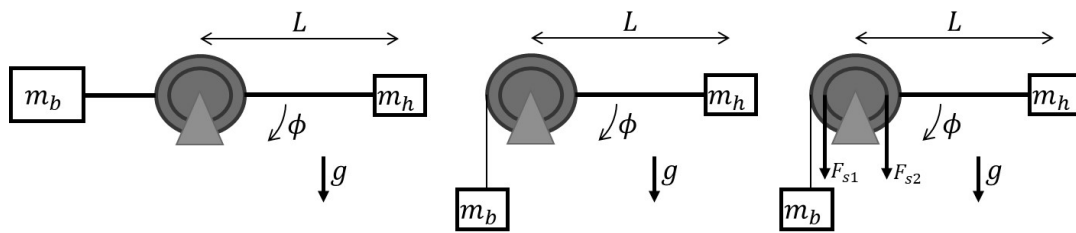


Figure A.3: Schematics of the application of the different torque profiles using the main pulley. From left to right sinusoidal, constant and linear. Here m_h is the mass of the hand and m_b the balance mass. F_{s1} and F_{s2} are the forces applied by the spring

of rotation of the wrist by adjusting its position on the frame. Additionally, the position of the forearm mount can be adjusted as previously discussed. Lastly, the connection between the hand and the rod is not a rigid connection but a cylindrical joint, thus the position along the rod can vary for different hand sizes. An additional advantage of this degree of freedom is that it compensates any remaining misalignment between the wrist joint and the pulley.

A.3. Generating the different force/torque profiles

With the setup three different force profiles can be generated a constant, linear and sinusoidal profile (Fig. A.3). The constant force is generated by hanging a set of weights with a cable on the main pulley. However, as the space near the main pulley is limited a set of two small pulleys is used to guide the cable, such that the weights can hang off the table the setup is placed on. By varying the mass hanging from the cable the level of compensation can be adjusted.

The linear profile is generated by attaching a spring to the main pulley. However, as changing the orientation of the setup results in a length change of the cable attached to the spring, the mounting of the spring needs to be adjustable. This adjustment is also required as the free length of the springs differs. One of the issues with using a cable to transmit the forces is that it can only sustain a tensile force. However, a force should be exerted by the springs during both palmar and dorsal flexion. To solve this, two cables are used which are wrapped in opposite directions around the main pulley. Through a set of two smaller pulleys the two cables are guided to the spring. Thus as the wrist palmar flexes, the upper cable becomes taut while the bottom cable relaxes. On the contrary, if the wrist is flexed dorsally the upper cable relaxes and the lower cable becomes taut, pulling the spring. To prevent the wires coming loose from the main pulley when they become slack, a cable guide is attached to it. To decrease the required stroke of the spring the radius of the main pulley is smaller for the spring ($R=20$ mm) than for the weights ($R=30$ mm). By changing the springs in combination with the weights, different levels of compensation can be achieved.

The sinusoidal profile is generated by hanging a weight on a rod attached to the axis of the main pulley. By adjusting the position of the weight along the rod, the level of compensation can be adjusted.

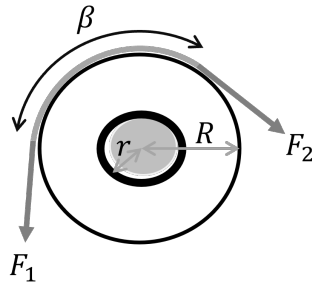


Figure A.4: Schematic of the pulley. Note that the axis the pulley is mounted on (light grey) is slightly smaller than the centre hole of the pulley, as in the case of a journal bearing there is always some play between the components.

Table A.1: Parameters of the pulleys, r indicate the inner radius of the pulley, R the outer, β the wrapping angle and μ the friction coefficient. Note that the first two pulleys have the same dimensions (r_1 and R_1) where as the main pulley has a variable lever arm (R_2 and R_3). As the dimensions of the first two pulleys are the same it is assumed that their coefficient of friction are both equal to μ_1

r_1	r_2	R_1	R_2	R_3	β_1	β_2	β_3	μ_1	μ_2
1.5 mm	2 mm	6 mm	30 mm	50 mm	30°	50°	100°	0.05	0.05

To minimise the friction in the system all pulleys are mounted on ball bearings. The friction has to be low to prevent its influence on the balancing. To make an estimate of the influence of the friction on the provided balancing forces some simple calculations have been performed. Based on the friction model of a journal bearing [96] the ratio between the input and output tension of a pulley can be expressed as (assuming motion is in the direction of F_2 and the reaction force is the bisector of the angle between F_1 and F_2)

$$\frac{F_2}{F_1} = \frac{R - r \cos\left(\frac{1}{2}\beta + \arctan \mu\right)}{R - r \cos\left(\frac{1}{2}\beta - \arctan \mu\right)} \quad (\text{A.1})$$

Here R is the radius of the pulley, r the radius of the journal bearing, β the wrapping angle and μ the coefficient of friction between the pulley and its axis. However, as the experiment is performed statically the level of friction is unknown and thus this equation can only be used for estimating the upper and lower bounds. Considering the more general case of a variable radius pulley (as is the case here with the main pulley), the expression is given by

$$\frac{F_2}{F_1} = \frac{R_1 - r \cos(\gamma + \arctan \mu)}{R_2 - r \cos(\beta - \gamma - \arctan \mu)} \quad (\text{A.2})$$

$$\gamma = \arctan\left(\frac{1}{\sin \beta} \left(\frac{R_2}{R_1} - \cos \beta\right)\right) \quad (\text{A.3})$$

As in total three pulleys are used for both the constant as the linear part the total influence of friction can be obtained by multiplying the previous two equations. For the constant torque profile, the friction is the highest when the forearm is placed in the horizontal position as the wrapping angle is the largest. For the calculation the parameters from Table A.1 are used. This results in a maximum deviation of approximately +/-3% of the balancing force. Thus the influence of the transmission will only be small.

A.4. Indicating the position of the hand

To indicate the level of flexion/extension of the hand a method is required by which the wrist position can be easily read by the participant. For this a dial is used attached to the axis of the pulley (Fig. A.6), because of its design simplicity and its ease of reading. The dial consists of four markings indicating the four levels of flexion/extension. After a short instruction about which marker correspond to which level of palmar-dorsal flexion, the participants had no problems of moving to the right position.

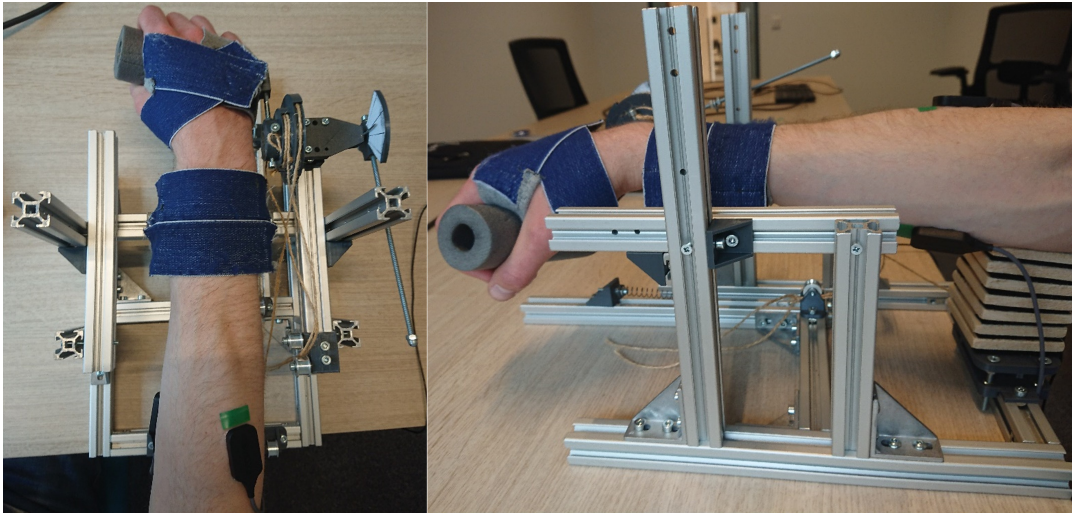


Figure A.5: Top and side view of the setup during an experiment. Consent was given for publication of this picture

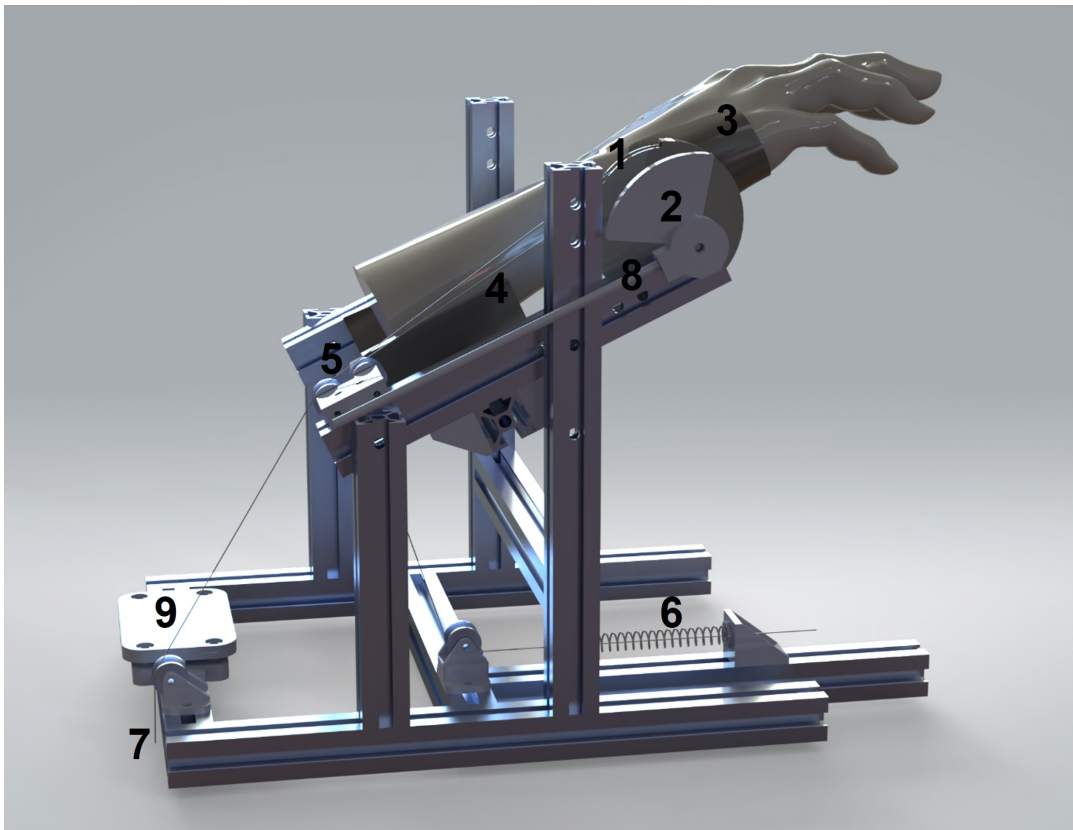


Figure A.6: Render of the test setup, including model of the hand. 1. Main pulley. 2. Dial. 3. Hand interface. 4. Forearm mount. 5. Pulley system. 6. Spring for linear profile. 7. Wire for constant profile. 8. Rod for sinusoidal profile. 9. Height adjustable baseplate of the elbow support.

B

Three springs

One of the simplest mechanisms for generating a nearly constant force across a certain range can be made with three springs (Fig. B.1). Two horizontally mounted compression springs are used to generate a negative force profile. The third spring, which is vertically mounted, generates a positive force profile, which if combined with the negative force profile results in an approximately constant force across a certain range. By changing the prestress in the vertical spring, the magnitude of the constant force can be varied between positive and negative values.

B.1. Model

Based on the model proposed by Lan et al. [83] the forces in the vertical direction of the horizontal (F_n) and vertical (F_p) springs can be expressed as

$$F_n = -k_n y \left(\frac{L_0}{\sqrt{(a_0 - x_h)^2 + y^2}} - 1 \right) \quad (\text{B.1})$$

$$F_p = k_p (y + h_0 - x_v) \quad (\text{B.2})$$

Here k_n is the stiffness of the horizontal springs, k_p the stiffness of the vertical spring, L_0 the initial length of the horizontal springs, a_0 the initial horizontal distance of the horizontal springs, h_0 the initial vertical distance of the horizontal springs, y the displacement of the three springs in the vertical direction and x_h and x_v the prestress length of the horizontal and vertical springs respectively (Fig. B.1). Note that $L_0^2 = a_0^2 + h_0^2$. Thus, the total force is given by

$$F = k_p (y + h_0 - x_v) - k_n y \left(\frac{L_0}{\sqrt{(a_0 - x_h)^2 + y^2}} - 1 \right) \quad (\text{B.3})$$

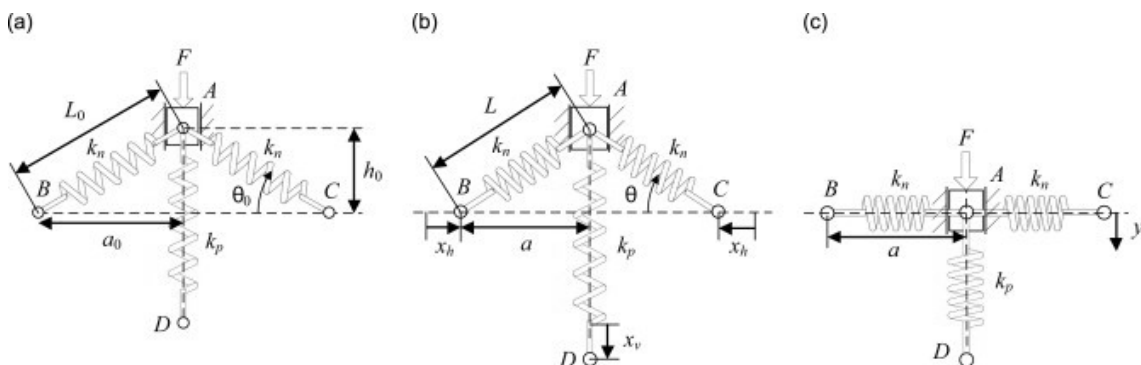


Figure B.1: Model of the three springs mechanism. Retrieved from [83]

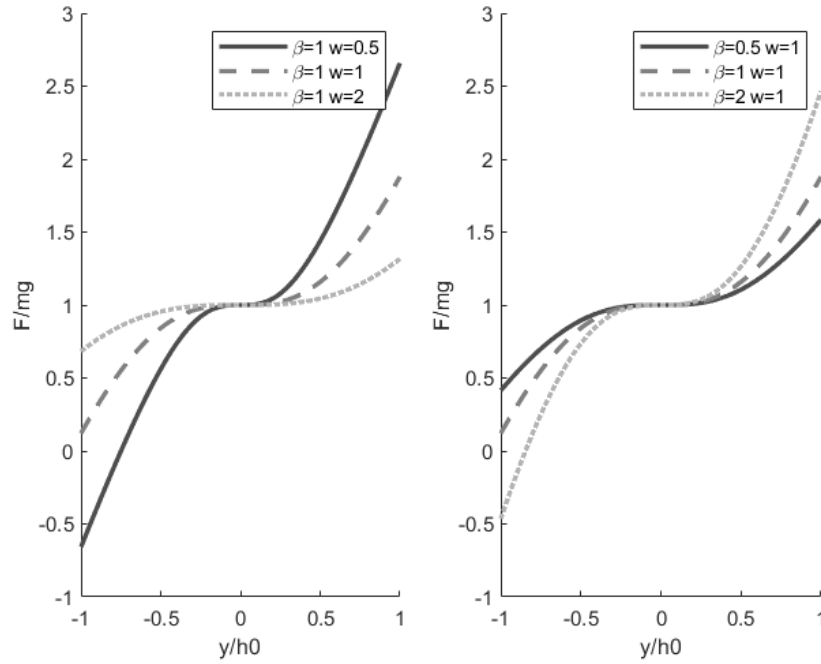


Figure B.2: Normalised load-displacement graph for different values of \hat{w} and β

For a constant force it must hold that $\frac{dF}{dy} = 0$ at $y = 0$, which puts the following requirement on the stiffness of the springs

$$\frac{k_n}{k_p} = \frac{a_0 - x_h}{2(L_0 - a_0 + x_h)} \quad (\text{B.4})$$

B.2. Sensitivity analysis

Making the variables dimensionless the behaviour of changing the variables can be studied more easily. By considering the input force to be a result of a mass lying on top of the system (e.g., the hand's mass) the following relations are used $k_p = \alpha \frac{mg}{h_0}$, $\beta = \frac{k_n}{k_p}$ and $w = a_0 - x_h$. Here m is the weight of the hand, α a scaling factor of the weight as a result of for instance a transmission and $2w$ the width of the mechanism. So, by considering all the variables of unit length with respect to h_0 ($\hat{w} = w/h_0$, $\hat{y} = y/h_0$ and $\hat{x}_v = x_v/h_0$) the total force can be expressed dimensionless as

$$\sigma = \frac{F}{\alpha mg} = (\hat{y} + 1 - \hat{x}_v) - 2\beta\hat{y} \left(\frac{\hat{w} \left(1 + \frac{1}{2\beta}\right)}{\sqrt{\hat{w}^2 + \hat{y}^2}} - 1 \right) \quad (\text{B.5})$$

Based on this equation, the force profile can be tuned by changing x_v, β or w . Changing x_v only influences the magnitude of the constant force region, while changing β or w affects the width of the constant force region. The effect of changing β or w is depicted in Fig. B.2. For a large constant force region, it is desired that the first and the consecutive derivatives of the force with respect to the y -displacement are zero. Considering these derivatives at zero displacement both the first and second derivatives are already zero. However, the third derivative is unequal to zero and is given by

$$\frac{d^3\sigma}{dy^3} = \frac{6(\beta + \frac{1}{2})}{\hat{w}^2} \quad (\text{B.6})$$

From this expression two things can be noticed. First of all, a small increase in w results in a larger increase in the constant force region than a small change in β . Decreasing β towards zero will at a

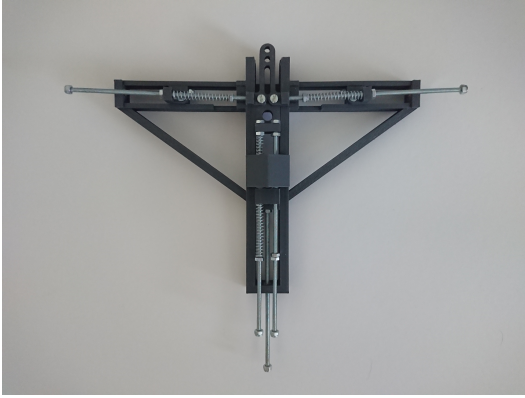


Figure B.3: Prototype of the mechanism

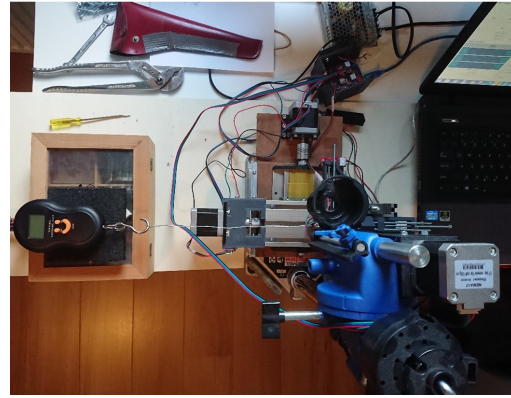


Figure B.4: Test setup, consisting of a scale and CNC xy-stage

certain stage no longer have a significant effect on the constant force region, because the $\frac{1}{2}$ will become dominant. However, when also allowing for negative values of β a perfect constant force region can be obtained for $\beta = -\frac{1}{2}$. This requires the horizontal springs or the vertical springs to have a negative stiffness profile. However, $\beta = -\frac{1}{2}$ results in a physically infeasible solution, because the normalised L_0 and a_0 can be expressed as

$$L_0 = \frac{\hat{w}}{2\beta} + \hat{w} \quad (\text{B.7})$$

$$a_0 = \sqrt{L_0 - 1} \quad (\text{B.8})$$

Thus as $\beta = -\frac{1}{2}$ $L_0 = 0$ and thus a_0 becomes an imaginary number. Thus, for a physically meaningful solution it should hold that

$$\hat{w}(1 + \frac{1}{2\beta}) > 1 \quad (\text{B.9})$$

As a result of changing x_v the spring can become subjected to either tension or compression during motion. So, because of this the spring must be capable of providing both tensile and compressive forces, ideally in the range of $\pm 2h_0$. However to be able to both compress and elongate a spring extra attention must be paid to mounting of the spring. So instead, when restricting the springs to work only in compression a different type of spring configuration is required. This can be achieved by mounting springs on opposite side of the sliding mechanism (Fig. B.3). These two springs exert opposite forces, thus depending on the movement direction of the mechanism one of the two springs will be compressed and thus applying a force.

B.3. Experimental validation

To validate the working of the mechanism a prototype was constructed to determine the force displacement relation (Fig. B.3). This prototype was constructed using additive manufacturing with PLA. For the springs coil springs were used with a spring stiffness of approximately 383 N/m. The value for the spring stiffness was determined by measuring the dimensions of the spring from which the stiffness can be calculated. However, because the material properties are unknown an estimate had to be made. Thus the actual value of the spring stiffness could be significantly different. For the measurement a computer controlled X-Y table was used to control the step size (Fig. B.4). The force were measured using a scale. The displacement was applied in steps of 2 mm after which the weight (force) was read off from the scale. This was done for a total displacement of 24 mm. Additionally the location of the positive spring was adjusted to change the total force profile. For this five different settings were used. In each setting all the measurements were repeated five times resulting in a total of 325 data points.

From the results, it can be seen that the mechanism has an approximate constant force region of which the magnitude can be changed by changing the pretension in the positive stiffness spring (Fig. B.5). However the magnitude of the force is considerably higher than expected from the model, which

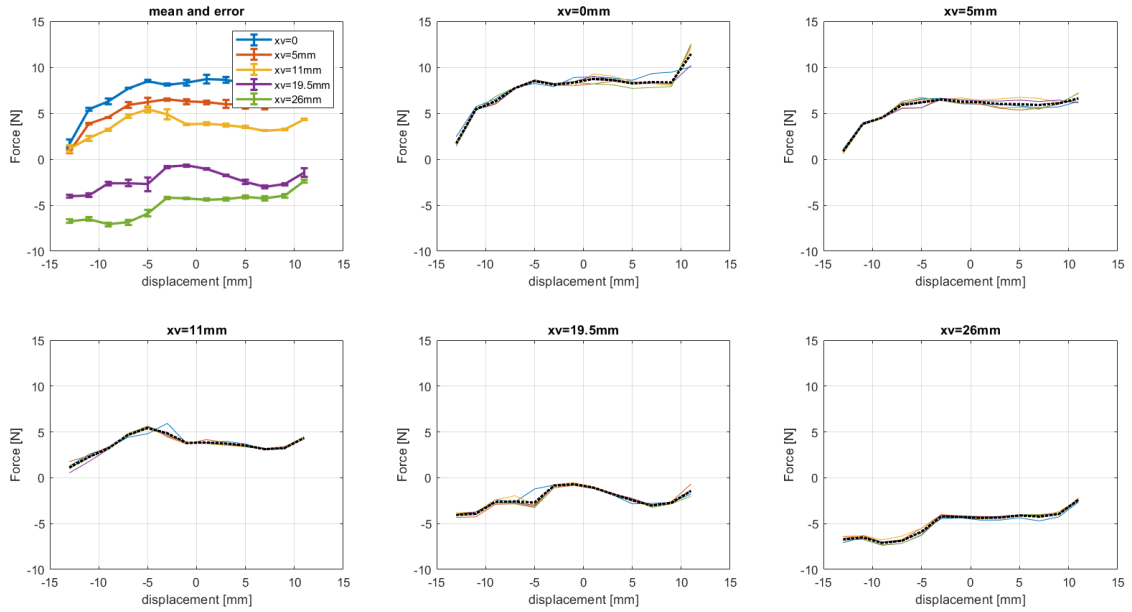
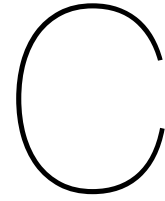


Figure B.5: Experimental results, showing the load-displacement characteristics for five adjustment levels

predicted forces in the range of ± 5 N. This difference is likely caused by the friction inside the mechanism, a wrong reference point of the force (the weight was measured relatively) and different spring properties then used in the model. In the model it has been assumed that the springs are linear, however because the springs are compressed significantly some nonlinearities can be expected here.

To improve the device performance a possible solution is to use flexures instead of springs to generate the negative stiffness part. The occurrence of this negative stiffness is generally a result of buckling of the flexures. The use of flexures enables a larger constant force region. Furthermore, with a flexure there are more possibilities for optimisation. Especially, when considering the flexure as a spatially curved beam, the spatial shape of the beam can be used as an additional optimisation parameter to produce the required force profile while aiming for a compact design.



3D cam

Instead of using a special configuration of springs the desired torque or force profile can also be constructed with a cam-follower mechanism. Although a standard cam-follower mechanism is capable of generating a large variety of torque profiles, these profiles can often not be changed directly. Thus, there are two methods to change the torque profile. Either change the properties of the spring or change the profile of the cam. By giving the cam a 3D shape instead of the more commonly used planar design is one possible method to change the torque profile. When moving the follower up or down along the additional dimension the desired torque profile, for the given orientation, can be chosen. This cam can be constructed by combining the individual planar profiles. However, for this the separate planar profiles must be determined. From a manufacturing point of view constructing such 3D shapes can become challenging using conventional manufacturing techniques such as milling or turning, however due to improvements in additive manufacturing techniques fabricating such complex surfaces can be done relatively easy. However, obtaining the desired surface hardness is still a point of concern.

C.1. Model

To determine the required profile a relation needs to be found between the displacement of the spring and the generated torque [97, 98]. Ignoring friction, the energy balance can be written as

$$U = \frac{1}{2}ks^2 - mgL \sin(\theta + \phi) \cos \psi \quad (\text{C.1})$$

Taking the torque fixed with respect to the flexion/extension of the wrist (a constant torque mechanism) the equation can be simplified to

$$U = \frac{1}{2}ks^2 - T(\theta, \psi, \phi_0)\phi \quad (\text{C.2})$$

Here k is the stiffness of the spring, s the displacement of the spring and T the torque as a function of the orientation of the arm. Assuming equilibrium across the entire motion range requires the total energy to be constant. This can be formulated as

$$\frac{dU}{d\phi} = ks \frac{ds}{d\phi} - T = 0 \quad (\text{C.3})$$

Solving this differential equation results in the desired displacement profile of the follower, which results in the compression/extension of the spring.

$$s = \sqrt{2 \frac{T}{k} \phi + C} \quad (\text{C.4})$$

To ensure real values for the displacement, C is set equal to

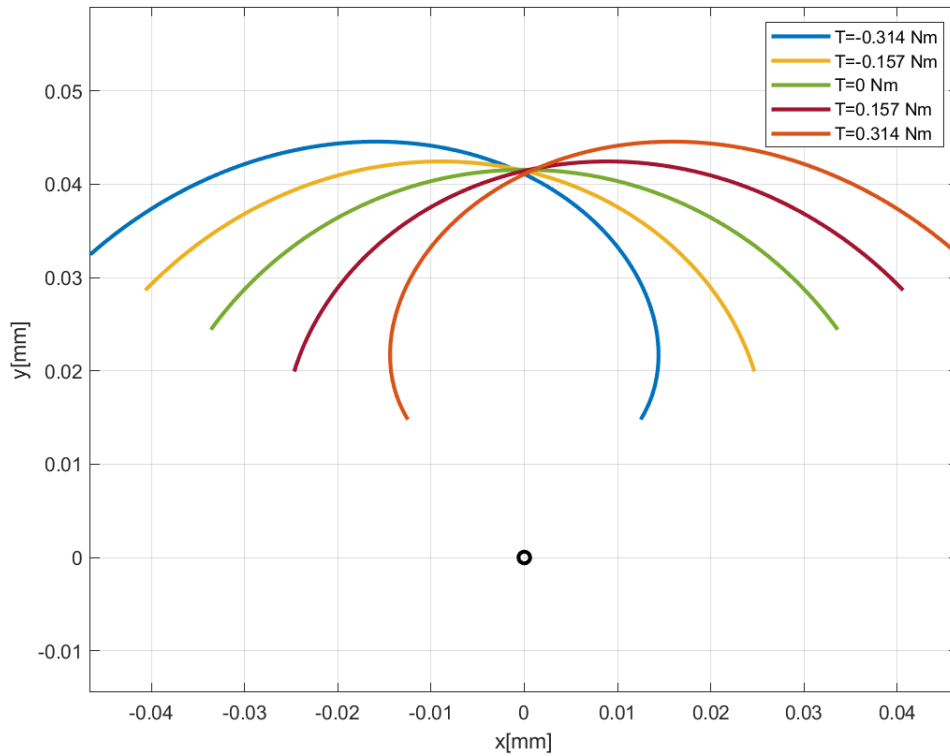


Figure C.1: Cam profiles to generate different constant torque outputs

$$C = 2 \frac{T_{max}}{k} \phi_{max} \quad (C.5)$$

From the equation of the spring deformation an expression can be found for the cam profile using various methods. Here the method proposed by Flores [97] is used to compute the cam profile. For this the pitch curve has to be determined first, which is given by

$$x_p = (R + r) * \sin \phi + \arcsin \frac{e}{r + R} + s * \sin \phi \quad (C.6)$$

$$y_p = (R + r) * \cos \phi + \arcsin \frac{e}{r + R} + s * \cos \phi \quad (C.7)$$

Here R , r and e stand for the base radius of the cam, radius of the follower and the eccentricity of the follower with respect to the cam respectively. Based on the expressions for the pitch curve the expression for the cam profile can be determined using

$$x_c = x_p + r \frac{\frac{dy_p}{d\phi}}{\sqrt{\frac{dx_p^2}{d\phi} + \frac{dy_p^2}{d\phi}}} \quad (C.8)$$

$$y_c = y_p + r \frac{\frac{dx_p}{d\phi}}{\sqrt{\frac{dx_p^2}{d\phi} + \frac{dy_p^2}{d\phi}}} \quad (C.9)$$

The resulting cam profiles for different levels of constant torque for $k=400$ N/m, $e=0$, $r=5$ mm, $R=0$ and $T_{max}=0.314$ Nm is shown in Fig. C.1. By offsetting these different profiles in the z -direction a three-dimensional cam surface profile can be constructed.

To verify that the different profiles result in a constant torque, simulations have been performed using COMSOL, from which can be concluded that the formulation of the shape is correct. However,

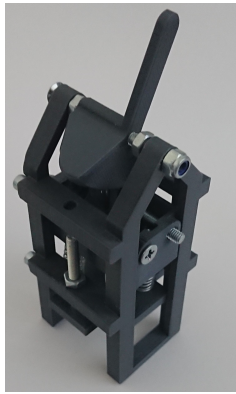


Figure C.2: Prototype of the 3D-cam mechanism

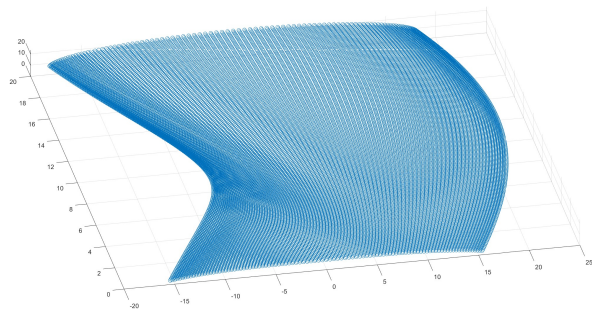


Figure C.3: Cam profile capable of generating the sinusoidal torque profile with a phase shift

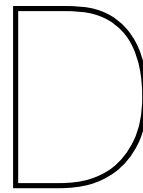
friction has not been included in the models, although it can potentially play a significant role because of the large contact forces.

C.2. Prototype

To further verify the functioning of the mechanism a simple prototype was constructed (Fig. C.2). All the parts were 3D printed out of PLA and joined together with bolts and nuts. From this prototype the following conclusions can be drawn

- Friction plays a significant role in the device performance.
- Due to the high friction and large contact forces adjusting the mechanism by moving it up or down along the cam surfaces requires a considerable amount of force. This can be improved by changing the follower to a ball (which can rotate freely) instead of a wheel. However, the issue with a ball is that it can come into contact with other levels of the cam during movement. Consequently, the curvature of the cam and the radius of the ball are limited.
- The dimensions of the cam pose a limitation on the overall dimensions of the mechanism. This means that further minimisation of the device becomes difficult. This is especially a matter of concern for the thickness because some offset is required between the different cam surface curves. Nonetheless there is still room for optimisation.
- The surface hardness was too low. Although this was somewhat expected from the use of PLA for the cam and follower, a substantial amount of wear was observed.

Since the profile of the cam can be adjusted to generate various torque profile, the mechanism is not limited to constant torques. In fact, “perfect” balancing is possible with this mechanism. An example of a cam surface capable of generating the required torque profile (a phase shift) is depicted in Fig. C.3. However, this perfect balancing can only be achieved for in-plane motion (only ϕ and θ). This is because the cam-surface can be considered as a two degrees of freedom system, while for balancing in space three degrees of freedom are required. Since the balancing of this third degree of freedom (ψ) only requires a scaling of the torque magnitude, it could potentially be achieved by changing the properties or pretension in the spring. However, in this case extra requirements are put on both the spring and the cam surface to ensure contact between the cam and follower throughout its range of motion.



Curved and prestressed flexures

D.1. Curved flexures

Instead of using two opposing springs to generate the negative stiffness it is also possible to use buckling beams. The use of such beams has a couple of advantages over the ordinary springs but also some drawbacks. Some advantages are

- Larger negative stiffness range, thus allowing for a smaller design
- More possibilities for optimization because the shape of the beam can be tailored [87, 99].

Nonetheless there are some drawbacks

- No straightforward analytical models. Only for simple geometries analytical models are available. For more complex shapes numerical methods such as finite element or elliptic integral methods are required.
- Smaller tolerances required on material properties and dimensions.

For an initial shape of the beam the geometry as discussed by Qiu et al. [87] is used, which is a double clamped beam of thickness t and length L (Fig. D.1). The shape can be described by the following equation.

$$w = \frac{h}{2} \left(1 - 2 \cos 2\pi \frac{x}{L} \right) \quad (\text{D.1})$$

Here h is the height at the centre of the beam. For the remaining discussion the y coordinate is defined with respect to the centre line passing through the clamped sides of the beam. Thus in the original shape of Fig. D.1 the beam centre is located at $y=h$. When a force is in the negative y direction at the centre of the beam, the beam will start to buckle. The buckled shape depends on the boundary conditions. Here it is assumed that the rotation of the centre of the beam is constrained, as several beams will be connected in parallel. Based on the beam equation and assuming the displacement to

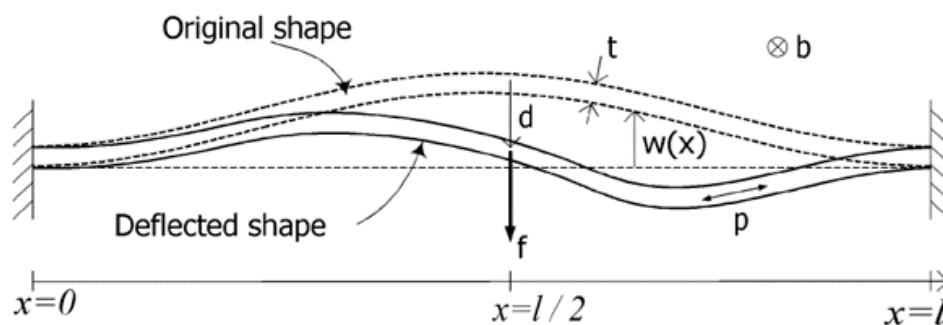


Figure D.1: Shape of the flexure. Retrieved from [87]

remain small with respect to the length, the forces in the negative stiffness regime can be expressed as (For a derivation see [87] or [100] for a more general discussion on buckling).

$$F_n = \left(8\pi^4 - 6\pi^4\left(\frac{y}{h} + 1\right)\right) \frac{EIh}{L^3} \quad (D.2)$$

Combining this with the previously discussed vertical spring (Appendix B). The total force can be expressed as

$$F = k_p(y + h - x_v) + \left(8\pi^4 - 6\pi^4\left(\frac{y}{h} + 1\right)\right) \frac{EIh}{L^3} \quad (D.3)$$

Based on this equation the stiffness required for neutral stability can be expressed as

$$k_p = 6\pi^4 \frac{EI}{L^3} \quad (D.4)$$

From this the required adjustment for the different force levels can be expressed as

$$x_v = \begin{cases} \frac{4}{3}h - \frac{F_0}{k_p} & \text{for } F = F_0 \\ \frac{4}{3}h & \text{for } F = 0 \\ \frac{4}{3}h + \frac{F_0}{k_p} & \text{for } F = -F_0 \end{cases} \quad (D.5)$$

The displacement of the vertical spring can now be expressed as

$$y_{min} + h - x_{vmax} \leq u \leq y_{max} + h - x_{vmin} \quad (D.6)$$

From this it can be noticed that the vertical spring will be subjected to both tensile and compressive forces, because of this it is more convenient to use two springs which are only compressed (similar to the prototype discussed in Appendix B). By choosing the required force range, stiffness and initial height the properties of the springs can be determined.

D.2. Prestressed flexures

Another possibility is to use straight flexures, which by prestressing buckle in approximately the same shape as the curved flexures. The advantage of using straight flexures is they can be cut from a flat sheet of which the thickness is more accurately controlled than in the case of additive manufacturing. The downside is that a proper prestress has to be applied to ensure the desired behaviour.

The first buckling mode of the beam is given by

$$w = \frac{h}{2} \left(1 - \cos \frac{2\pi x}{L}\right) \quad (D.7)$$

The required lateral displacement (for prestressing) to obtain the desired stroke can now be approximated using the equations from [100] resulting in

$$\lambda = \frac{1}{2} \int_0^L \left(\frac{dw}{dx}\right)^2 dx = \frac{1}{4} \pi^2 \frac{h^2}{L} \quad (D.8)$$

An expression of the force generated during buckling is now approximately equal to (For derivation see [101])

$$F_n = -631.7y \frac{EI}{L^3} \quad (D.9)$$

When considering the positive stiffness spring, the required adjustment range changes, because for the prestressed straight flexures the force-displacement relation is symmetric. The adjustment range can now be expressed as

$$x_v = \begin{cases} -\frac{F_0}{k_p} & \text{for } F = F_0 \\ 0 & \text{for } F = 0 \\ \frac{F_0}{k_p} & \text{for } F = -F_0 \end{cases} \quad (D.10)$$

Giving a total displacement range of the positive stiffness spring as

$$-\frac{F}{k_p} - y_{min} \leq u \leq \frac{F}{k_p} + y_{max} \quad (\text{D.11})$$

D.3. Experimental evaluation

D.3.1. method

To verify the validity of the model and test if the pre-curved beams can be used for a constant force mechanism a prototype was made. For this prototype the pre-curved flexures were 3D-printed out of PLA, with a thickness of 0.4 mm, length of 100 mm and height of 9.76 and 10 mm. The flexures were grouped in a set of three. Additionally, instead of one long flexure as depicted in Fig. D.1 the flexures were split down the middle, which is allowed because of the symmetry of the boundary conditions (similar configuration as in Chapter 4).

So, to assess the performance of the prototype the load-displacement behaviour was measured using a motion stage (PI M-505.4DG) in combination with a 45N force sensor (futek). The stage applies a predefined displacement to the mechanism, while in the meantime the force sensor measures the required force. With this, two different tests were performed. First the load-displacement behaviour of two different types of flexures was determined without the coil springs attached. This has been done to assess the validity of the production technique. The second experiment was done to assess the performance of one of the flexures sets in combination with a coil spring. Additionally, the level of pretension in the coil springs was varied.

For the first experiment two flexure sets were evaluated, one with a theoretical height of 9.76 mm and the other of 10 mm. The flexures were 3D printed using a Creality Ender 3 v2 out of PLA with a nozzle size of 0.4 mm. The flexures had a width of only one layer, thus having a thickness of approximately 0.4 mm. Due to issue with slicing such small features, two different slicers were used for comparison. The first flexure set was sliced using Ultimaker Cura 4.12.1 and the second using PrusaSlicer 2.4.1. A displacement of 20 mm was applied with respect to the neutral position after which it was moved back to the neutral position. During both the forward and backward motion, the forces were measured. For each flexure set the measurement was repeated three times. For the 9.76 mm an additional measurement was performed using a slower displacement speed, resulting in a higher measurement resolution.

For the second experiment the 9.76 mm flexure set was used in combination with two coil springs (Fig. D.2) having a stiffness of 440 N/m (as determined by the manufacturer). The method of performing the measurements were similar to the previously discussed methods for the independent flexure sets. However, the pretension in the coil springs was varied by applying a prescribed displacement using a separate motion stage. For this, four levels of pretension were used, expressed as the displacement of the motion stage (-9.39, 0, 13.33 and 36.06 mm). For each level of pretension five measurements were performed resulting in a total of twenty measurements. These measurements were randomized to accommodate for nuisance variables such as the occurrence of plasticity or fatigue inside the flexures.

D.3.2. results and discussion: Experiment 1

During the experiments the following observations could be made

- Some of the flexures initially did not deform or deformed in the opposite direction, after which they suddenly snapped and continued following the expected path just as the other flexures. The snapback was clearly audible and could also be seen in the force-deflection data as a sudden jump in force.
- The 10 mm flexure sets contained a thickening near the centre of one of the flexures, which was caused by the start-stop point of the printer.
- The 9.76 mm flexure set contained discontinuities in some of the layers, however no large differences in thickness were observed.
- The forces at the neutral position were not equal to zero due to pretension inserted in the system during mounting of the force sensor.

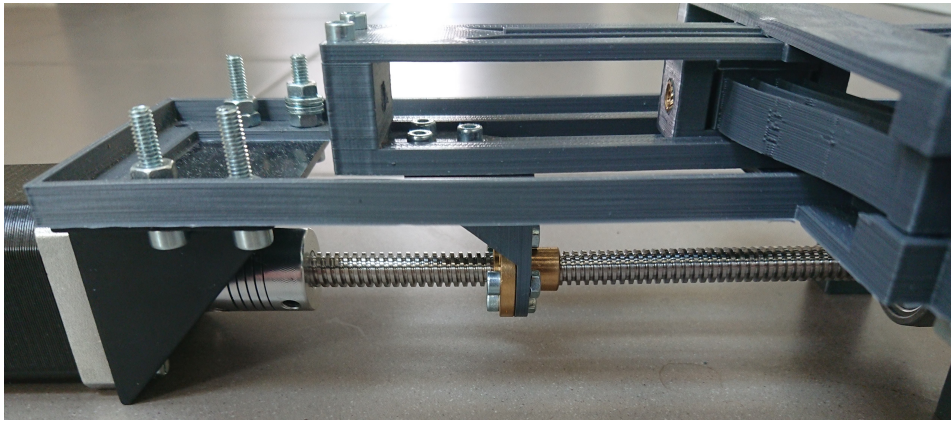


Figure D.2: Image of the prototype. Note that the coil springs are not shown in this image

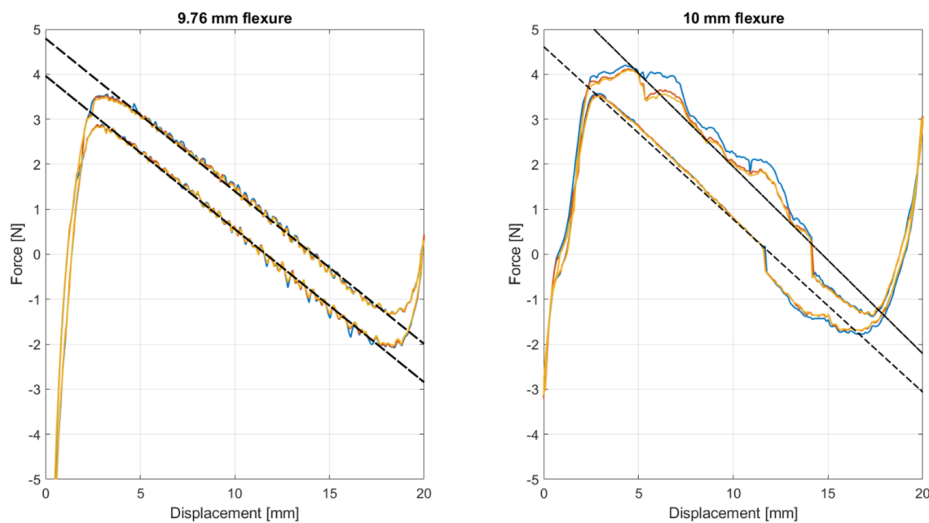


Figure D.3: Load-displacement graph of the two different flexures

The results of the first experiment for the two different flexure sets are depicted in Fig. D.3. From these results the following observations can be made

- The difference between the three measurements is small, almost completely overlapping each other, especially for the 9.76 mm flexure.
- The forward motion (upper part) and the backward motion (lower part) do not coincide thus indicating a considerable loss of energy in the system.
- The slope of the forward and backward motion is nearly the same for the 9.76 mm, both being approximately equal to -340 N/m. This is noticeably smaller than the stiffness the flexure set was designed for, namely 440 N/m.
- The 10 mm flexure shows only during the backward motion a nearly constant stiffness. The forward motion is more erratic.

Some of these findings can be explained as follows

- The energy loss (hysteresis) is caused by hysteresis inside the material and (primarily) the friction between the flexure set and the supporting frame. Thus, when improving the prototype the friction between the different parts must be reduced, by for instance preventing contact between components.
- The stiffness is noticeably different than designed for. This can be attributed to four things. The thickness of the flexures was not equal to 0.4 mm. As the stiffness scales cubic with the thickness

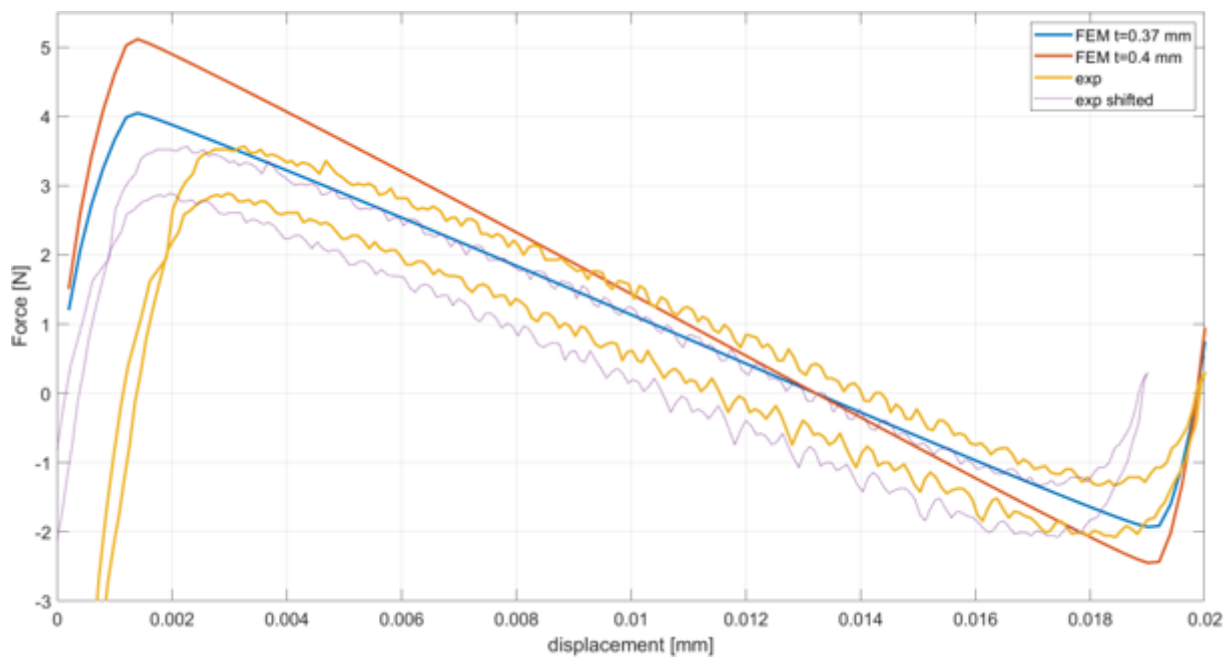


Figure D.4: Comparison between simulation and experiment of the load-displacement characteristics of the flexures

a small deviation in the thickness can have a significant effect on the stiffness. The material properties were not known exactly. Thus, there was possibly a difference between the material properties used in the simulations and the actual properties of the filament. Due to the limited resolution of the printer the height of the flexures was not exactly equal to 9.76 mm. Lastly, the flexures showed some discontinuities. Although this has not a large effect on the overall stiffness it does have a large effect on the total strength.

- The jumps in force for the 10 mm flexure correspond to the fact that not all flexures moved similarly and even making contact at some times, followed by a snapping of one of the flexures. This behaviour is likely the result of a thickness variations inside each flexure and between the different flexures. This was also observed when looking at the flexures, where one of the flexures showed a considerable thickening near the centre as a result of the start-stop location of the print head.
- The occurrence of the first buckling mode is likely caused by a low torsional stiffness of the flexure set and imperfect alignment. Because of the long flexures in combination with an imperfect alignment can results in a small rotational deviation, making the system to follow the first buckling mode. Additionally, a small rotation of the flexure set can have a considerable impact on the width of the negative stiffness region.

Comparing the results from the experiment with the FEM simulations, as depicted in Fig. D.4. It can be observed that the simulated 0.4 mm thick flexures have a higher stiffness than the fabricated flexures. Taking a thickness of 0.37 mm follows the experimental results better. This difference is likely the result of the previously discussed issues with the manufacturing of the flexures. A similar problem was observed by Qiu et al. [87]. Additionally, the experimental results seem somewhat shifted to the right, correcting this causes the FEM results and experimental results to better overlap each other. Note that this shifting does not influence the stiffness of the flexures, since the slope remains the same. However, the endpoints no longer coincide. This difference is likely caused by the presence of initial stresses in the setup.

D.3.3. Conclusion: Experiment 1

Based on the experiments and the comparison with the FEM solutions it can be concluded that using pre-curved flexures is an option to obtain a nearly linear negative stiffness profile. However, the fabrication of these flexures is a matter of concern, because of the small thickness of the flexures. Using FDM printing to produce the flexures is possible, but extra attention must be paid to the slicing process

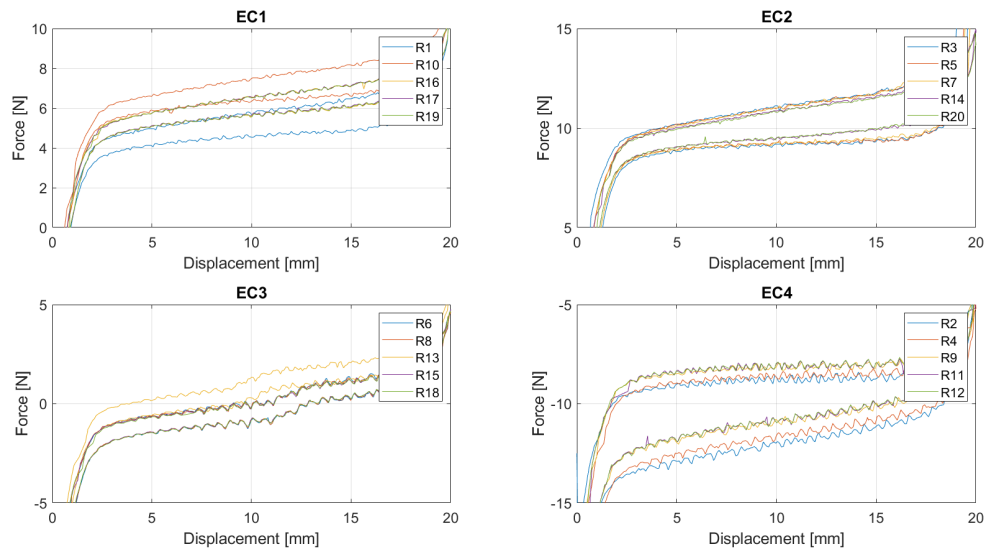


Figure D.5: Experimental load-displacement graph of the constant force mechanism for four different levels of adjustment

to obtain uniform flexures. Other production methods worth considering are waterjet cutting and wire edm. Another possible solution would be to use strips cut from a metal sheet, because the thickness of these sheets is considerably more accurate. However, this requires the metal strips to be pretensioned. Furthermore it can be concluded that FEM can be used to model the behaviour of the flexures, however extra attention must be paid to the manufacturing constraints and the material properties, since a slight change in thickness can have a considerable impact on the stiffness both experimentally and in simulations. Additionally, misalignment of the components can have a considerable impact on the mechanism's behaviour. Consequently, care must be taken during manufacturing and assembly.

D.3.4. Results and discussion: Experiment 2

The results of the second experiment where the flexures were used in combination with an ordinary coil spring are depicted in Fig. D.5 and Fig. D.6. In Fig. D.5 the four different experimental conditions are shown separately. Fig. D.6 shows the combined results of the second, third and fourth experimental condition. For clarity the first experimental condition has been omitted in these figures. Based on these two figures the behaviour of the mechanism can be explained as follows

- The difference in force between the forward and backward path is likely the result of friction within the system.
- The jump around the zero-force crossing in EC3 is likely the result of play in the system. Thus, a change in the direction of the force results in a small movement of the coil springs thus resulting in a different force magnitude.
- The difference in stiffness between the forward and backward motion especially for EC2 and EC4 is likely caused by a direction dependent stiffness term, which also makes the effect more pronounced in EC2 and EC4 compared with EC1 and EC3 as the forces in the first two are larger. The exact origin of this additional stiffness could not be found in the system but is likely caused by the presence of some form of contact. Having a large stiffness under compression and a low stiffness under tension.
- The fact that all the measurements start at a negative value is the result of prestress inserted in the system during mounting of the force sensor.
- The difference within the results for the different EC's cannot necessarily be attributed to the presence of plasticity in the flexures as the results for EC3 do not change between the first and last run.

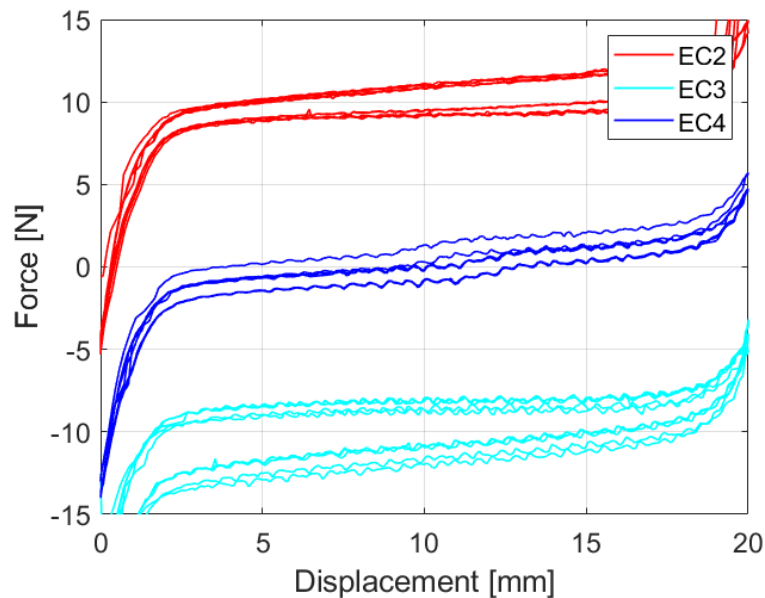


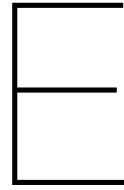
Figure D.6: Experimental load-displacement graph of the second, third and fourth level of adjustment

D.3.5. Conclusion: Experiment 2

From the experiments it can be concluded that the mechanism is adjustable across the desired force range. However, the stiffness of the flexures should be tuned more thoroughly to the stiffness of the coil springs. Additionally, the stiffness of the support structure must be taken into account as well, because some form of parasitic stiffness can be observed in the results.

D.4. Conclusion

One of the issues with using curved beam is the manufacturing process, because of the small feature size. The initial prototypes were made using an FDM printer with PLA. The thickness of the flexures was similar to the nozzle size thus limiting the accuracy of the flexure thickness. Additionally, the slicing of the flexures resulted in some issues, either the flexures showed discontinuities or start-stop points resulting in a local thickening. Especially this local thickening can have a considerable impact on the stiffness of the flexures. A possible solution would be to use a smaller nozzle size. However, the thickness accuracy remains an issue as the nozzle size has also limitations. Another drawback of FDM printing is the low stiffness of the materials such as PLA. However, for the intended application a stiffness of 1000-3000 N/m is required. As a single PLA flexure with a thickness of 0.4 mm and length of 100 mm can generate a negative stiffness of around 100 N/m a considerable number of flexures is required. Thus, for a more compact design stiffer materials such as titanium are desired. However, manufacturing such thin flexures is challenging using 3D printing or waterjet cutting, especially because for stiffer materials thinner flexures are likely required to prevent yielding.



Experimental results of inclined flexures

To validate the performance of inclined flexures several experiments have been performed with several configurations of the flexures. For this experiment the same setup has been used as discussed in Appendix D. The experiment involved measuring the force displacement characteristics of a mechanism consisting of straight flexures under inclination (Fig. E.1). Due to the way the mechanism is made the flexures can be mounted in two ways, resulting either in a compression or a tensile unit. All flexures are made of stainless spring steel of 0.2 mm, with a width of 4.2 mm and a free length of 50 mm. The following conditions have been evaluated.

- 4 flexures under an inclination of 15 degrees in the tensile configuration (one flexure per set) (C1)
- 8 flexures under an inclination of 18 degrees in the compressive configuration (two flexures per set) (C2)
- 4 flexures under an inclination of 15 degrees in the compressive configuration (one flexure per set) (C3)
- 8 flexures under an inclination of 15 degrees in the tensile configuration (two flexures per set) (C4)
- 8 flexures under an inclination of 19 degrees in the compressive configuration (two flexures per set) (C5)
- 8 flexures under an inclination of 18 degrees in the compressive configuration with reinforced mount (Two flexures per set) (C6)

The 8 flexures under 15° was not evaluated in the compressive configuration as this experiment was performed in an earlier stage after which the set of flexures was no longer available, because the

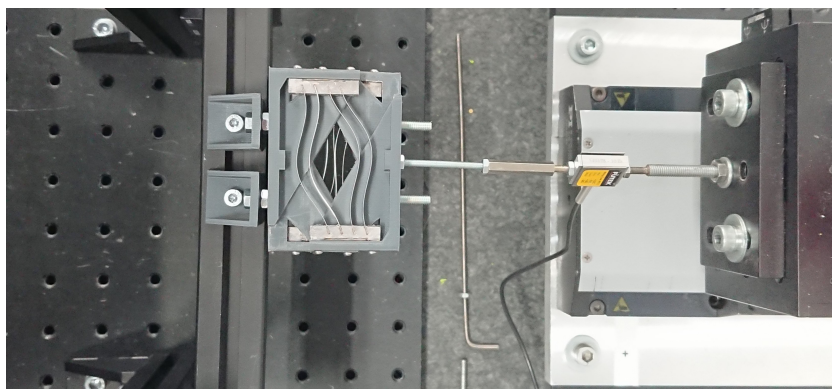


Figure E.1: Setup for measuring the load-displacement characteristics of the inclined flexures. The mechanism shown consists of 16 flexures, consisting of four flexures per set (as used in the final configuration). Note that the mechanism is already compressed by the motion stage.

flexures were reused to construct to other sets of flexures. The 8 flexures under 18° (C2) was only tested in the compressive configuration because the tensile configuration would not fit in the support structure as this was originally designed for the 15° . The same applies to C5.

During the experiments a couple of observations could be made

- During the C2 experiments it was observed that one of the flexures buckled in the opposite direction. This is likely caused by manufacturing errors as the flexures already showed some curvature in the undeformed shape.
- During the C2 experiments the first two measurements were performed with a lower total displacement.
- During the C5 experiments it was noticed that multiple flexures buckled in the opposite direction. This is likely caused by manufacturing errors as the flexures already showed some curvature in the undeformed shape. Additionally, some plastic deformation might have occurred in the flexures from previous experiments, as the flexures have been reused.
- For the C5 measurement a sharp increase in stiffness was observed at the end of the measurement. This increase was caused by mechanical contact between the mechanism and the measurement setup. This was not an issue during the other measurements as during those measurements an additional spacer was placed between the measurement setup frame and the mechanism.

E.1. Results and discussion

When looking at the C1, C3 and C4 measurements in Fig. E.2. it can be noticed that the differences within each experiment are relatively small. However, when looking at C2 some larger differences can be observed especially between the first two and the consecutive measurements. This difference is likely caused by some initial plasticity occurring in one of the flexures, possibly in the flexure which buckled in the opposite direction as the other flexures.

When comparing the results from the elliptic integral method with the measurements, two distinct differences can be observed. First of all, for all configurations the stiffness is significantly different from the simulation. This is likely caused by the influence of the stiffness of the support structure which acts in series to the flexures, thus decreasing the overall stiffness. When looking at C1, C3 and C4 it can be observed that the negative stiffness range is considerably smaller. The difference at the beginning can be explained due to the finite stiffness of the support structure, while the difference at the end is likely caused by some differences between the flexure length, inclination angle and support stiffness. However, when looking at the C2 measurement the last part of the negative stiffness range is almost similar.

Comparing the different experiments with each other it can be noticed that changing the inclination angle will considerably increase the negative stiffness range, while having a little effect on the stiffness itself. This is also in accordance with the results from the simulations. Another remarkable thing which can be observed is that the zero-crossing (the unstable equilibrium point) occurs at roughly the same location for the simulations and the experiments.

Some small differences can be observed between C1 and C3. One of the possible causes of the difference is the alignment with the force sensor. As the mechanism had to be removed and reassembled between the different experiments it is possible that the mechanism was slightly tilted during the connection to the force sensor. This has likely the largest effect on C1 and C3, while they have a very low torsional stiffness. In fact, in this configuration these types of flexures are also used for compliant hinges and are called cross-flexural hinges.

For the calculation of the stiffness a linear curve is fitted through the data of the forward and backward part of the curve between 4 and 12 mm for C1, C3 and C4, between 5 and 15 mm for C2 and 6 and 16 mm for C5 as the movement range for C2 and C5 is larger. Since the first two measurement of C2 are different from the rest they are not considered in determining the stiffness, the same applies to the higher resolution measurements. The results are tabulated in Table E.1 from which can be concluded

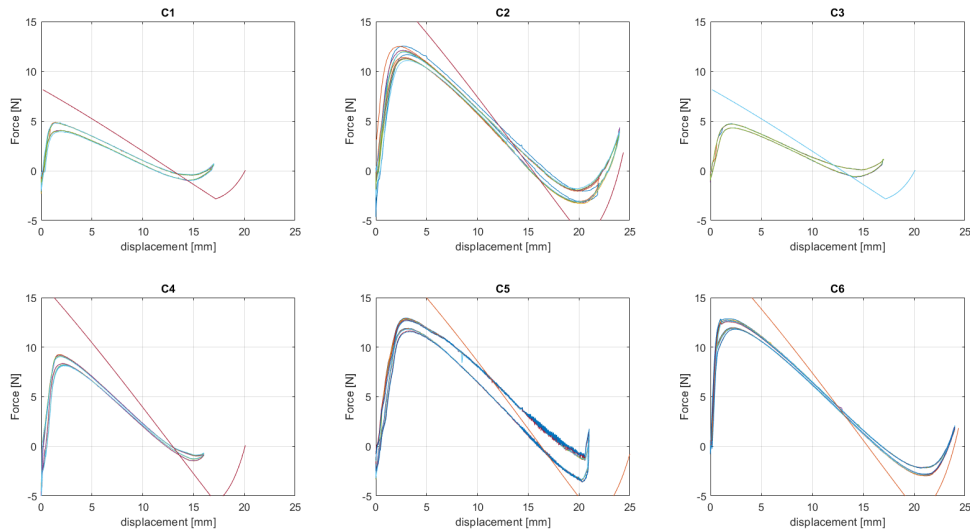


Figure E.2: Load-displacement graphs of the different experiments

Table E.1: Stiffness (N/m) of the flexures in the negative stiffness regime. Obtained by performing a curve fit through a part of the region

	C1 (n=5)	C2 (n=3)	C3 (n=5)	C4 (n=4)	C5 (n=6)	C6 (n=6)
Forward	-0.48	-0.97	-0.45	-0.94	-0.95	-0.95
Backward	-0.48	-1.02	-0.48	-0.91	-1.03	-0.95
Mean	-0.48	-0.99	-0.46	-0.92	-0.99	-0.95
Simulation	-0.64	-1.29	-0.64	-1.28	-1.29	-1.29

that there is a large difference between the simulations and experiment. Additionally, some difference can be observed between the forward and backward motion, which differ by at most 6%. As C2 and C3 involve a different flexure orientation as C1 the results of the forward and backward motion cannot be compared directly.

To study the effect of the support stiffness of the flexures experiments were performed using a reinforced flexure mount. This flexure mount was made by plating the original 3D printed block with stainless steel plates. Comparing the results of C2 and C6 a noticeable influence of this increased support stiffness can be observed as the initial phase in the load-displacement graph (Fig. E.2) is shorter.

E.2. Evaluation of final configuration

For this experiment the same setup was used as in the previous section. The experiment involved measuring the force displacement characteristics of a mechanism consisting of straight flexures under an inclination of 18° . All flexures are made of stainless spring steel of 0.2 mm, with a width of 5.08 mm and a free length of 50 mm. A total of sixteen flexures were used, which were mounted in groups of four (Fig. E.1). Each mount was made of PLA and reinforced on both sides and the bottom with 0.5mm stainless steel plates, cut in the same profile is the PLA. The stiffness of each run is determined for a displacement of 5 till 12 mm.

E.2.1. results and discussion

Based on Table 2 the mean stiffness is equal to -2.60 N/mm, which was slightly larger than expected (7.4%) as it was designed for -2.42 N/mm. This design was based on the stiffness value determined during the C6 experiment by looking at the total width of the flexures. Changing the width of the flexures

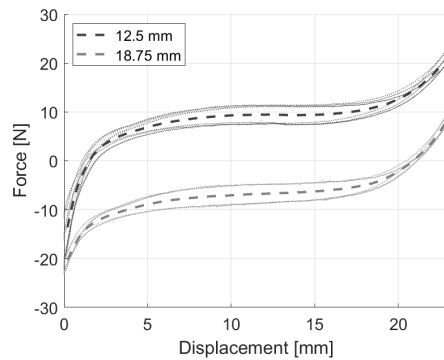


Figure E.3: Load-displacement graph of the improved prototype of the adjustable constant force mechanism for two adjustment levels. The dashed line indicate the mean curve of the complete motion cycle. The dotted lines display the raw data

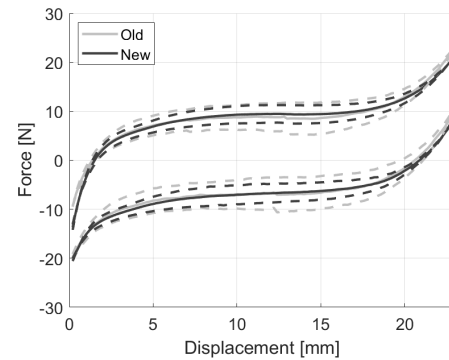


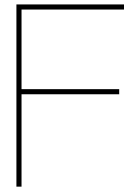
Figure E.4: Comparison between the old and new prototype of the mechanism

is the easiest parameter to tune, as the (negative) stiffness scales linearly with the width. So, for the C6 experiment the total flexure width was equal to $4.2 \cdot 8 = 33.6$, which resulted in a stiffness of -1 N/mm. By extrapolating this to a stiffness of -2.42 the required flexure width is 88.312 mm, dividing this by sixteen flexures results in a flexure width of 5.08 . The fact that now a higher stiffness is observed than expected can be attributed to several factors

- Manufacturing errors. The flexures were cut to size, however with this it is difficult to cut with an accuracy lower than 0.1 mm, thus the width of the C6 flexures can deviate a bit from 4.2 mm (used for C6) and the same applies to the new flexures.
- Presence of pretension. When disassembling the flexures, it was observed that a considerable amount of plasticity had occurred and the length of the different sets was different. The change in length is also likely caused by microslip of the flexures inside the mount, causing them to move partially out of the mount.
- Contact between flexures
- Higher overall stiffness. Looking at the stiffness in the first part of the C6 and the current experiment (linear positive stiffness), which can to some extent be considered as a measure of the systems stiffness. The initial stiffness during the current experiment was slightly larger than for the C6 experiment (25 against 19 N/mm). As a lower stiffness of the support structure results in a lower negative stiffness, this can possibly explain the higher negative stiffness as the system stiffness is somewhat larger. Note however that having more flexures also results in a higher stiffness (e.g., when comparing C1 (6 N/mm) and C4 (12 N/mm) of the previous experiment).

E.3. Constant force mechanism

As extensively discussed in Chapter 4 the inclined flexures were combined with a coil spring having a similar stiffness to generate a constant force mechanism. While the hysteresis in both the coil springs and negative stiffness element was observed to be small (e.g. Fig. E.2) after combining them the hysteresis was considerably larger. One of the origins of this hysteresis is the occurrence of contact between the two components of the negative stiffness element. Although this was not an issue in the separate configuration, a slight eccentric loading caused the parts to come into contact. So a new prototype was fabricated with a larger spacing between the two parts of the negative stiffness element. The load-displacement characteristics were again evaluated experimentally (Fig. E.3) showing a similar constant force region as the results from Chapter 4. Comparing the results between the two experiments it can be observed that as a result of the increased spacing the width of the hysteresis curve decreased by almost a half (Fig. E.4). Another source of hysteresis is the contact between the side-walls of the mechanism and the negative stiffness mechanism. Although not considered further, this can be solved by increasing the spacing between the sidewalls and the negative stiffness mechanism, by increasing the overall width of the mechanism.



Interface

For a wrist support the interface with the body is of importance to consider. As such, different types of interfaces were investigated. The design of the interface involves two factors. The transmission of the force and the attachment to the hand and forearm.

F.1. Transmission

Different methods of force transmissions have already been investigated by Haarman [7] for the finger in the development of a hand orthosis. However most of these mechanisms can be directly translated to the wrist. An overview of these transmissions including additional ones are given in Fig. F.1.

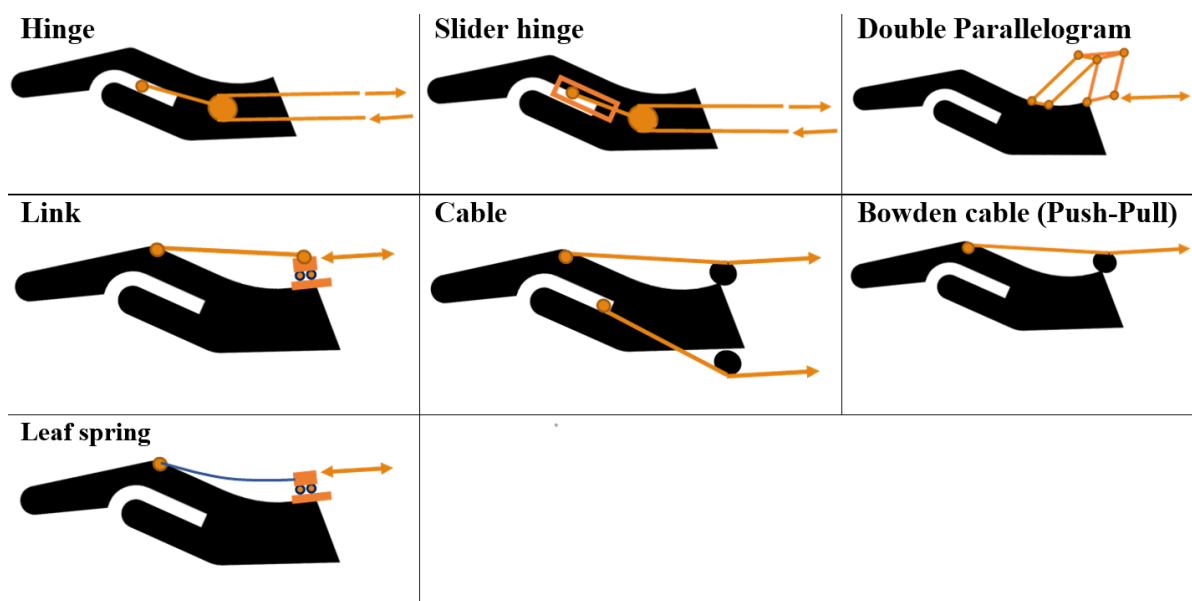


Figure F.1: Overview of different methods to apply a force or torque the hand

For choosing the type of transmission two important points must be taken into account the relation between the input-output torque must be constant and the prevention of misalignment. The constant relation is of importance as the output should be an approximately constant torque around the wrist when a constant force is provided as input. Misalignment should be prevented as it results in excessive forces being exerted on the wrist joint and hand potentially causing discomfort. When considering the linearity between the input and output only the hinge is capable of providing a constant relation. However, when a rigid hinge is used a small misalignment of the hinge joint axis and the wrist joint axis can already cause problems. All other proposed methods are capable of handling some misalignment.

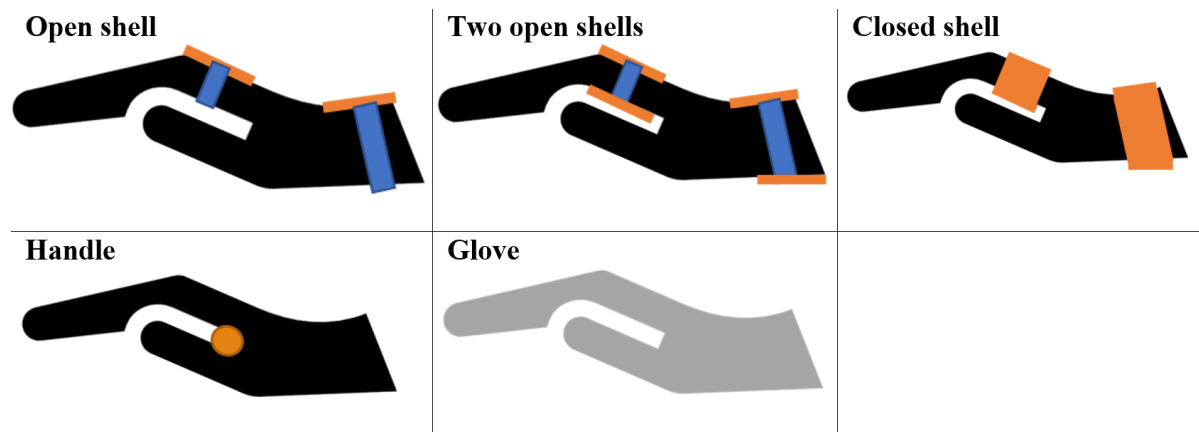


Figure F.2: Overview of different methods to interface with the hand and forearm



Figure F.3: First prototype of the interface, the mounting holes can be used for the attachment of a transmission



Figure F.4: Second prototype of the interface, the elastic band in combination with the Velcro® strap allow for easy donning and doffing of the interface. The transmission can be attached through a hole at the side of the interface

Of these methods the slider hinge is the most favourable as it is capable of handling some misalignment whereas the relation between input and output is almost constant (if no misalignment is present the mechanism behaves similar to the hinge)(Appendix G). On the other hand, for the other methods the relation between input and output forces depends on the position of the wrist, resulting in a non-constant transmission. Another drawback of most transmissions placed on top of the hand (e.g., link or cable), is that due to the small lever arm, a large force must be exerted to balance the weight. However this large force has to be taken up by the wrist, potentially causing some discomfort

F.2. Attachment

Besides the transmission the method of connecting the mechanism to the hand and forearm is of importance. Some possible solutions are depicted in Fig. F.2. For the attachment of the mechanism to the hand several factors must be considered, which are the comfort, ease of donning and doffing and restriction of movement. When considering the ease of donning and doffing a glove or a closed shell is less favourable as they have to be moved over the hand, whereas the other methods can make use of for instance Velcro® straps to tighten or loosen it. When looking at the restriction of movement having a rigid part located in the palm of your hand is less favourable as it obstructs closing of the hand. Based on these considerations the use of an open shell was further investigated through some prototype.

F.2.1. Prototypes

The first prototype is depicted in Fig. F.3. It was made using a thermoplastic material, which can be easily modelled to the hand's shape upon heating with hot water. Velcro® straps were used to attach it to the hand and forearm. However based on some user feedback it became clear that donning-doffing

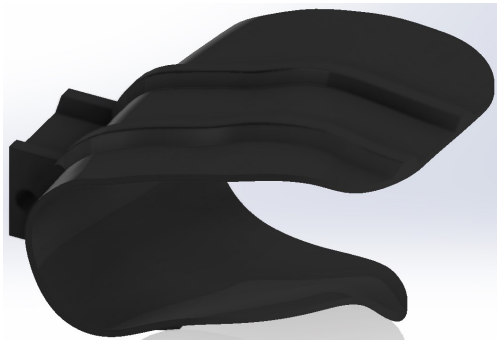


Figure F.5: Model of the shell for the hand interface. The rims are included to increase the stiffness of the shell. To block on the left side contains a hole for the attachment of the transmission

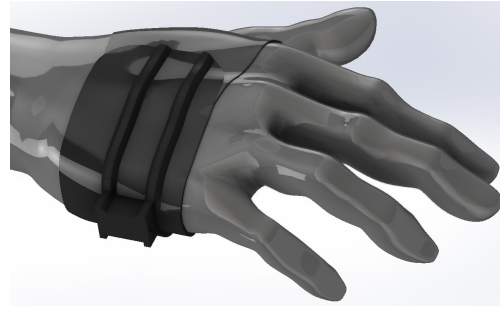


Figure F.6: Model of the shell in combination with a model of the hand. From this image it can be observed that the interface follows the curvature of the hand

was challenging due to the configuration of the Velcro® straps, while sufficiently tightening it was also challenging. Additionally this prototype was not suitable for combining with a hinge type of transmission as the connections are located at the dorsal side of the hand. As such a new prototype was made (Fig. F.4), which was also used in the test setup of the experiment (Appendix A). The shell part of this prototype was 3D printed (Fig. F.5 and Fig. F.6) based on a CAD model of the hand [102]. To improve the comfort the shell was covered with cloth. The interface can be donned-doffed using a Velcro® strip and an elastic band, which also allows tightening of the interface to accommodate different hand sizes.

The comfort of this prototype was evaluated during the experiment. In general it was considered as comfortable, but for some participants it was a bit too small or too large. Consequently, using various standard sizes, such as S, M or L would be a solution. As the prototype is based on a CAD model of the hand, making different sizes for the interface can be achieved relatively straightforward by scaling the CAD model.

G

Interface models

To determine which type of interface to choice from, some mathematical models were made to evaluate the required compensation force/torque and its deviation from the constant input force.

G.1. Cable and Bowden cable

Applying the forces using some form of cable, the required balancing force can be expressed as

$$F_b = mgL_h \cos(\phi + \theta) \cos \psi \frac{\sqrt{L^2 + a^2 + b^2 + c^2 - 2aL \sin \phi + 2bL \cos \phi - 2ac \cos \phi - 2bc \sin \phi}}{aL \cos \phi - ac \sin \phi + bL \sin \phi + bc \cos \phi} \quad (\text{G.1})$$

Here the variables are defined according to Fig. G.1. Additionally, the cable length and the stroke are given by

$$l(\phi) = \sqrt{L^2 + a^2 + b^2 + c^2 - 2aL \sin \phi + 2bL \cos \phi - 2ac \cos \phi - 2bc \sin \phi} \quad (\text{G.2})$$

$$s = l(\phi_2) - l(\phi_1) \quad (\text{G.3})$$

This model depends on several variables. An example of the influence of changing one of these parameters is depicted in Fig. G.3 and Fig. G.4. From this it can be observed that especially for large angles the forces start to deviate when an offset is applied. Consequently, b should preferably be as small as possible. Although these variables can be considered as design variables, some uncertainty in these values should be taken into account as the location of the wrist joint centre is in general not exactly known.

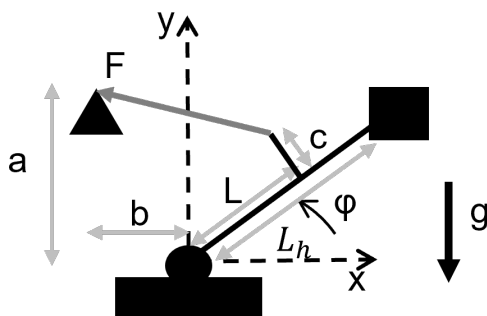


Figure G.1: Schematic of the cable transmission

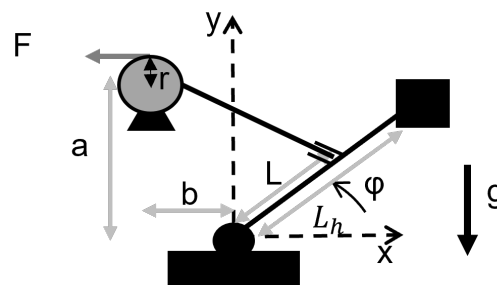


Figure G.2: Schematic of the slider hinge transmission

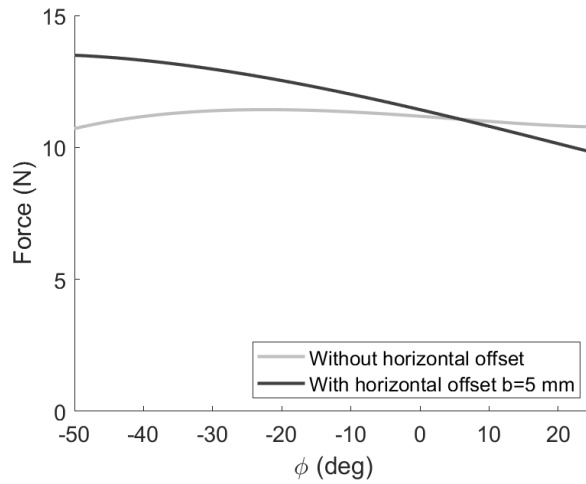


Figure G.3: Influence of horizontal offset on the required balancing force based on the cable model. Showing the force for the same conditions as in Chapter 5 and $a=20$ mm, $b=0$ mm, $c=15$ mm and $L=50$ mm.

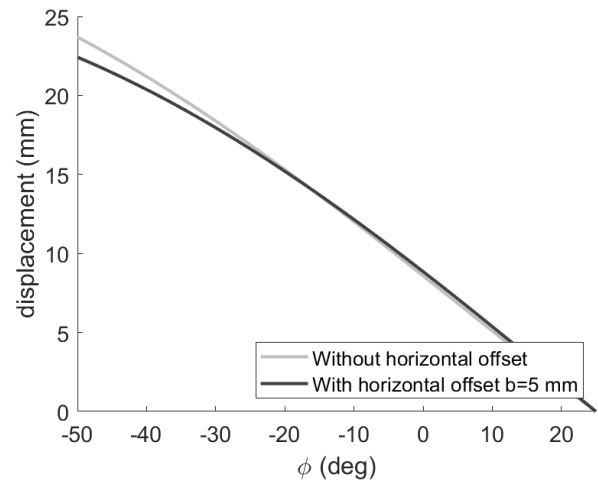


Figure G.4: Influence of horizontal offset on the stroke of the mechanism based on the cable model.

G.2. Slider hinge

Applying the forces using a slider in combination with a hinge to accommodate misalignment the required balancing force can be expressed as

$$F_b = mg \frac{L_h}{r} \cos(\phi + \theta) \cos \psi \frac{\sqrt{(a - L \sin \phi)^2 + (b + L \cos \phi)^2}}{L^2 + bL \cos \phi - aL \sin \phi} \sqrt{a^2 + b^2 + L^2 - 2L\sqrt{a^2 + b^2} \cos\left(\pi - \phi - \arctan \frac{a}{b}\right)} \quad (\text{G.4})$$

Here the variables are defined according to Fig. G.2. Note in the case there is no misalignment ($a, b=0$) the equations can be simplified to the equation for an ordinary hinge

$$F_b = mg \frac{L_h}{r} \cos(\phi + \theta) \cos \psi \quad (\text{G.5})$$

Additionally the stroke of the mechanism can be expressed as

$$l(\phi) = r \arcsin \left(\frac{c \sin\left(\phi + \arctan\left(\frac{a}{b}\right)\right)}{\sqrt{a^2 + b^2 + c^2 + 2c \cos\left(\phi + \arctan\left(\frac{a}{b}\right)\right) \sqrt{a^2 + b^2}}} \right) \quad (\text{G.6})$$

$$s = l(\phi_2) - l(\phi_1) \quad (\text{G.7})$$

Which for no misalignment simplifies to

$$l(\phi) = r\phi \quad (\text{G.8})$$

The influence of the misalignment can be observed from Fig. G.5, showing a shift and slight deformation of the torque curve compared to the case of no misalignment. Consequently as the delivered torque is based on the hinge model the delivered torque will underestimate the required torque in the case of a misalignment. Additionally from Fig. G.6 it can be observed that there is an offset between the input and output angle, but the relation remains approximately linear

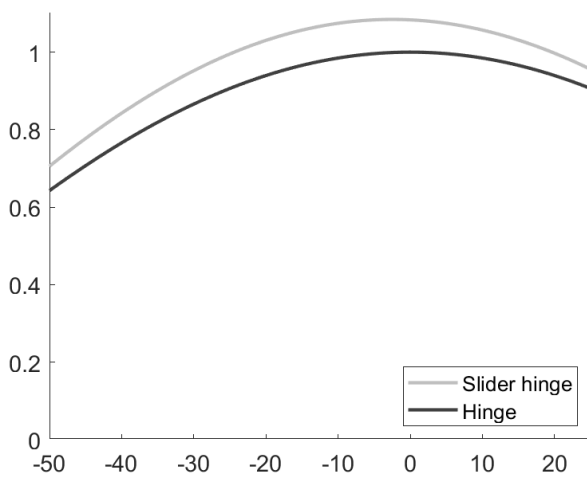


Figure G.5: Influence of misalignment based on the hinge slider model. Showing the torque for the hinge slider and the hinge with a misalignment of 5 mm ($a=3$ mm, $b=4$ mm, $L=50$ mm and $c=50$ mm).

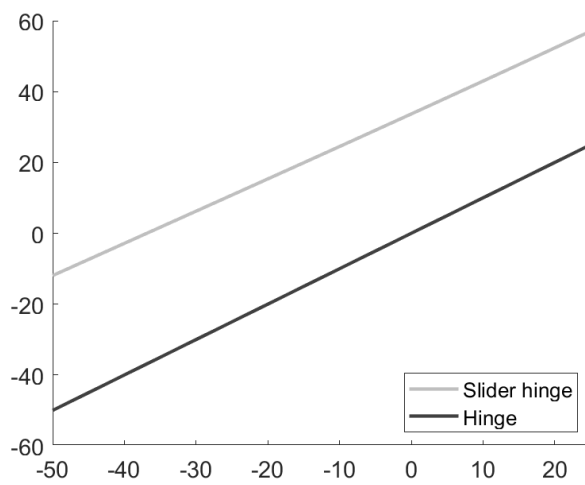


Figure G.6: Influence of misalignment on the relation between the input and output angle. Here the input angle is considered as the flexion of the wrist (ϕ) and the output angle the rotation of the hinge where the forces are applied to.



Wrist support evaluation

To evaluate the performance of the wrist support a prototype was made. However from this prototype it immediately became clear that a considerable amount of friction was present in the transmission from the constant force mechanism to the hand. Although these issues were not insurmountable it required a redesign of the transmission, requiring manufacturing of a large part of the device over again. However by using a different transmission based on a cable and a pulley the majority of the mechanism could be retained. The drawback of using this different transmission is that the forces no longer behave perfectly constant, making it inappropriate for evaluating the use of a constant force. Despite these limitations an experiment was performed as an initial investigation of the device.

H.1. Method

For this exploratory experiment the same setup was used as in the main experiment as discussed in Chapter 3. However in the current experiment the forces are generated through the wrist support mounted to the forearm. Furthermore for this experiment the same protocol (e.g., sensor placement, MVC measurements and forearm orientation) as the main experiment. However due to restrictions of the mechanism the 50° palmar flexion of the wrist could not be evaluated. Besides no support, four different levels of compensation were evaluated based on four different adjustment levels of the constant force mechanism (17, 18, 19 and 20 mm). These four adjustment levels approximately correspond to an output force of the mechanism of respectively 2.7, 5.2, 7.8 and 10.4 N (based on the model presented in Chapter 4). The order of both the wrist position and level of compensation was randomised and the measurements were repeated five times. However the measurements for no support were repeated six times, three times before and three times after the measurements with compensation, to limit the required donning and doffing of the mechanism.

H.2. Results

The experiment was performed with one participant of which the characteristics are depicted in Table H.1. The results of the experiment is depicted in Fig. H.1, showing the influence of the different compensation methods.

H.3. Discussion

From the results of the experiment it can be observed that there is an effect of the wrist support. However these effects are not all expected. For instance when considering the activity of the extensor muscle at 25° dorsal flexion an increase in activity is observed when the level of support is increased.

Table H.1: Participant characteristics, reported as mean and standard deviation.

Gender	Age (years)	Weight (kg)	Height (m)	Hand weight (g)	Centre of mass (mm)
Male	24	61	1.88	353	43.6

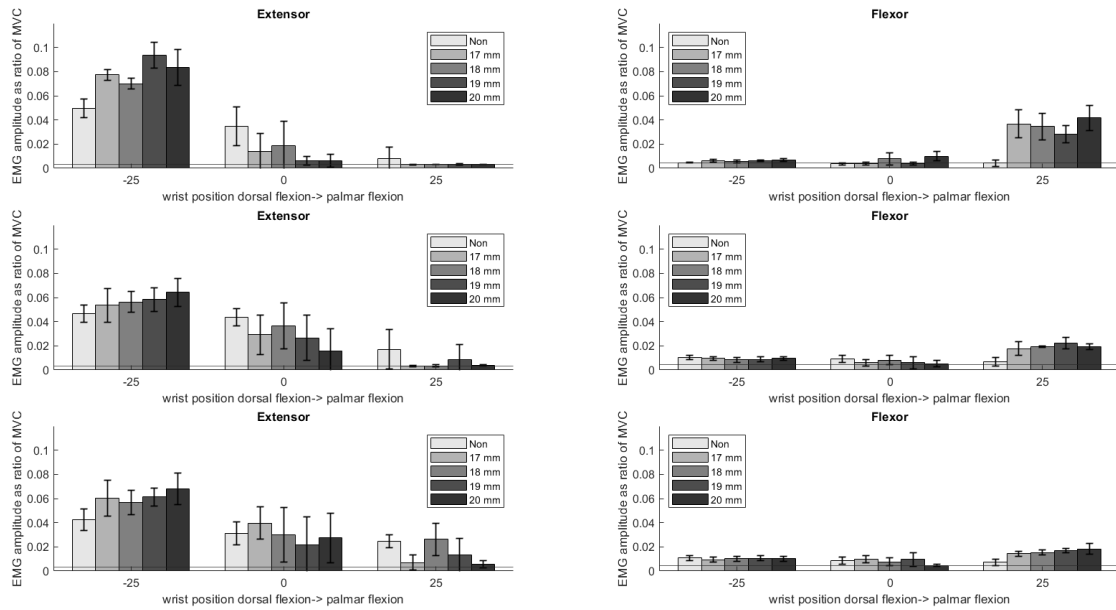


Figure H.1: Mean sEMG magnitude relative to the MVC of the ECR (left) and FCR (right) for different forearm, wrist positions and balance methods

This increase is likely a consequence of how the forces are applied by the cable and pulley system, resulting in an opposing force instead of an assisting force at the level of dorsal flexion. During the experiment it also became clear that friction had a substantial influence, as clearly a stick-slip motion was observed, causing the cable to become slack at some instances, consequently providing no support. This was especially of an issue with the 17 mm adjustment, which is also something to be expected as the output force is close to zero. Considering the results of the flexor muscle the outcomes are more in line with the expectations based on the main experiment, showing an increase in activity for palmar flexion when a form of support is used. Nonetheless, the increase is larger than observed in the main experiment, which primarily showed an increase at 50 palmar° flexion.

H.4. Conclusion

Based on this experiment the following recommendations can be made related to the future design of the wrist support. First of all, more attention must be paid to the transmission of the forces to the hand, as the current implementation of a cable-pulley system is unable to provide a constant torque and has a limited motion range as the cable must be kept taut. Second, the friction should be decreased, which became especially apparent due to the occurrence of stick-slip motion. Despite these issues related to the transmission and friction, it can be concluded from the experiment that the mechanism is wearable and with some improvements is capable of being implemented in a wrist support.

Interaction effects

As in Chapter 3 only a part of the experimental results could be considered a more extensive overview of the results is presented here. Although the main results are considered here as well the focus of this section is on the interaction effects between the three different experimental factors (forearm position, wrist orientation and balancing method)

I.1. Extensor muscle

Using Mauchly's test it was observed that the assumption of sphericity had been violated for the main effects of wrist position, $\chi^2(5) = 21.04, p < .001$ and balance method $\chi^2(5) = 15.04, p = .011$. Consequently, the degrees of freedom were corrected using Greenhouse-Geisser estimates of sphericity. The effect of wrist position and balance method were observed to be significant ($p < .001$). When considering the effect of balance method, a significant main effect was observed of the method on the EMG activity, $F_{1,31,9,18} = 28.93, r = 0.87$. Contrasts showed that the activity using a form of support were 51% ($p < .001, F_{1,7} = 62.234, r = 0.95$), 53% ($p < .001, F_{1,7} = 73.243, r = 0.96$), and 46% ($p < .001, F_{1,7} = 70.027, r = 0.95$) lower than without support for respectively constant, linear and sinusoidal. Additionally the overall activity reduction for the linear profile is significantly higher than the sinusoidal profile ($p = .041, F_{1,7} = 6.23, r = 0.68$). When looking at the interaction effects a significant interaction was observed between the wrist position and the balance method ($p = .002, F_{1,92,13,42} = 10.06, r = 0.65$) and the wrist position, balance method and forearm position ($p < .001, F_{3,77,26,37} = 7.66, r = 0.47$).

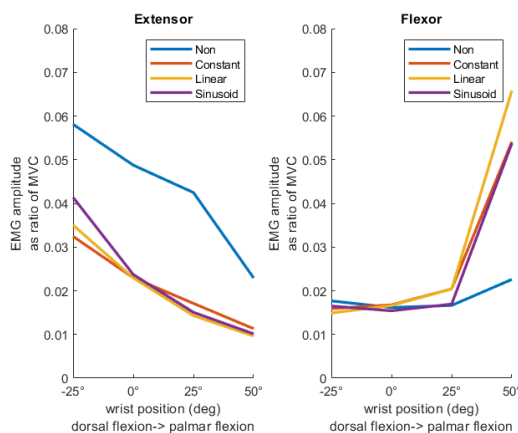


Figure I.1: Interaction plot showing the interaction between the balance method and the wrist position

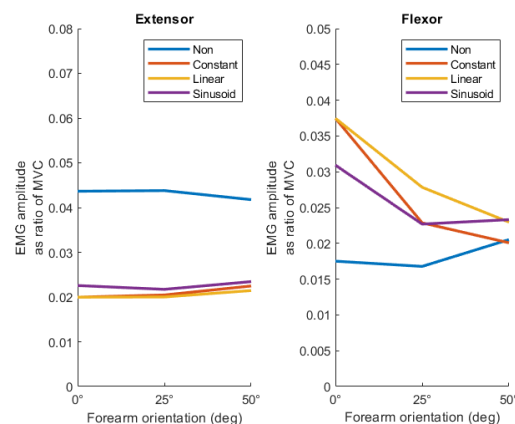


Figure I.2: Interaction plot showing the interaction between the balance method and the forearm position

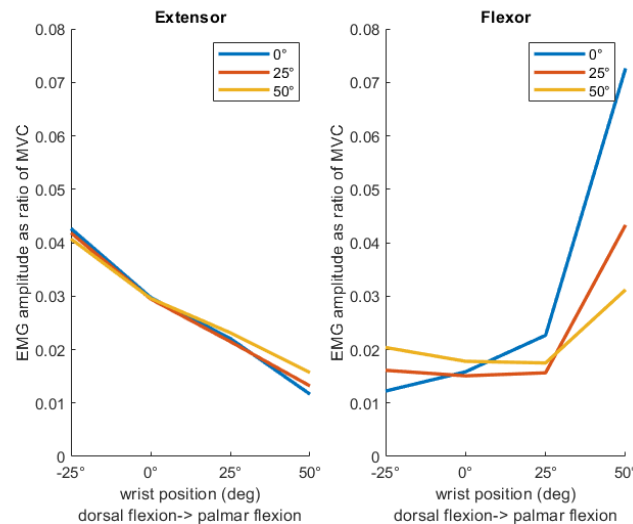


Figure I.3: Interaction plot showing the interaction between the wrist position and the forearm position

I.1.1. Interaction effects

To further investigate the interaction effects, contrasts were performed. For this the no support, 0° wrist flexion and 0° forearm position were considered as baseline. Considering the interaction between the wrist position and balance method the following observations can be made. For dorsal flexion only a significant interaction effect was observed for the sinusoidal profile ($p = 0.007, F_{1,7} = 14.52, r = 0.82$). This can also be observed from Fig. I.1, showing a steeper slope than the other balancing methods. For 50° palmar flexion a significant effect is observed for all compensation methods (constant ($p = .009, F_{1,7} = 12.531, r = 0.80$), linear ($p = .044, F_{1,7} = 6.04, r = 0.68$) and sinusoidal ($p = .028, F_{1,7} = 7.567, r = 0.72$)), showing a lower decrease in activity than for no support. Besides comparing no support to any type of support this study also investigated the difference between the sinusoidal torque profile and the simplified torque profiles. Consequently, performing again contrast, but now with the sinusoidal torque profile as a reference some additional observations can be made. For dorsal flexion only a significant interaction effect was observed for no support ($p = .007, F_{1,7} = 14.52, r = 0.82$), constant ($p < .001, F_{1,7} = 37.91, r = 0.92$) and linear ($p = .006, F_{1,7} = 15.458, r = 0.83$). This can also be observed from Fig. I.1, showing a steeper slope than the other balancing methods. When considering the other interaction graphs (Fig. I.2 and Fig. I.3) no large differences in slope are present, indicating only a small interaction.

I.2. Flexor muscle

Using Mauchly's test it was indicated that the assumption of sphericity had been violated for the main effects of wrist position, $\chi^2(5) = 29.78, p < .001$. Consequently, the degrees of freedom were corrected using Greenhouse-Geisser estimates of sphericity. The effect of wrist position ($p < .001$), balance method ($p < .001$) and forearm orientation ($p = .008$) were observed to be significant. Contrasts showed that the activity using a form of support were 50% ($p = .002, F_{1,7} = 22.76, r = 0.87$), 61% ($p < .001, F_{1,7} = 30.66, r = 0.90$) and 44% ($p < .001, F_{1,7} = 31.13, r = 0.90$) higher than without support for respectively constant, linear and sinusoidal. Additionally the activity increase for the linear profile is significantly higher than for the constant profile ($p = 0.016, F_{1,7} = 10.06, r = 0.77$). When looking at the interaction effects a significant interaction was observed between the forearm and wrist position ($p = 0.047, F_{1,19,8.32} = 5.20, r = 0.62$), forearm position and balance method ($p < .001, F_{6,42} = 5.64, r = 0.34$) and wrist position and balance method ($p = .001, F_{1,443,10.01} = 16.75, r = 0.79$)

I.2.1. Interaction effects

To further investigate the interaction effects, contrasts were performed. For this the no support, 0° wrist flexion and 0° forearm position were considered as baseline. Considering the interaction between the wrist position and balance method the following observations can be made. For all levels of palmar

flexion there is a significant interaction effect for all compensation methods except the sinusoidal profile at 25° palmar flexion. This can also be observed from Fig. I.1, where the constant and linear profile start to deviate from no support after 0° palmar flexion and the sinusoidal after 25° palmar flexion. Considering the interaction between the forearm and wrist position only a significant interaction is observed at 25° palmar flexion for the forearm at 50° ($p = .024, F_{1,7} = 8.26, r = 0.74$). This can also be observed from Fig. I.3, showing an increase in activity from 0° to 25° palmar flexion for the forearm at 0°, whereas for the forearm at 25° and 50° there is no increase or even a slight decrease. Considering the interaction between the forearm position and balance method all compensation methods show a significant interaction effect for the different forearm positions with respect to the horizontal position except for the sinusoidal profile with respect to no support. This can also be observed from Fig. I.2, showing an overall decrease of activity for increasing forearm orientation for the constant and linear torque profile, whereas the sinusoidal profile and no support start to increase slightly after the 25° position. When considering the sinusoidal torque profile as the reference for the contrasts the following observations can be made. For the interaction between the wrist position and balance method, besides the significant interaction effect for no support, there is also an effect for the linear profile at 25° palmar flexion ($p = 0.047, F_{1,7} = 5.79, r = 0.67$). There is no significant interaction effect for forearm and balance method considering the different forearm positions and balance methods.

I.3. Discussion

When comparing the results presented in this section with the results from Chapter 3 it can be noticed that some conditions are considered as significant which were not the case in the Chapter 3. This is a consequence of the fact that here simple contrast were used instead of a post hoc test. Here contrasts are used for the investigation of the interaction effects and it allows for more straightforward calculation of the effect sizes. Chapter 3 involved a post hoc test as it was not yet a clear if the simplified torque profiles would result in a smaller or larger effect on the muscle activity compared to the sinusoidal torque profile (e.g., no assumptions on the direction of the hypothesis). The differences in outcomes are caused by the fact the post hoc test can be considered as more conservative [103] and the post hoc test assumes a two-tailed hypothesis, while the contrasts assume a one-tailed hypothesis. Although between the two methods there are some differences between what is considered as significant, the general conclusions are the same, showing an overall increase in activity of the anti-gravity muscle when a form of support is used, while the difference between the different compensation methods are small.

Another remarkable thing which can be observed is the limited effect the forearm orientation has on the extensor activity, while the torques generated by gravity show a far larger decrease. However this ignores the influence of the wrist position, when only considering the neutral position of the wrist a decrease of activity of 24% is observed compared to a decrease in the required balancing torque of 36%. Some differences between these two values are expected as for the calculation of the required torque it is assumed that the wrist behaves as a frictionless pendulum. Additionally the relation between activity and torque is not necessarily linear [104].

J

Manufacturing

J.1. Prototype

A large part of the adjustable constant force mechanism was 3D printing using an FDM printer and can thus be easily replicated. However the manufacturing of the flexures sets was a bit more complicated and thus deserves some elaboration.

Each flexure set consisted of several components which were glued together using an epoxy.

- Stainless spring steel flexures, cut from a flat sheet of 0.2 mm thick
- PLA mounting block, for mounting of the flexures. The challenge in designing this block was determining the required gap width to allow insertion of the flexures. After some tests using various gap sizes it was concluded that a width of 0.23 mm was the most appropriate, enabling relatively easy insertion of the flexures, while having only a limited amount of play.
- Stainless steel reinforcements. As the stiffness of the PLA mounting block is relatively small, whereas the forces exerted on it by the flexures are relatively high, it was decided to reinforce the mounting blocks, to limit the influence the mounting block has on the behaviour of the flexures. As such, 0.5 mm stainless steel plates were cut to the same profile as the mounting block and glued to the sides of the mounting block. Consequently, the flexures are fixed in both the stainless steel plate and the mounting block.

The assembly of the flexure sets from this components consisted of two steps. First the stainless steel reinforcements were glued on to the mounting block. After this, two of these components were mounted in a frame, as a reference for the shape of the flexure set (Fig. J.1). Second, with the reinforced mounting block fixed in place in the frame the flexures were glued inside the mounting block. This process was repeated for each flexure set.



Figure J.1: Flexures and the reinforced mounting block attached to the frame used for keep the position of the mounting block fixed during insertion of the flexures.

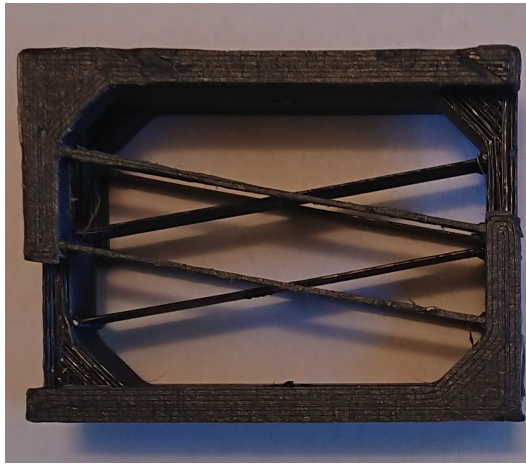


Figure J.2: Prototype of the monolithic negative stiffness mechanism using inclined flexures in its undeformed state



Figure J.3: Prototype of the monolithic negative stiffness mechanism using inclined flexures in its deformed state

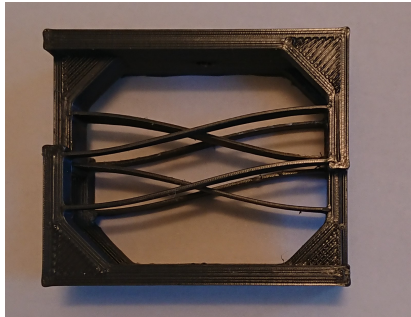


Figure J.4: Prototype of the monolithic negative stiffness mechanism, using curved flexures, in its undeformed shape

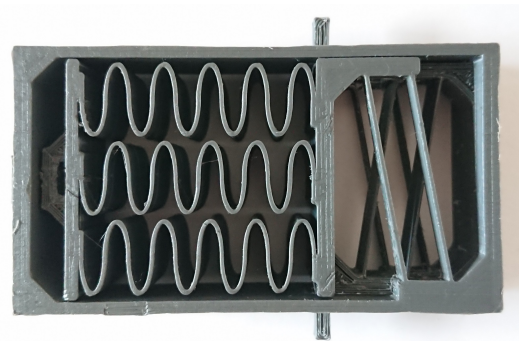


Figure J.5: Prototype of the monolithic constant force mechanism

J.2. Monolithic design

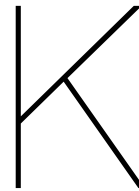
Although the adjustable constant force mechanism was largely 3D printed, manufacturing and assembly took a considerably amount of time, especially the construction of the flexure sets. To decrease the assembly time some initial investigations were performed in making the design at least partially monolithic.

As an initial test an FDM printer was used for the fabrication of the monolithic prototype. The first prototype was based on the same design as the negative stiffness mechanism, but with the flexures now being an integral part of the mechanism. However, as the mechanism contains free hanging surfaces, such as the flexures, support material had to be printed. The flexures were printed having a thickness of 0.4 mm, consisting of a single line, as the printing nozzle was of the same size. The printed prototype is depicted in Fig. J.2 and Fig. J.3 proving the possibility of using an FDM printer to print such structures. Note however that the negative stiffness generated by this design is insufficient to be of use in the wrist support prototype.

Instead of the inclined flexures, the use of pre-curved flexures was also investigated. As such a separate prototype was made using curved flexures, which is depicted in Fig. J.4. Although, some snap-through behaviour was observed the mechanism did not show a bi-stable behaviour as expected from simulations. This is likely caused by a combination of manufacturing uncertainty and the limited stroke as the stroke was limited by endstops to prevent accidentally damaging the part.

Lastly, as printing the negative stiffness element was successful an attempt was made to make the complete adjustable constant force mechanism out of one part. Thus, combining both the positive

stiffness element and the negative stiffness element in one design. Based on a combination of FEM simulations and the elliptic integral method the stiffness of the positive and negative stiffness elements were calculated and tuned such that they were approximately equal (although not validated experimentally). The prototype of this mechanism is depicted in Fig. J.5. Proving that it is also possible to completely 3D printing the mechanism, decreasing the difficulties of manufacturing. However, using PLA the obtainable level of constant force is too small for application in a wrist support. However using different materials having a higher stiffness implementation should be possible. An additional advantage is that the mechanism can be easily scaled, although it is still dependent on the available printing resolution.



Concept generation

The initial concept generation did not focus on obtaining the adjustable constant force mechanism as the major part of this thesis is concerned with. Instead, initially solutions were investigated capable of potentially perfect compensation of the weight of the hand. A large part of this initial investigation focussed on methods to change stiffness to adjust the torque profile for different orientations of the arm. Some possible methods to change stiffness are depicted in Fig. K.1 which are to a large extent based on literature [74–76, 105].

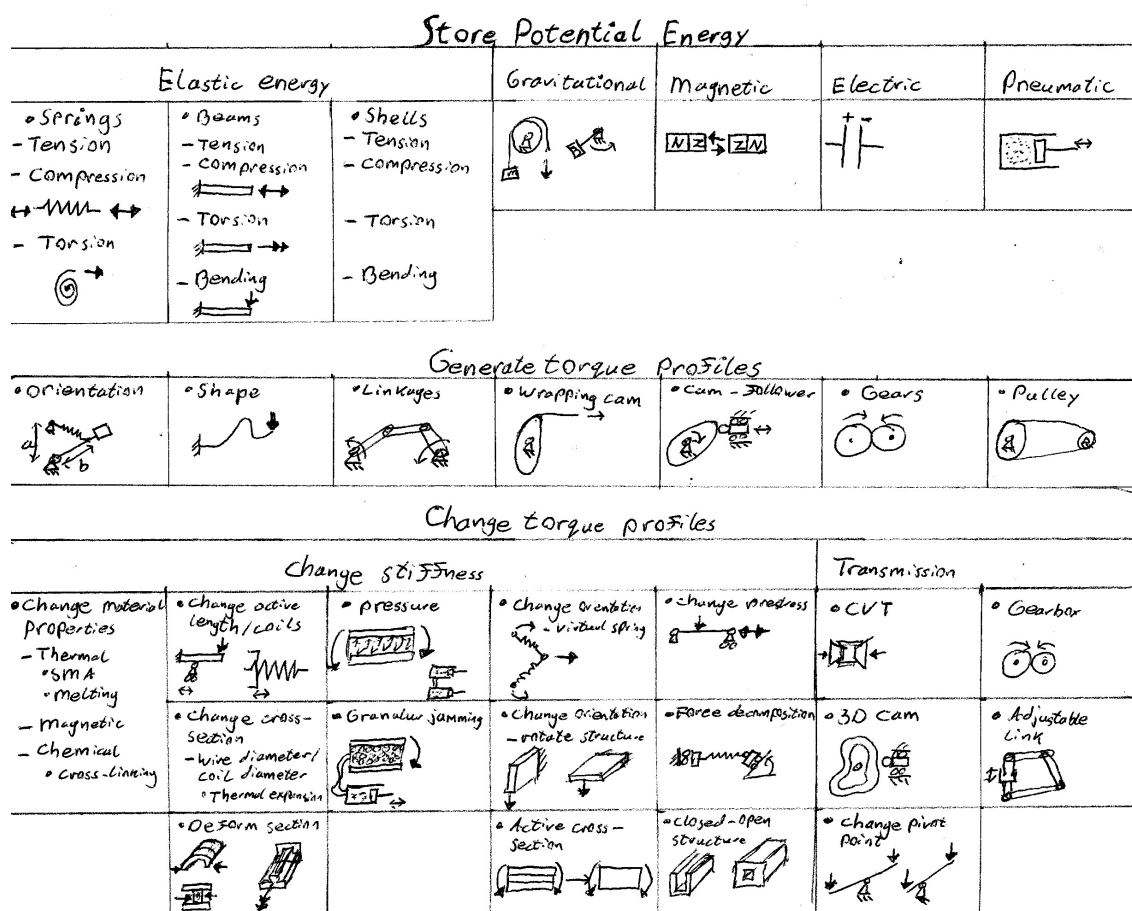
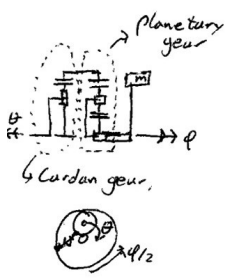


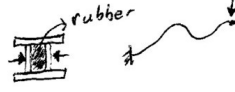
Figure K.1: Various solutions to the three sub-problems, storing energy, generating the required torque profile and adjusting the profile for different orientations of the arm

Cardan gear + Planetary gear



- Remarks
- Phase shift of stiffness profile
 - Requires non-backdrivable mechanism
 - Rotation of θ is not balanced yet

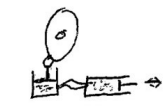
Spatially curved beams + Cross-section change



- Applying force to the sides of the beam compresses the rubber causing it to expand vertically. This changes the distances between the flanges and thus the bending stiffness

- Remarks
- Change amplitude of constant moment
 - Instead of rubber some meta material/auxetic material can be used.

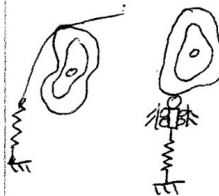
Gas Spring + Cam Follower



- Use a cam follower to generate the desired torque profile
- Store potential energy in gas spring

• Stiffness of gas spring can be changed with a piston, by increasing or decreasing the pressure in the gas spring cylinder

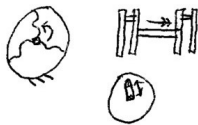
3D-Cam



• Use a cam as a non-circular pulley or as a cam-follower to generate desired torque profile

- Shape of cam changes in out of plane direction. Thus moving the cam, wire or follower in the out of plane direction results in a change of torque profile

Torsion spring + CVT

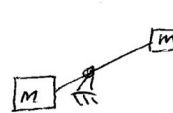


- Two constant torque springs connected, such that when prestressed generate opposite torques

• The two springs are connected through a CVT, such that the resulting torque can be varied from $-T$ to T

• A possible CVT is a variable lever arm

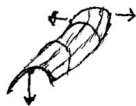
Counterweight



• Use a counterweight to compensate the weight of the hand

- Possibly combine with a transmission to decrease stroke of the counterweight or decrease its mass

Double curvature shell + Deform section



- Use a double curvature shell to generate a constant moment

• By compressing/stretching the sides the second area moment can be changed, changing the bending stiffness/torque

Triple springs



- Approximate constant force mechanism. Force output can be changed by moving point A up or down

Figure K.2: Concepts generated by combining the partial solutions from Fig. K.1

Bibliography

- [1] Eugenio Mercuri and Francesco Muntoni. “Muscular dystrophies”. In: *The Lancet* 381.9869 (Mar. 2013), pp. 845–860. ISSN: 01406736. DOI: 10.1016/S0140-6736(12)61897-2. URL: <https://linkinghub.elsevier.com/retrieve/pii/S0140673612618972>.
- [2] Eugenio Mercuri, Carsten G Bönnemann, and Francesco Muntoni. “Muscular dystrophies”. In: *The Lancet* 394.10213 (Nov. 2019), pp. 2025–2038. ISSN: 01406736. DOI: 10.1016/S0140-6736(19)32910-1. URL: <https://linkinghub.elsevier.com/retrieve/pii/S0140673619329101>.
- [3] Alan EH Emery. “The muscular dystrophies”. In: *The Lancet* 359.9307 (Feb. 2002), pp. 687–695. ISSN: 01406736. DOI: 10.1016/S0140-6736(02)07815-7. URL: <https://linkinghub.elsevier.com/retrieve/pii/S0140673602078157>.
- [4] Joan Lobo Prat. “Control Interfaces to Actively Support the Arm Function of Men with Duchenne Muscular Dystrophy”. PhD thesis. Enschede, 2016.
- [5] Kostas Nizamis. “Hand neuro-motor characterization and motor intention decoding in Duchenne muscular dystrophy”. PhD thesis. Enschede, The Netherlands: University of Twente, June 2019. ISBN: 9789036547833. DOI: 10.3990/1.9789036547833. URL: <http://purl.org/utwente/doi/10.3990/1.9789036547833>.
- [6] A G Dunning. “Slender Spring Systems, for a close-to-body dynamic arm support for people with Duchenne muscular dystrophy”. PhD thesis. 2016.
- [7] C J W Haarman. “Development of a functional hand orthosis for boys with Duchenne muscular dystrophy”. PhD thesis. 2016.
- [8] MMHP Janssen. “Upper extremity function in Duchenne Muscular Dystrophy. Mechanisms of declined task performance”. PhD thesis. 2017.
- [9] *Wearable Robotics*. URL: <https://www.wearablerobotics.nl/>.
- [10] Ronald A. Bos et al. “A structured overview of trends and technologies used in dynamic hand orthoses”. In: *Journal of NeuroEngineering and Rehabilitation* 13.1 (Dec. 2016), p. 62. ISSN: 1743-0003. DOI: 10.1186/s12984-016-0168-z. URL: <http://jneuroengrehab.biomedcentral.com/articles/10.1186/s12984-016-0168-z>.
- [11] Piyu Wang and Qingsong Xu. “Design and modeling of constant-force mechanisms: A survey”. In: *Mechanism and Machine Theory* 119 (Jan. 2018), pp. 1–21. ISSN: 0094114X. DOI: 10.1016/j.mechmachtheory.2017.08.017. URL: <https://linkinghub.elsevier.com/retrieve/pii/S0094114X17302525>.
- [12] Thanh-Vu Phan, Huy-Tuan Pham, and Cong-Nam Truong. “Design and Analysis of a Compliant Constant-Torque Mechanism for Rehabilitation Devices”. In: Cham: Springer International Publishing, 2020, pp. 541–549. DOI: 10.1007/978-3-030-45120-2_{_}44. URL: http://link.springer.com/10.1007/978-3-030-45120-2_44.
- [13] Parker W. Hill, Eric T. Wolbrecht, and Joel C. Perry. “Gravity Compensation of an Exoskeleton Joint Using Constant-Force Springs”. In: *2019 IEEE 16th International Conference on Rehabilitation Robotics (ICORR)*. IEEE, June 2019, pp. 311–316. ISBN: 978-1-7281-2755-2. DOI: 10.1109/ICORR.2019.8779422. URL: <https://ieeexplore.ieee.org/document/8779422/>.
- [14] Salvatore Crisafulli et al. “Global epidemiology of Duchenne muscular dystrophy: an updated systematic review and meta-analysis”. In: *Orphanet Journal of Rare Diseases* 15.1 (Dec. 2020), p. 141. ISSN: 1750-1172. DOI: 10.1186/s13023-020-01430-8. URL: <https://ojrd.biomedcentral.com/articles/10.1186/s13023-020-01430-8>.

- [15] Dongsheng Duan et al. "Duchenne muscular dystrophy". In: *Nature Reviews Disease Primers* 7.1 (Dec. 2021), p. 13. ISSN: 2056-676X. DOI: 10.1038/s41572-021-00248-3. URL: <http://www.nature.com/articles/s41572-021-00248-3>.
- [16] Susana Garcia et al. "Identification of *de novo* Mutations of Duchénnè/Becker Muscular Dystrophies in Southern Spain". eng. In: *International Journal of Medical Sciences* 11.10 (2014), pp. 988–993. ISSN: 1449-1907. DOI: 10.7150/ijms.8391. URL: <http://www.medsci.org/v11p0988.htm>.
- [17] Emma Ciafaloni et al. "Delayed Diagnosis in Duchenne Muscular Dystrophy: Data from the Muscular Dystrophy Surveillance, Tracking, and Research Network (MD STARnet)". In: *The Journal of Pediatrics* 155.3 (Sept. 2009), pp. 380–385. ISSN: 00223476. DOI: 10.1016/j.jpeds.2009.02.007. URL: <https://linkinghub.elsevier.com/retrieve/pii/S0022347609001188>.
- [18] Shelagh M. Szabo et al. "The clinical course of Duchenne muscular dystrophy in the corticosteroid treatment era: a systematic literature review". In: *Orphanet Journal of Rare Diseases* 16.1 (Dec. 2021), p. 237. ISSN: 1750-1172. DOI: 10.1186/s13023-021-01862-w. URL: <https://ojrd.biomedcentral.com/articles/10.1186/s13023-021-01862-w>.
- [19] S. Ryder et al. "The burden, epidemiology, costs and treatment for Duchenne muscular dystrophy: an evidence review". In: *Orphanet Journal of Rare Diseases* 12.1 (Dec. 2017), p. 79. ISSN: 1750-1172. DOI: 10.1186/s13023-017-0631-3. URL: <http://ojrd.biomedcentral.com/articles/10.1186/s13023-017-0631-3>.
- [20] Takeshi Tsuda. "Clinical Manifestations and Overall Management Strategies for Duchenne Muscular Dystrophy". In: *Duchenne Muscular Dystrophy: Methods and Protocols*. Ed. by Camilla Bernardini. New York, NY: Springer New York, 2018, pp. 19–28. DOI: 10.1007/978-1-4939-7374-3{_}2. URL: http://link.springer.com/10.1007/978-1-4939-7374-3_2.
- [21] Michelle Eagle et al. "Survival in Duchenne muscular dystrophy: improvements in life expectancy since 1967 and the impact of home nocturnal ventilation". In: *Neuromuscular Disorders* 12.10 (Dec. 2002), pp. 926–929. ISSN: 09608966. DOI: 10.1016/S0960-8966(02)00140-2. URL: <https://linkinghub.elsevier.com/retrieve/pii/S0960896602001402>.
- [22] Michelle Eagle et al. "Managing Duchenne muscular dystrophy – The additive effect of spinal surgery and home nocturnal ventilation in improving survival". In: *Neuromuscular Disorders* 17.6 (June 2007), pp. 470–475. ISSN: 09608966. DOI: 10.1016/j.nmd.2007.03.002. URL: <https://linkinghub.elsevier.com/retrieve/pii/S0960896607000831>.
- [23] P. Kieny et al. "Evolution of life expectancy of patients with Duchenne muscular dystrophy at AFM Yolaine de Kepper centre between 1981 and 2011". In: *Annals of Physical and Rehabilitation Medicine* 56.6 (Sept. 2013), pp. 443–454. ISSN: 18770657. DOI: 10.1016/j.rehab.2013.06.002. URL: <https://linkinghub.elsevier.com/retrieve/pii/S1877065713000869>.
- [24] Luigia Passamano et al. "Improvement of survival in Duchenne Muscular Dystrophy: retrospective analysis of 835 patients." eng. In: *Acta myologica : myopathies and cardiomyopathies : official journal of the Mediterranean Society of Myology* 31.2 (Oct. 2012), pp. 121–5. ISSN: 1128-2460. URL: <http://www.ncbi.nlm.nih.gov/pubmed/23097603%20http://www.pubmedcentral.nih.gov/articlerender.fcgi?artid=PMC3476854>.
- [25] Amy S. Rosenberg et al. "Immune-mediated pathology in Duchenne muscular dystrophy". eng. In: *Science Translational Medicine* 7.299 (Aug. 2015), pp. 4–299. ISSN: 1946-6234. DOI: 10.1126/scitranslmed.aaa7322. URL: <https://www.science.org/doi/10.1126/scitranslmed.aaa7322>.
- [26] Christophe Cornu, Francis Goubel, and Michel Fardeau. "Muscle and joint elastic properties during elbow flexion in Duchenne muscular dystrophy". In: *The Journal of Physiology* 533.2 (June 2001), pp. 605–616. ISSN: 0022-3751. DOI: 10.1111/j.1469-7793.2001.0605a.x. URL: <https://onlinelibrary.wiley.com/doi/10.1111/j.1469-7793.2001.0605a.x>.

- [27] Mariska M. H. P. Janssen et al. "Dynamic arm study: quantitative description of upper extremity function and activity of boys and men with duchenne muscular dystrophy". In: *Journal of NeuroEngineering and Rehabilitation* 14.1 (Dec. 2017), p. 45. ISSN: 1743-0003. DOI: 10.1186/s12984-017-0259-5. URL: <http://jneuroengrehab.biomedcentral.com/articles/10.1186/s12984-017-0259-5>.
- [28] S.F. Bensamoun et al. "Elastic properties of skeletal muscle and subcutaneous tissues in Duchenne muscular dystrophy by magnetic resonance elastography (MRE): A feasibility study". In: *IRBM* 36.1 (Feb. 2015), pp. 4–9. ISSN: 19590318. DOI: 10.1016/j.irbm.2014.11.002. URL: <https://linkinghub.elsevier.com/retrieve/pii/S195903181400147X>.
- [29] Joseph G. M. Hendriksen and Johan S. H. Vles. "Neuropsychiatric Disorders in Males With Duchenne Muscular Dystrophy: Frequency Rate of Attention-Deficit Hyperactivity Disorder (ADHD), Autism Spectrum Disorder, and Obsessive—Compulsive Disorder". In: *Journal of Child Neurology* 23.5 (May 2008), pp. 477–481. ISSN: 0883-0738. DOI: 10.1177/0883073807309775. URL: <http://journals.sagepub.com/doi/10.1177/0883073807309775>.
- [30] Yi-Jing Lue et al. "Measurement of the Functional Status of Patients with Different Types of Muscular Dystrophy". In: *The Kaohsiung Journal of Medical Sciences* 25.6 (June 2009), pp. 325–333. ISSN: 1607551X. DOI: 10.1016/S1607-551X(09)70523-6. URL: [http://doi.wiley.com/10.1016/S1607-551X\(09\)70523-6](http://doi.wiley.com/10.1016/S1607-551X(09)70523-6).
- [31] J. Houdijn Beekhuis et al. "Design of a self-aligning 3-DOF actuated exoskeleton for diagnosis and training of wrist and forearm after stroke". In: *2013 IEEE 13th International Conference on Rehabilitation Robotics (ICORR)*. IEEE, June 2013, pp. 1–5. ISBN: 978-1-4673-6024-1. DOI: 10.1109/ICORR.2013.6650357. URL: <http://ieeexplore.ieee.org/document/6650357/>.
- [32] Mariska M. H. P. Janssen et al. "Patterns of decline in upper limb function of boys and men with DMD: an international survey". In: *Journal of Neurology* 261.7 (July 2014), pp. 1269–1288. ISSN: 0340-5354. DOI: 10.1007/s00415-014-7316-9. URL: <http://link.springer.com/10.1007/s00415-014-7316-9>.
- [33] Lilian Lacourpaille et al. "Non-invasive assessment of muscle stiffness in patients with duchenne muscular dystrophy". In: *Muscle & Nerve* 51.2 (Feb. 2015), pp. 284–286. ISSN: 0148639X. DOI: 10.1002/mus.24445. URL: <https://onlinelibrary.wiley.com/doi/10.1002/mus.24445>.
- [34] Lilian Lacourpaille et al. "Effects of Duchenne muscular dystrophy on muscle stiffness and response to electrically-induced muscle contraction: A 12-month follow-up". In: *Neuromuscular Disorders* 27.3 (Mar. 2017), pp. 214–220. ISSN: 09608966. DOI: 10.1016/j.nmd.2017.01.001. URL: <https://linkinghub.elsevier.com/retrieve/pii/S0960896616308148>.
- [35] Kostas Nizamis et al. "Characterization of Forearm Muscle Activation in Duchenne Muscular Dystrophy via High-Density Electromyography: A Case Study on the Implications for Myoelectric Control". In: *Frontiers in Neurology* 11 (Apr. 2020). ISSN: 1664-2295. DOI: 10.3389/fneur.2020.00231. URL: <https://www.frontiersin.org/article/10.3389/fneur.2020.00231/full>.
- [36] Mariska M.H.P. Janssen, Jaap Harlaar, and Imelda J.M. de Groot. "Surface EMG to assess arm function in boys with DMD: A pilot study". In: *Journal of Electromyography and Kinesiology* 25.2 (Apr. 2015), pp. 323–328. ISSN: 10506411. DOI: 10.1016/j.jelekin.2015.01.008. URL: <https://linkinghub.elsevier.com/retrieve/pii/S1050641115000279>.
- [37] Craig M. McDonald et al. "Profiles of neuromuscular diseases: Duchenne muscular dystrophy". In: *American Journal of Physical Medicine & Rehabilitation* 74.Supplement 1 (Sept. 1995), S70–S92. ISSN: 0894-9115. DOI: 10.1097/00002060-199509001-00003. URL: <http://journals.lww.com/00002060-199509001-00003>.
- [38] M Jansen. "No use is disuse. Physical training in Duchenne muscular dystrophy". PhD thesis. 2014.
- [39] Fabiana Luisa Mattar and Claudia Sobreira. "Hand weakness in Duchenne muscular dystrophy and its relation to physical disability". In: *Neuromuscular Disorders* 18.3 (Mar. 2008), pp. 193–198. ISSN: 0960-8966. DOI: 10.1016/J.NMD.2007.11.004.

- [40] Marilyn B. Wagner, Paul J. Vignos, and Chris Carlozzi. "Duchenne muscular dystrophy: A study of wrist and hand function". In: *Muscle & Nerve* 12.3 (Mar. 1989), pp. 236–244. ISSN: 0148-639X. DOI: 10.1002/mus.880120313. URL: <https://onlinelibrary.wiley.com/doi/10.1002/mus.880120313>.
- [41] Andrea M. Reinig, Sara Mirzaei, and Daniel J. Berlau. "Advances in the Treatment of Duchenne Muscular Dystrophy: New and Emerging Pharmacotherapies". In: *Pharmacotherapy: The Journal of Human Pharmacology and Drug Therapy* 37.4 (Apr. 2017), pp. 492–499. ISSN: 1875-9114. DOI: 10.1002/PHAR.1909. URL: <https://onlinelibrary-wiley-com.tudelft.idm.oclc.org/doi/full/10.1002/phar.1909%20https://onlinelibrary-wiley-com.tudelft.idm.oclc.org/doi/abs/10.1002/phar.1909%20https://accpjournals-onlinelibrary-wiley-com.tudelft.idm.oclc.org/doi/10.1002/phar.1909>.
- [42] Jean K. Mah. "Duchenne and Becker Muscular Dystrophies: Underlying Genetic and Molecular Mechanisms". In: *Muscular Dystrophy*. Ed. by Raymond A Huml. Cham: Springer International Publishing, 2015, pp. 21–35. DOI: 10.1007/978-3-319-17362-7_{_}4. URL: http://link.springer.com/10.1007/978-3-319-17362-7_4.
- [43] Laura E. Case. "Physical Therapy and Orthotic Devices". In: *Muscular Dystrophy*. Ed. by Raymond A Huml. Cham: Springer International Publishing, 2015, pp. 73–104. DOI: 10.1007/978-3-319-17362-7_{_}8. URL: http://link.springer.com/10.1007/978-3-319-17362-7_8.
- [44] David J Birnkrant et al. "Diagnosis and management of Duchenne muscular dystrophy, part 1: diagnosis, and neuromuscular, rehabilitation, endocrine, and gastrointestinal and nutritional management". In: *The Lancet Neurology* 17.3 (Mar. 2018), pp. 251–267. ISSN: 14744422. DOI: 10.1016/S1474-4422(18)30024-3. URL: <https://linkinghub.elsevier.com/retrieve/pii/S1474442218300243>.
- [45] David J Birnkrant et al. "Diagnosis and management of Duchenne muscular dystrophy, part 3: primary care, emergency management, psychosocial care, and transitions of care across the lifespan". In: *The Lancet Neurology* 17.5 (May 2018), pp. 445–455. ISSN: 14744422. DOI: 10.1016/S1474-4422(18)30026-7. URL: <https://linkinghub.elsevier.com/retrieve/pii/S1474442218300267>.
- [46] David J Birnkrant et al. "Diagnosis and management of Duchenne muscular dystrophy, part 2: respiratory, cardiac, bone health, and orthopaedic management". In: *The Lancet Neurology* 17.4 (Apr. 2018), pp. 347–361. ISSN: 14744422. DOI: 10.1016/S1474-4422(18)30025-5. URL: <https://linkinghub.elsevier.com/retrieve/pii/S1474442218300255>.
- [47] Andrew J. Skalsky and Craig M. McDonald. "Prevention and Management of Limb Contractures in Neuromuscular Diseases". In: *Physical Medicine and Rehabilitation Clinics of North America* 23.3 (Aug. 2012), pp. 675–687. ISSN: 10479651. DOI: 10.1016/j.pmr.2012.06.009. URL: <https://linkinghub.elsevier.com/retrieve/pii/S1047965112000484>.
- [48] **SaeboMAS | Mobile Arm Support Device | Saebo, Inc.** URL: <https://www.saebo.com/shop/saebomas/>.
- [49] **Pura from Armon - Armon Products BV.** URL: <http://www.armonproducts.com/products/pura/>.
- [50] Ali Amoozandeh Nobaveh, Giuseppe Radaelli, and Just L. Herder. "A Design Tool for Passive Wrist Support". In: *Biosystems and Biorobotics* 27 (2022), pp. 13–17. ISSN: 21953570. DOI: 10.1007/978-3-030-69547-7_{_}3/TABLES/1. URL: https://link-springer-com.tudelft.idm.oclc.org/chapter/10.1007/978-3-030-69547-7_3.
- [51] Elaine N Marieb and Katja Hoehn. *Human Anatomy & Physiology*. Essex: Pearson, 2016.
- [52] Stephen D Forro, Akul Munjal, and Jason B Lowe. *Anatomy, Shoulder and Upper Limb, Arm Structure and Function*. StatPearls [Internet]. Treasure Island (FL), 2021. URL: <https://www.ncbi.nlm.nih.gov/books/NBK507841/>.

- [53] Paul Jackson Mansfield and Donald A. Neumann. "Structure and Function of the Elbow and Forearm Complex". In: *Essentials of Kinesiology for the Physical Therapist Assistant*. Ed. by Paul Jackson Mansfield and Donald A Neumann. St. Louis (MO): Elsevier, 2019, pp. 91–119. DOI: 10.1016/B978-0-323-54498-6.00005-9. URL: <https://linkinghub.elsevier.com/retrieve/pii/B9780323544986000059>.
- [54] Paul Jackson Mansfield and Donald A. Neumann. "Structure and Function of the Wrist". In: *Essentials of Kinesiology for the Physical Therapist Assistant*. Ed. by Paul Jackson Mansfield and Donald A Neumann. St. Louis (MO): Elsevier, 2019, pp. 120–140. DOI: 10.1016/B978-0-323-54498-6.00006-0. URL: <https://linkinghub.elsevier.com/retrieve/pii/B9780323544986000060>.
- [55] Nives Klopčar and Jadran Lenarčič. "Kinematic Model for Determination of Human Arm Reachable Workspace". In: *Meccanica* 40.2 (Apr. 2005), pp. 203–219. ISSN: 0025-6455. DOI: 10.1007/s11012-005-3067-0. URL: <http://link.springer.com/10.1007/s11012-005-3067-0>.
- [56] Çiğdem Ayhan and Egemen Ayhan. "Kinesiology of the wrist and the hand". In: *Comparative Kinesiology of the Human Body*. Ed. by Salih Angin and Ibrahim Engin Şimşek. Elsevier, 2020, pp. 211–282. DOI: 10.1016/B978-0-12-812162-7.00013-8. URL: <https://linkinghub.elsevier.com/retrieve/pii/B9780128121627000138>.
- [57] Robert Kaufmann et al. "Kinematics of the Midcarpal and Radiocarpal Joints in Radioulnar Deviation: An In Vitro Study". In: *The Journal of Hand Surgery* 30.5 (Sept. 2005), pp. 937–942. ISSN: 03635023. DOI: 10.1016/j.jhsa.2005.05.016. URL: <https://linkinghub.elsevier.com/retrieve/pii/S0363502305004089>.
- [58] C.P Neu, J.J Crisco, and S.W Wolfe. "In vivo kinematic behavior of the radio-capitate joint during wrist flexion–extension and radio-ulnar deviation". In: *Journal of Biomechanics* 34.11 (Nov. 2001), pp. 1429–1438. ISSN: 00219290. DOI: 10.1016/S0021-9290(01)00117-8. URL: <https://linkinghub.elsevier.com/retrieve/pii/S002192901001178>.
- [59] L. Leonard et al. "Development of an in-vivo method of wrist joint motion analysis". In: *Clinical Biomechanics* 20.2 (Feb. 2005), pp. 166–171. ISSN: 02680033. DOI: 10.1016/j.clinbiomech.2004.09.005. URL: <https://linkinghub.elsevier.com/retrieve/pii/S0268003304002141>.
- [60] Junya Aizawa et al. "Three-dimensional motion of the upper extremity joints during various activities of daily living". In: *Journal of Biomechanics* 43.15 (Nov. 2010), pp. 2915–2922. ISSN: 00219290. DOI: 10.1016/j.jbiomech.2010.07.006. URL: <https://linkinghub.elsevier.com/retrieve/pii/S0021929010003878>.
- [61] Deanna H. Gates et al. "Range of Motion Requirements for Upper-Limb Activities of Daily Living". eng. In: *The American Journal of Occupational Therapy* 70.1 (Jan. 2016), pp. 1–7001350010. ISSN: 0272-9490. DOI: 10.5014/ajot.2016.015487. URL: <https://research.aota.org/ajot/article/70/1/7001350010p1/6119/Range-of-Motion-Requirements-for-Upper-Limb>.
- [62] Vigen Arakelian. "Gravity compensation in robotics". In: *Advanced Robotics* 30.2 (Jan. 2016), pp. 79–96. ISSN: 0169-1864. DOI: 10.1080/01691864.2015.1090334. URL: <http://www.tandfonline.com/doi/full/10.1080/01691864.2015.1090334>.
- [63] A. G. Dunning and J. L. Herder. "A review of assistive devices for arm balancing". In: *2013 IEEE 13th International Conference on Rehabilitation Robotics (ICORR)*. IEEE, June 2013, pp. 1–6. ISBN: 978-1-4673-6024-1. DOI: 10.1109/ICORR.2013.6650485. URL: <http://ieeexplore.ieee.org/document/6650485/>.
- [64] Justus Laurens Herder. *Energy-free Systems. Theory, conception and design of statically*. Vol. 2. 2001. ISBN: 9037001920.
- [65] Gabriëlle J.M. Tuijthof and Just L. Herder. "Design, actuation and control of an anthropomorphic robot arm". In: *Mechanism and Machine Theory* 35.7 (July 2000), pp. 945–962. ISSN: 0094114X. DOI: 10.1016/S0094-114X(99)00051-8. URL: <https://linkinghub.elsevier.com/retrieve/pii/S0094114X99000518>.

- [66] Abhishek Agrawal and Sunil K. Agrawal. "Design of gravity balancing leg orthosis using non-zero free length springs". In: *Mechanism and Machine Theory* 40.6 (June 2005), pp. 693–709. ISSN: 0094114X. DOI: 10.1016/j.mechmachtheory.2004.11.002. URL: <https://linkinghub.elsevier.com/retrieve/pii/S0094114X05000054>.
- [67] Richard L. Smith et al. "Design of a perfect balance system for active upper-extremity exoskeletons". In: *2013 IEEE 13th International Conference on Rehabilitation Robotics (ICORR)*. IEEE, June 2013, pp. 1–6. ISBN: 978-1-4673-6024-1. DOI: 10.1109/ICORR.2013.6650376. URL: <http://ieeexplore.ieee.org/document/6650376/>.
- [68] Wouter D. van Dorsser et al. "Gravity-Balanced Arm Support With Energy-Free Adjustment". In: *Journal of Medical Devices* 1.2 (June 2007), pp. 151–158. ISSN: 1932-6181. DOI: 10.1115/1.2736400. URL: <https://asmedigitalcollection.asme.org/medicaldevices/article/1/2/151/445015/GravityBalanced-Arm-Support-With-EnergyFree>.
- [69] W D van Dorsser et al. "Energy-free adjustment of gravity equilibrators by adjusting the spring stiffness". In: *Proceedings of the Institution of Mechanical Engineers, Part C: Journal of Mechanical Engineering Science* 222.9 (Sept. 2008), pp. 1839–1846. ISSN: 0954-4062. DOI: 10.1243/09544062JMES832. URL: <http://journals.sagepub.com/doi/10.1243/09544062JMES832>.
- [70] Boudewijn M. Wisse et al. "Energy-Free Adjustment of Gravity Equilibrators Using the Virtual Spring Concept". In: *2007 IEEE 10th International Conference on Rehabilitation Robotics*. IEEE, June 2007, pp. 742–750. ISBN: 978-1-4244-1319-5. DOI: 10.1109/ICORR.2007.4428508. URL: <http://ieeexplore.ieee.org/document/4428508/>.
- [71] Wouter D. van Dorsser et al. "Energy-Free Adjustment of Gravity Equilibrators With Application in a Mobile Arm Support". In: *Volume 2: 30th Annual Mechanisms and Robotics Conference, Parts A and B*. Vol. 2006. ASMEDC, Jan. 2006, pp. 591–599. ISBN: 0-7918-4256-8. DOI: 10.1115/DETC2006-99745. URL: <https://asmedigitalcollection.asme.org/IDETC-CIE/proceedings/IDETC-CIE2006/42568/591/318153>.
- [72] Peter N Kooren et al. "Design and pilot validation of A-gear: a novel wearable dynamic arm support". In: *Journal of NeuroEngineering and Rehabilitation* 12.1 (Dec. 2015), p. 83. ISSN: 1743-0003. DOI: 10.1186/s12984-015-0072-y. URL: <http://www.jneuroengrehab.com/content/12/1/83>.
- [73] T Rahman et al. "A body-powered functional upper limb orthosis." In: *Journal of rehabilitation research and development* 37.6 (2000), pp. 675–80. ISSN: 0748-7711. URL: <http://www.ncbi.nlm.nih.gov/pubmed/11321003>.
- [74] Loïc Blanc, Alain Delchambre, and Pierre Lambert. "Flexible Medical Devices: Review of Controllable Stiffness Solutions". In: *Actuators* 6.3 (July 2017), p. 23. ISSN: 2076-0825. DOI: 10.3390/act6030023. URL: <http://www.mdpi.com/2076-0825/6/3/23>.
- [75] Mariangela Manti, Vito Cacucciolo, and Matteo Cianchetti. "Stiffening in Soft Robotics: A Review of the State of the Art". In: *IEEE Robotics & Automation Magazine* 23.3 (Sept. 2016), pp. 93–106. ISSN: 1070-9932. DOI: 10.1109/MRA.2016.2582718. URL: <http://ieeexplore.ieee.org/document/7565718/>.
- [76] B. Vanderborght et al. "Variable impedance actuators: A review". In: *Robotics and Autonomous Systems* 61.12 (Dec. 2013), pp. 1601–1614. ISSN: 09218890. DOI: 10.1016/j.robot.2013.06.009. URL: <https://linkinghub.elsevier.com/retrieve/pii/S0921889013001188>.
- [77] Renzhen Chen et al. "A variable positive-negative stiffness joint with low frequency vibration isolation performance". In: *Measurement* 185 (Nov. 2021), p. 110046. ISSN: 02632241. DOI: 10.1016/j.measurement.2021.110046. URL: <https://linkinghub.elsevier.com/retrieve/pii/S0263224121009714>.
- [78] David J. Braun, Vincent Chalvet, and Abhinav Dahiya. "Positive–Negative Stiffness Actuators". In: *IEEE Transactions on Robotics* 35.1 (Feb. 2019), pp. 162–173. ISSN: 1552-3098. DOI: 10.1109/TRO.2018.2872284. URL: <https://ieeexplore.ieee.org/document/8492364/>.
- [79] R F Chandler et al. *Investigation of inertial properties of the human body*. Tech. rep. 1975.

- [80] Charles E Clauser, John T McConville, and John W Young. *Weight, volume, and center of mass of segments of the human body*. Tech. rep. 1969.
- [81] Wilfrid Taylor Dempster and George R. L. Gaughran. "Properties of body segments based on size and weight". In: *American Journal of Anatomy* 120.1 (Jan. 1967), pp. 33–54. ISSN: 0002-9106. DOI: 10.1002/aja.1001200104. URL: <https://onlinelibrary.wiley.com/doi/10.1002/aja.1001200104>.
- [82] Jennifer L. Durkin and James J. Dowling. "Analysis of Body Segment Parameter Differences Between Four Human Populations and the Estimation Errors of Four Popular Mathematical Models". In: *Journal of Biomechanical Engineering* 125.4 (Aug. 2003), pp. 515–522. ISSN: 0148-0731. DOI: 10.1115/1.1590359. URL: <https://asmedigitalcollection.asme.org/biomechanical/article/125/4/515/447637/Analysis-of-Body-Segment-Parameter-Differences>.
- [83] Chao-Chieh Lan, Sheng-An Yang, and Yi-Syuan Wu. "Design and experiment of a compact quasi-zero-stiffness isolator capable of a wide range of loads". In: *Journal of Sound and Vibration* 333.20 (Sept. 2014), pp. 4843–4858. ISSN: 0022460X. DOI: 10.1016/j.jsv.2014.05.009. URL: <https://linkinghub.elsevier.com/retrieve/pii/S0022460X1400399X>.
- [84] Christine Vehar Jutte and Sridhar Kota. "Design of Nonlinear Springs for Prescribed Load-Displacement Functions". In: *Journal of Mechanical Design* 130.8 (Aug. 2008). ISSN: 1050-0472. DOI: 10.1115/1.2936928. URL: <https://asmedigitalcollection.asme.org/mechanicaldesign/article/doi/10.1115/1.2936928/418190/Design-of-Nonlinear-Springs-for-Prescribed>.
- [85] G. Radaelli and J.L. Herder. "A monolithic compliant large-range gravity balancer". In: *Mechanism and Machine Theory* 102 (Aug. 2016), pp. 55–67. ISSN: 0094114X. DOI: 10.1016/j.mechmachtheory.2016.03.015. URL: <https://linkinghub.elsevier.com/retrieve/pii/S0094114X16300088>.
- [86] Minhaz Ur Rahman. "Design of constant force compliant mechanisms". PhD thesis. 2014.
- [87] J. Qiu, J.H. Lang, and A.H. Slocum. "A Curved-Beam Bistable Mechanism". In: *Journal of Microelectromechanical Systems* 13.2 (Apr. 2004), pp. 137–146. ISSN: 1057-7157. DOI: 10.1109/JMEMS.2004.825308. URL: <http://ieeexplore.ieee.org/document/1284352/>.
- [88] A. G. Dunning et al. "Bistable Compliant Mechanisms: Corrected Finite Element Modeling for Stiffness Tuning and Preloading Incorporation". In: *Journal of Mechanical Design* 134.8 (Aug. 2012). ISSN: 1050-0472. DOI: 10.1115/1.4006961. URL: <https://asmedigitalcollection.asme.org/mechanicaldesign/article/doi/10.1115/1.4006961/467019/Bistable-Compliant-Mechanisms-Corrected-Finite>.
- [89] A.H.A. Stienen et al. "Self-Aligning Exoskeleton Axes Through Decoupling of Joint Rotations and Translations". In: *IEEE Transactions on Robotics* 25.3 (June 2009), pp. 628–633. ISSN: 1552-3098. DOI: 10.1109/TRO.2009.2019147. URL: <http://ieeexplore.ieee.org/document/4815531/>.
- [90] Serdar Ates et al. "SCRIPT Passive Orthosis: Design and technical evaluation of the wrist and hand orthosis for rehabilitation training at home". In: *2013 IEEE 13th International Conference on Rehabilitation Robotics (ICORR)*. IEEE, June 2013, pp. 1–6. ISBN: 978-1-4673-6024-1. DOI: 10.1109/ICORR.2013.6650401. URL: <http://ieeexplore.ieee.org/document/6650401/>.
- [91] Serdar Ates, Claudia J. W. Haarman, and Arno H. A. Stienen. "SCRIPT passive orthosis: design of interactive hand and wrist exoskeleton for rehabilitation at home after stroke". In: *Autonomous Robots* 41.3 (Mar. 2017), pp. 711–723. ISSN: 0929-5593. DOI: 10.1007/s10514-016-9589-6. URL: <http://link.springer.com/10.1007/s10514-016-9589-6>.
- [92] Karin L. de Gooijer-van de Groep et al. "Estimation of tissue stiffness, reflex activity, optimal muscle length and slack length in stroke patients using an electromyography driven antagonistic wrist model". In: *Clinical Biomechanics* 35 (June 2016), pp. 93–101. ISSN: 02680033. DOI: 10.1016/j.clinbiomech.2016.03.012. URL: <https://linkinghub.elsevier.com/retrieve/pii/S0268003316300274>.

- [93] Steven K. Charles and Neville Hogan. "Dynamics of wrist rotations". In: *Journal of Biomechanics* 44.4 (Feb. 2011), pp. 614–621. ISSN: 00219290. DOI: 10.1016/j.jbiomech.2010.11.016. URL: <https://linkinghub.elsevier.com/retrieve/pii/S0021929010006408>.
- [94] Niek Rijnveld and Hermano I. Krebs. "Passive Wrist Joint Impedance in Flexion - Extension and Abduction - Adduction". In: *2007 IEEE 10th International Conference on Rehabilitation Robotics*. IEEE, June 2007, pp. 43–47. ISBN: 978-1-4244-1319-5. DOI: 10.1109/ICORR.2007.4428404. URL: <http://ieeexplore.ieee.org/document/4428404/>.
- [95] Domenico Formica et al. "The passive stiffness of the wrist and forearm". In: *Journal of Neurophysiology* 108.4 (Aug. 2012), pp. 1158–1166. ISSN: 0022-3077. DOI: 10.1152/jn.01014.2011. URL: <https://www.physiology.org/doi/10.1152/jn.01014.2011>.
- [96] R C Hibbeler. *Engingeering Mechanics: Statics*. Pearson Education, Limited, 2016. ISBN: 9781292089232. URL: <https://books.google.nl/books?id=ItoVrgEACAAJ>.
- [97] Paulo Flores. "A Computational Approach for Cam Size Optimization of Disc Cam-Follower Mechanisms With Translating Roller Followers". In: *Journal of Mechanisms and Robotics* 5.4 (Nov. 2013). ISSN: 1942-4302. DOI: 10.1115/1.4025026. URL: <https://asmedigitalcollection.asme.org/mechanismsrobotics/article/doi/10.1115/1.4025026/380578/A-Computational-Approach-for-Cam-Size-Optimization>.
- [98] Fei Gao, Yannan Liu, and Wei-Hsin Liao. "Cam Profile Generation for Cam-Spring Mechanism With Desired Torque". In: *Journal of Mechanisms and Robotics* 10.4 (Aug. 2018). ISSN: 1942-4302. DOI: 10.1115/1.4040270. URL: <https://asmedigitalcollection.asme.org/mechanismsrobotics/article/doi/10.1115/1.4040270/366555/Cam-Profile-Generation-for-CamSpring-Mechanism>.
- [99] Hussein Hussein et al. "On the design of a preshaped curved beam bistable mechanism". In: *Mechanism and Machine Theory* 131 (Jan. 2019), pp. 204–217. ISSN: 0094-114X. DOI: 10.1016/J.MECHMACHTHEORY.2018.09.024.
- [100] S P Timoshenko and J M Gere. *Theory of Elastic Stability*. Dover Publications, 2012. ISBN: 9780486134802. URL: <https://books.google.nl/books?id=98B6JOW2HiUC>.
- [101] Mattias Vangbo. "An analytical analysis of a compressed bistable buckled beam". In: *Sensors and Actuators A: Physical* 69.3 (Sept. 1998), pp. 212–216. ISSN: 09244247. DOI: 10.1016/S0924-4247(98)00097-1. URL: <https://linkinghub.elsevier.com/retrieve/pii/S0924424798000971>.
- [102] Alexander Story. *Right Hand Reference*. 2020. URL: <https://grabcad.com/library/right-hand-reference-1>.
- [103] Andy Field. *Discovering statistics using IBM SPSS statistics*. sage, 2013. ISBN: 1446274586.
- [104] Didier Staudenmann et al. "Methodological aspects of SEMG recordings for force estimation – A tutorial and review". In: *Journal of Electromyography and Kinesiology* 20.3 (June 2010), pp. 375–387. ISSN: 1050-6411. DOI: 10.1016/J.JELEKIN.2009.08.005.
- [105] Izabela K. Kuder et al. "Variable stiffness material and structural concepts for morphing applications". In: *Progress in Aerospace Sciences* 63 (Nov. 2013), pp. 33–55. ISSN: 0376-0421. DOI: 10.1016/J.PAEROSCI.2013.07.001.